การแลกเปลี่ยนของสปีชีส์คอปเปอร์ในโพรง แซดเอสเอ็ม-5 ที่ปริมาณคอปเปอร์สูง

นางสาวกัญจน์รัตน์ สุขรัตน์

EXCHANGE OF COPPER SPECIES IN THE CAVITY OF ZSM-5 AT HIGH COPPER LOADING

Miss Kanjarat Sukrat

A Thesis Submitted in Partial Fulfillment of the Requirements
for the Degree of Master of Science in Chemistry
Department of Chemistry
Faculty of Science
Chulalongkorn University
Academic year 2004

Thesis Title	EXCHANGE OF COPPER SPECIES IN THE CAVITY OF ZSM-5 AT HIGH COPPER LOADING
By	Miss Kanjarat Sukrat
Field of Study	Chemistry
Thesis Advisor	Associate Professor Vudhichai Parasuk, Ph. D.

Accepted by the Faculty of Science, Chulalongkorn University in Partial Fulfillment of the Requirements for the Master's Degree

………………………………… Dean of the Faculty of Science

(Professor Piamsak Menasveta, Ph. D.)

THESIS COMMITTEE

……………………………… Chairman

(Associate Professor Sirirat Kokpol, Ph. D.)

……………………………… Thesis Advisor

(Associate Professor Vudhichai Parasuk, Ph. D.)

……………………………… Member

(Associate Professor Supot Hannongbua, Ph. D.)

……………………………… Member

(Aticha Chaisuwan, Ph. D.)

นางสาวกัญจน์รัตน์ สุขรัตน์ : การแลกเปลี่ยนของสปีชีส์คอปเปอร์ในโพรง แซดเอสเอ็ม-5 ที่ปริมาณคอปเปอร์สูง (EXCHANGE OF COPPER SPECIES IN THE CAVITY OF ZSM-5 AT HIGH COPPER LOADING) อ. ที่ปรึกษา : รศ. ดร. วุฒิชัย พาราสุข, 103 หน้า. ISBN 974-17-6084-1.

ได้มีการค้นพบว่าแซดเอสเอ็ม-5ที่แลกเปลี่ยนไอออนคอปเปอร์ สามารถก่อกัมมันต์ในปฏิกิริยาการสลายตัวของไนโตรเจนออกไซด์แบบตรง งานวิจัยนี้ได้ศึกษาตำแหน่งแลกเปลี่ยนและคอปเปอร์สปีชีส์ที่เหมาะสมในโพรงของแซดเอสเอ็ม-5 ที่ปริมาณคอปเปอร์สูง โดยเปรียบเทียบโครงสร้างและพลังงานแลกเปลี่ยนของ $CuOH^+$ ในแต่ละตำแหน่งแลกเปลี่ยน เช่นตำแหน่ง T6 T12, T8 T8, T7 T12 แบบที่ 1 (M1T7 T12) และ T7 T12 แบบที่ 2 (M2T7 T12) โดยใช้แบบจำลองคลัสเตอร์ที่โครงสร้างที่ปลายของคลัสเตอร์ทั้งหมด (อันประกอบด้วยความยาวพันธะระหว่างออกซิเจนกับไฮโดรเจนและมุมระหว่างเตตระฮีดรอล-ออกซิเจน-ไฮโดรเจนทั้งหมดซึ่งได้กำหนดให้มีค่าความยาวพันธะเดียวกันและค่ามุมเดียวกัน) และตำแหน่งของโปรตอนที่ได้ปรับให้มีพลังงานเสถียรที่สุดโดยใช้วิธี B3LYP/6-31G(d,p) ขณะที่แช่แข็งค่าตัวแปรโครงสร้างส่วนอื่น จากผลการปรับโครงสร้างเสถียรแบบบางส่วน พบว่าความยาวพันธะระหว่างออกซิเจนกับไฮโดรเจนเท่ากับ 0.96 อังสตรอม และมุมระหว่างเตตระฮีดรอล-ออกซิเจน-ไฮโดรเจน มีค่าระหว่าง 115.0-119.0º จากแบบจำลอง CuZSM-5 ที่เตรียมจากการแทนที่โปรตอนและการหาโครงสร้างเสถียรบางส่วนของโปรตอนและ $CuOH^+$ เราพบว่าระยะระหว่าง Cu-O(Z) หรือคอปเปอร์กับออกซิเจนในโครงร่างมีค่าระหว่าง 1.84-2.15 อังสตรอม สำหรับการแลกเปลี่ยน $CuOH^+$ หนึ่งไอออนที่ตำแหน่งแลกเปลี่ยน M2T7 T12 และ T8 T8 มีค่าพลังงานแลกเปลี่ยนเป็นบวกและลบน้อยคือระหว่าง -5.36-3.47 กิโลแคลอรีต่อโมล การแลกเปลี่ยนที่ตำแหน่ง M1T7 T12 ให้ค่าพลังงานแลกเปลี่ยนสูงที่สุด สำหรับการแลกเปลี่ยน $CuOH^+$ สองไอออนทั้งหมดเราได้ค่าพลังงานแลกเปลี่ยนเป็นบวกทั้งหมดโดยมีค่าระหว่าง 12.61-75.61 กิโลแคลอรีต่อโมล ตำแหน่งที่มีค่าพลังงานแลกเปลี่ยนต่ำที่สุดของทั้งการแลกเปลี่ยนแบบหนึ่งและสองไอออนคือตำแหน่ง T6 T12 โดยมีพลังงานแลกเปลี่ยน -32.47 และ +12.61 กิโลแคลอรีต่อโมล ตามลำดับ สรุปได้ว่าตำแหน่งแลกเปลี่ยนที่เหมาะสมคือตำแหน่ง T6 T12 โดยแลกเปลี่ยนเพียงหนึ่งไอออนต่อตำแหน่งแลกเปลี่ยน อย่างไรก็ตามสปีชีส์ที่แลกเปลี่ยนไม่ใช่ $CuOH^+$ แต่เป็น $[CuOH_2]^{2+}$ มากกว่า ซึ่งโครงสร้างแบบหลังสามารถลดแรงซึ่งทำให้แรงผลักระหว่างสปีชีส์ที่มีประจุมากกว่า สำหรับการศึกษาเสถียรภาพของสารประกอบเชิงซ้อนคอปเปอร์-น้ำ ได้มีการปรับโครงสร้างเสถียรที่เป็นไปได้ของ $[Cu(H_2O)_n]^{2+}$ สำหรับ n เท่ากับ 1-7 โดยวิธี HF/6-31G(d,p) และพลังงานของสารประกอบเชิงซ้อนนี้ได้รับการคำนวณด้วยความแม่นยำมากขึ้นที่ MP2/6-31G(d,p) และ B3LYP/6-31G(d,p) สำหรับ n เท่ากับ 6 และ 7 ได้ทำการคำนวณพลังงานที่ HF/6-31++G(d,p), HF/6-311G(d,p) และ HF/6-311G(2df,p) ด้วย พบว่าสำหรับ n เท่ากับ 6 และ 7 จะพบสารประกอบเชิงซ้อนแบบ 5 และ 6 โคออร์ดิเนชันเท่านั้น สำหรับโครงสร้างแบบ 5 โคออร์ดิเนชันประกอบด้วยโครงสร้างแบบปิรามิดฐานสี่เหลี่ยม (spy) และปิรามิดคู่ฐานสามเหลี่ยม (tbp) และโครงสร้างแบบ 6 โคออร์ดิเนชัน พบโครงสร้างบิดเบี้ยวของออกตะฮีดรอล (oct) สำหรับโครงสร้าง n เท่ากับ 6 จากระเบียบวิธีที่คำนวณด้วยเบสิส เซต 6-31G(d,p) ทำนายโครงสร้าง tbp มีเสถียรภาพสูงสุดแต่เมื่อขยายเบสิส เซต และคำนวณด้วยวิธี HF โครงสร้างแบบ oct มีความเสถียรภาพมากกว่า สำหรับโครงสร้าง n เท่ากับ 7 ทุกระเบียบวิธีและทุกเบสิส เซต เห็นพ้องว่าโครงสร้าง tbp มีเสถียรภาพสูงสุด ในขณะที่โครงสร้าง oct มีพลังงานสูงกว่าเพียงเล็กน้อย ดังนั้นเราสามารถพบทั้งโครงสร้าง tbp และ oct ในสารละลายแต่จะพบโครงสร้างแบบ tbp ในปริมาณมากกว่า

ภาควิชา	เคมี	ลายมือชื่อนิสิต	
สาขาวิชา	เคมี	ลายมือชื่ออาจารย์ที่ปรึกษา	
ปีการศึกษา	2547		

KANJARAT SUKRAT : EXCHANGE OF COPPER SPECIES IN THE CAVITY OF ZSM-5 AT HIGH COPPER LOADING. THESIS ADVISOR : ASSOC. PROF. VUDHICHAI PARASUK, Ph. D. 103 pp., ISBN 974-17-6084-1

Copper ion-exchanged ZSM-5 (CuZSM-5) has been found to be active for the direct decomposition of NO_x. The suitable exchanged sites and copper species in the cavity of ZSM-5 at high copper loading were studied by comparing configurations and exchanged energies of $CuOH^+$ in each exchanged site such as T6 T12, T8 T8, T7 T12 model 1 (M1T7 T12) and T7 T12 model 2 (M2T7 T12) using cluster models. All edges of cluster (all O-H bond lengths and T-O-H bond angles were set same bond length and same bond angle parameter) and positions of H^+ were optimized using B3LYP/6-31G(d,p) while freezing other geometrical parameters. The results of partial optimizations gave O-H bond length of 0.96 Å and T-O-H bond angle between 115.0°-119°. By replacing H^+ with $CuOH^+$ and partial optimization of H^+ and $CuOH^+$, models of CuZSM-5 were prepared. We found Cu-O(Z) distances, Cu to framework oxygen distance, ranging between 1.84-2.15 Å. For one-ion exchanged $CuOH^+$ at M2T7 T12 and T8 T8 exchanged sites, small positive and negative exchanged energies between -5.36-3.47 kcal/mol were observed. The M1T7 T12 exchanged site possess as the highest exchanged energies. For all two-ion exchanged $CuOH^+$, positive exchanged energies which ranging from 12.61-75.61 kcal/mol were opatined. T6 T12 exchanged sites give the lowest exchanged energies for both one- and two-ion exchanged $CuOH^+$, -32.47 and +12.61 kcal/mol respectively. It can be concluded that preferable exchanged sites for $CuOH^+$ is T6 T12 site and there is only one ion exchanged per site. However, the exchanged species are not in the form of $CuOH^+$ but rather $[CuOH_2]^{2+}$ where the repulsion between charge species as minimized. For structures and stabilizations of copper- water complexes, possible structures of $[Cu(H_2O)_n]^{2+}$ for n=1-7 were geometry optimized at HF/6-31G(d,p) level and their energies were more accurately determined at MP2/6-31G(d,p) and B3LYP/6-31G(d,p) level of theory. In addition, for n=6 and 7, single point calculations using HF/6-31++G(d,p), HF/6-311G(d,p) and HF/6-311G(2df,p) were also performed. We found that for n=6 and n=7 only 5-fold and 6-fold coordination complexes were found. The 5-fold consists of square pyramidal (spy) and trigonal bipyramidal (tbp) structures and the 6-fold consists of distorted octahedral (oct) structure. For n=6, at 6-31G(d,p) basis all methods predicted tbp as the most stable from of $[Cu(H_2O)_n]^{2+}$. However, with HF method but larger basis set, the oct become more stable. For n=7 all methods and basis sets agree that tbp is the most stable and the oct lies slightly above tbp structure. Thus, oct and tbp structures could co-exist in solution but tbp is more abundant.

Department	Chemistry	Student's signature	
Field of study	Chemistry	Advisor's signature	
Academic year	2004		

ACKNOWLEDGEMENTS

CONTENTS

CONTENTS (continued)

CONTENTS (continued)

LIST OF FIGURES

LIST OF FIGURES (continued)

LIST OF FIGURES (continued)

LIST OF TABLES

LIST OF TABLES (continued)

CHAPTER 1

INTRODUCTION

1.1 Research Rational

Although selective catalytic reduction (SCR) is the current best available technology for reducing NO_x emissions but this process has several disadvantages such as high cost of facilities as well as running and leakage of unreacted ammonia. The uniqueness and properties of catalysts involve transition metals within their materials. Copper ion-exchanged zeolites (CuZSM-5) are among those interesting materials, which have been widely studied in the past decades because of their important industrial applicability. They have been found to be active in catalytic direct decomposition of NO_x (NO, N_2O) into N_2 and O_2.[1-3] Copper ions have been recognized as active sites in many redox reactions involved in the processes of catalytic decomposition. However, little is known about the activity of copper ion in CuZSM-5. The central goal of research is on pursuing the rational for the natures of the active sites or exchanged sites and the prefer exchanged site and species in the cavity of ZSM-5 catalyst, especially at high copper loading (Al/Cu = 1) using quantum calculations. The results could be used to develope and design highly active CuZSM-5 catalysts for direct decomposition of NO_x.

In aqueous solution, first-row transition metal dication (M^{2+}) are surrounded by an inner solvation shell of six water molecules resulting in an octahedral or nearly octahedral, $[M(H_2O)_n]^{2+}$ species.[73] Pasquarello et al.[74] determined the structure of the hydrated Cu(II) complex by both neutron diffraction and first-principles molecular dynamics and reported fivefold coordination complex. The simulation reveals that the solvated complex undergoes frequent transformations between square pyramidal and trigonal bipyramidal configurations. This is in contrast to QM/MM MD simulation which favors an octahedrally solvated Cu(II) ion.[75] Because of its electronic d^9 configuration, a Jahn-Teller distortion is generally assumed to axially elongate two bonds of the octahedral $[Cu(H_2O)_6]^{2+}$ complex, yielding an unusually fast water

exchange rate.[75-77] In addition, an even shorter time scale has been observed and has been attributed to rapid transformations between configurations differing by the orientation of the elongation. Thus, the behavior of its simplest aqueous form, the Cu(II) ion, remains poorly understood. Again, we have studied the solvation of divalent copper by water through the optimization of the structure of copper water complex $[Cu(H_2O)_n]^{2+}$, n=1-7 by static density functional theory and ab initio to confirm geometries of $[Cu(H_2O)_n]^{2+}$ complexes.

1.2 Zeolites

Zeolites[4,5] are crystalline, hydrated aluminosilicates of group I and group II elements, in particular, sodium, potassium, magnesium, calcium, strontium and barium. Structurally, zeolites are "framework" aluminosilicates, which are based on an infinitely extending three-dimensional network of tetrahedral aluminate (AlO_4^{5-}) and silicate (SiO_4^{4-}) linked to each other by sharing oxygen atoms at the corner of each tetrahedral as shown in Figure 1.1.
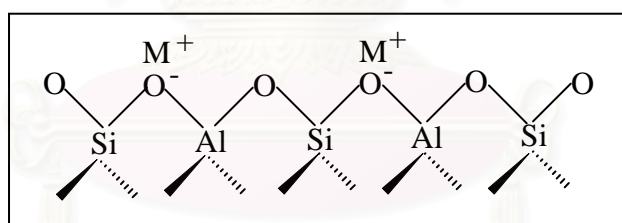
Figure 1.1 The general structure of zeolites.[4]

The AlO_2^- tetrahedra in the structure determine the framework charge. This is balanced by cations that occupy nonframework positions. The general formula for the composition of zeolites is

$$M_{x/n} [(AlO_2)_x (SiO_2)_y] \cdot z\ H_2O$$
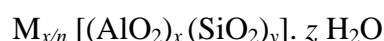
Where M is the cation of valency n, generally from the group I or II ions, although other metals, nonmetals, and organic cations are also possible. The symbols x and y are

the number of tetrahedral aluminate and silicate, respectively. z is the number of water molecules in the channels and cavities of zeolites.

1.3 Structures of Zeolites

All zeolites[4-6] are constructed from a common subunit of structure so called primary building unit of silicate or aluminate tetrahedral. Figure 1.2 shows the two primary building units connecting by sharing an oxygen.
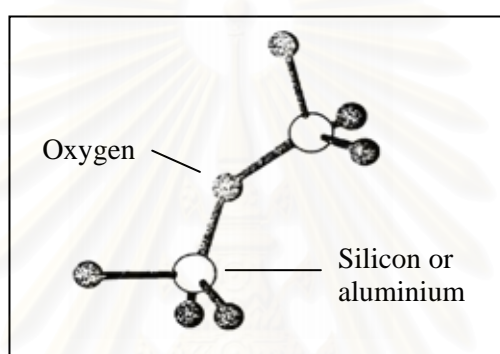
Figure 1.2 Two primary building units of zeolites, two SiO_4/AlO_4 tetrahedra are linked by corner-sharing.[6]

Many zeolite structures are based on a secondary building unit which consists of selected geometric groupings of these tetrahedra. There are 9 such building units, which can be used to describe all of known zeolite structures. The secondary building units can consist of 4, 6, and 8-membered single rings, 4-4, 6-6, and 8-8 membered double rings, and 4-1, 5-1, and 4-4-1 branched rings as illustrated in Figure 1.3.

The secondary building unit provides a convenient method for topologically describing and relating different zeolites. However, in many instances, describing structural differences and similarities requires a building unit that takes into account the arrangement of these secondary building units. The chain building unit adds further dimension to the building unit. An example of such structural mixing within a zeolite framework is the intergrowth of ZSM-5 and ZSM-11. The chain-building unit of both ZSM-5 and ZSM-11 is shown in Figure 1.4. The difference between these two zeolite

structures is the way the chain-building units linking to generate the structure. ZSM-5 is generated such that the chains forming sheets are related through a center of inversion, while ZSM-11 is generated through linkage such that the sheets are related through a mirror plane.
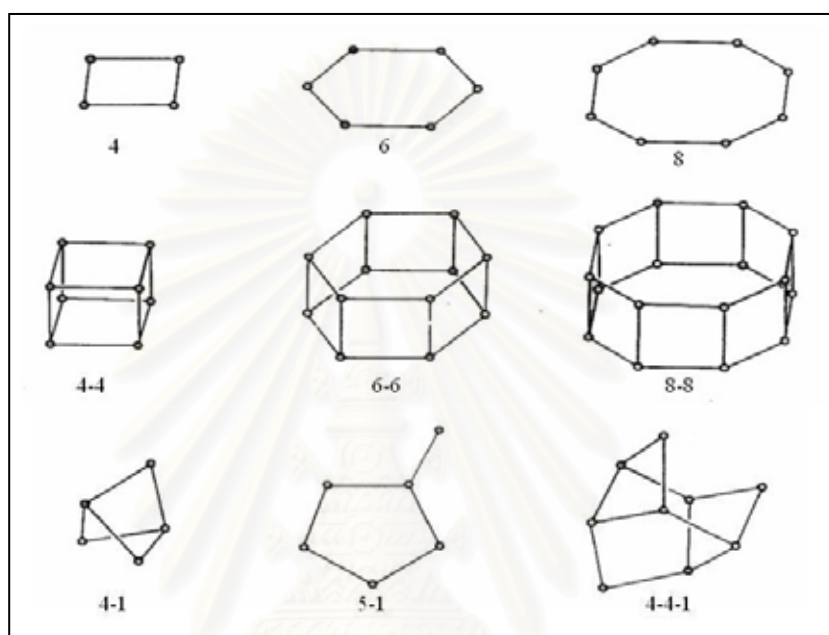
Figure 1.3 Secondary building units found in zeolite structures.[4]
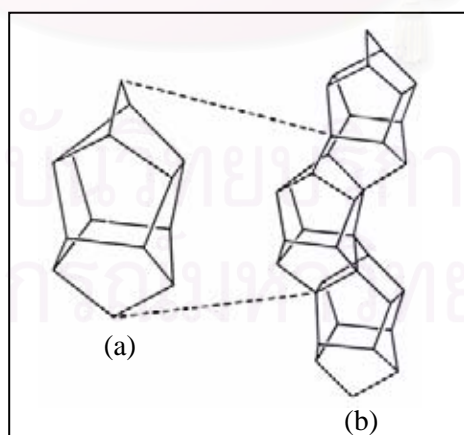
Figure 1.4 The 5-1 secondary building unit (a) to form the chain units (b) found in the ZSM-5 and ZSM-11 structures.[4]

Most of these materials have been synthesized in a laboratory. The large variety of materials arises from (1) many ways the tetrahedral can be connected to form networks with channels and cavities of different sizes, (2) the different type of cations present for charge compensation in extra-framework positions and (3) the different combination of cations in the tetrahedral framework positions (T = Si, Al, P, …). The structure types and the examples found or synthesized are collected in the 'Atlas of the Zeolite Structure Types' which is currently updated and also available on the internet.[8,9]

1.4 Zeolite ZSM-5

The oil company 'Mobil' first synthesized ZSM-5, which is abbreviated from Zeolite Socony Mobil-five, in 1972 with structure code 'MFI'.[7] The tetrahedral units are linked to form the chain-type building block as shown in Figure 1.4. Rings consisted of five oxygen atoms are evident in this structure; the name pentasil is therefore used for describing this ring type. Structure of ZSM-5 contains 96 silicon and 192 oxygen atoms (SiO_2), resulting in a framework density of 17.9 T sites/1000 $Å^3$. The synthetic zeolite, ZSM-5, has the same framework structure as silicalite, with a proportion of the silicon sites occupied by Al^{3+}. Two phases of the purely siliceous zeolite, silicalite, are known: the first to be identified was the orthorhombic phase which contains 12 independent T sites; the second, a low-temperature monoclinic phase (which is ascribed to a shift of neighboring (010) pentasil layers), contains 24 independent T sites as shown in Figure 1.5.[10,11]
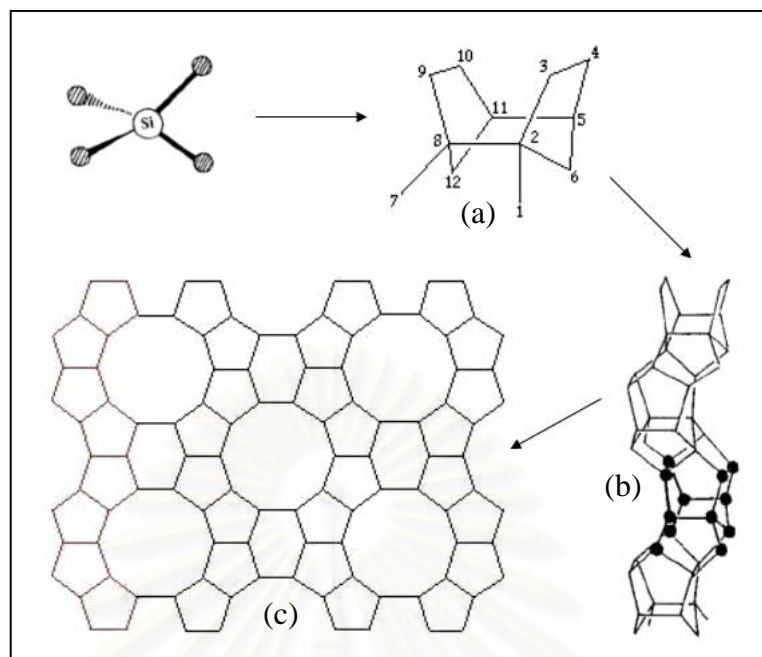
Figure 1.5 Diagrammatic representation of the ZSM-5 structure. (a) Secondary building blocks illustrating the 12 T sites which combine to form chain-type building blocks (pentasil layers (b)). These pentasil layers can combine to form the channel system of the ZSM-5 structure (c). A displacement of these pentasil layers along the (010) direction results in the monoclinic phase of the zeolite, and the subsequent reduction in symmetry allows for 24 independent T sites.[10,11]

ZSM-5 is a medium-pore zeolite having an orthorhombic crystalline structure. The pore opening is composed of a 10-member ring. The ZSM-5 framework contains two types of intersection channels: one type is straight, has elliptical (0.51x0.58 nm) openings, and run parallel to the b-axis of the orthorhombic unit cell, while the other has near-circular (0.54 x 0.56 nm) openings, is sinusoidal (zigzag) and directed along the a-axis.[11] Figure 1.6 exhibits structure of ZSM-5 and schematic of three-dimensional channel.
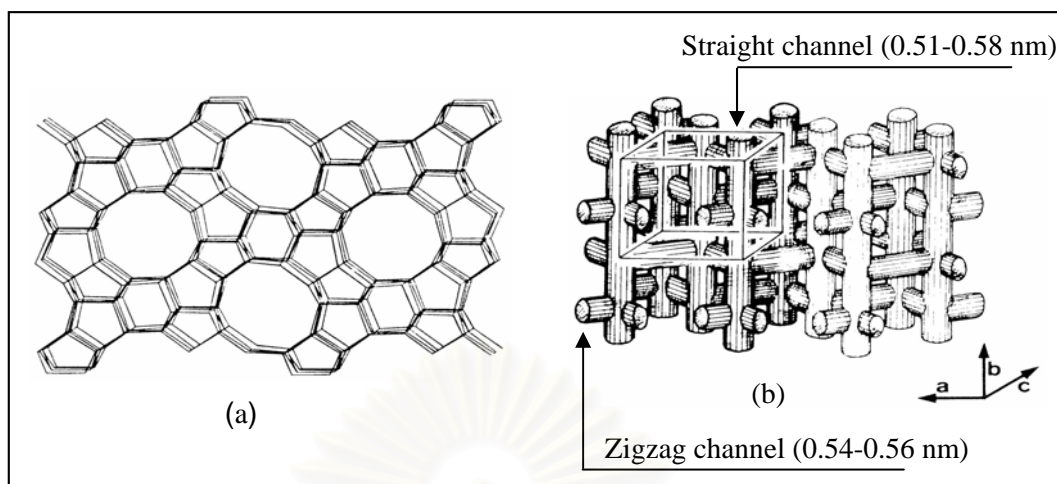
Figure 1.6 (a) Structure of ZSM-5 (MFI). View shows the straight channels. The sinusoidal channels run perpendicular to the straight channels.[4] (b) Schematic illustration of the three-dimensional channels in ZSM-5.[6,10]

1.4.1 Chemical Composition of Zeolite ZSM-5

The chemical formula of a typical unit cell of hydrated Na-ZSM-5 is

$$Na_n[Al_nSi_{96-n}O_{192}.16H_2O], n < 27.$$
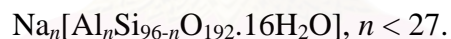
There seems to be a limit on the Al incorporation in the framework. The Si/Al ratio cannot be lower than 1. The lowest Si/Al ratio known in the ZSM-5 lattice is 10. Pairs of AlO_4^- tetrahedra are forbidden by the Löewenstein rule (*i.e.*, no neighboring Al's directly bonded by one oxygen).[12] Zeolite ZSM-5 was used in many industrially catalytic processes and had been the subject of extensive research.[6] Since the catalytic activity of the material was inextricably linked to its composition and structure, recent work attempted to modify these properties by introducing heteroatoms, such as Cu, Ti, Ga, and Ge into the framework.

1.4.2 Shape Selectivity Properties of Zeolite ZSM-5

The accessibility to the catalytic sites in ZSM-5 is best viewed by considering its channel system as schematized in Figure 1.6(b).[6,10] The particular shape selectivity properties of ZSM-5 result from the conjugation of four different structurally interrelated features:

A channel (or pore) opening consisting of 10-member oxygen rings which is intermediate between that of classical shape-selective zeolites (such as erionite, ferrierite, gmelinite, chabazite, or zeolite A) and that of large pore zeolites (such as faujasite, mordenite, and fault-free offretite) as shown in Figure 1.7.
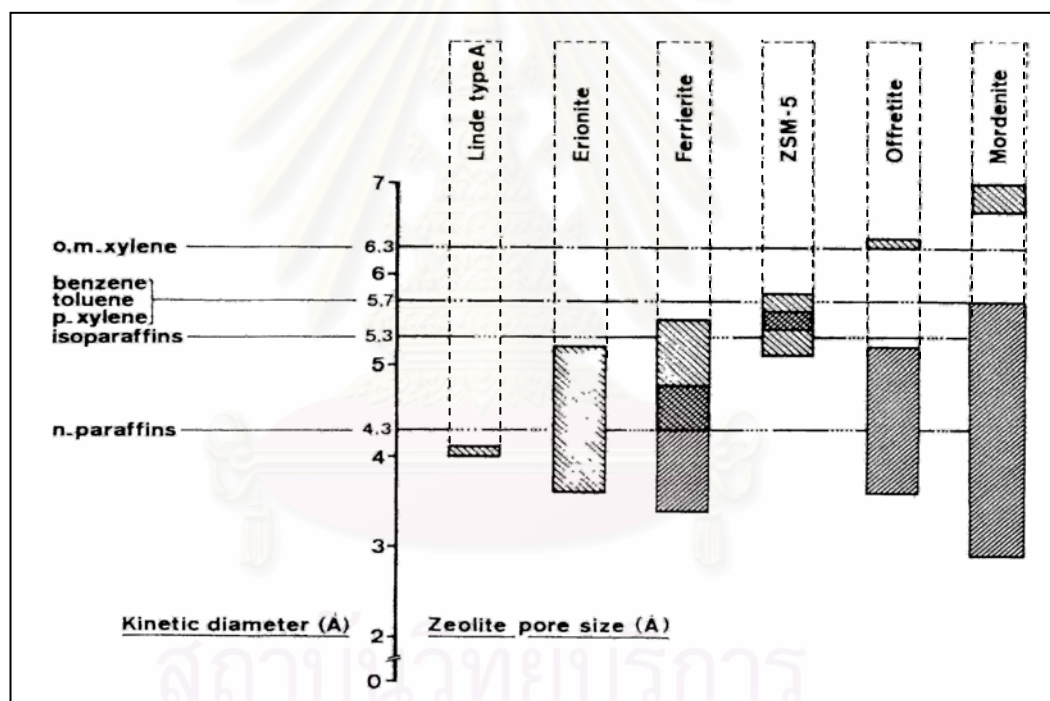
Figure 1.7 Correlation between pore size of various zeolites and kinetic diameter of some molecules.[6]

ZSM-5 are known as *molecular sieves* since they accept for adsorption molecules of certain dimensions while rejecting those of larger dimensions.[4,6,7] They possess shape selectivity, which plays a very important role in zeolite catalysis. Shape

selectivity is divided into 3 types: reactant, product, and transition-state shape selectivity, as shown in Figure 1.8.[4]

Reactant shape selectivity, Figure 1.8(a), results from the limited diffusivity of some of the reactants, *e.g.,* linear *vs.* branched, which cannot effectively enter and diffuse inside the crystal. Product shape selectivity, Figure 1.8(b), occurs when slowly diffusing product molecules, for example *o-* and *m*-xylene, cannot rapidly escape from the crystal, and undergo secondary reactions, for example, to *p*-xylene. Restricted transition-state shape selectivity can be explained by the decrease of the rate constant for a certain reaction mechanism when the required transition state is too bulky to form readily, Figure 1.8(c).
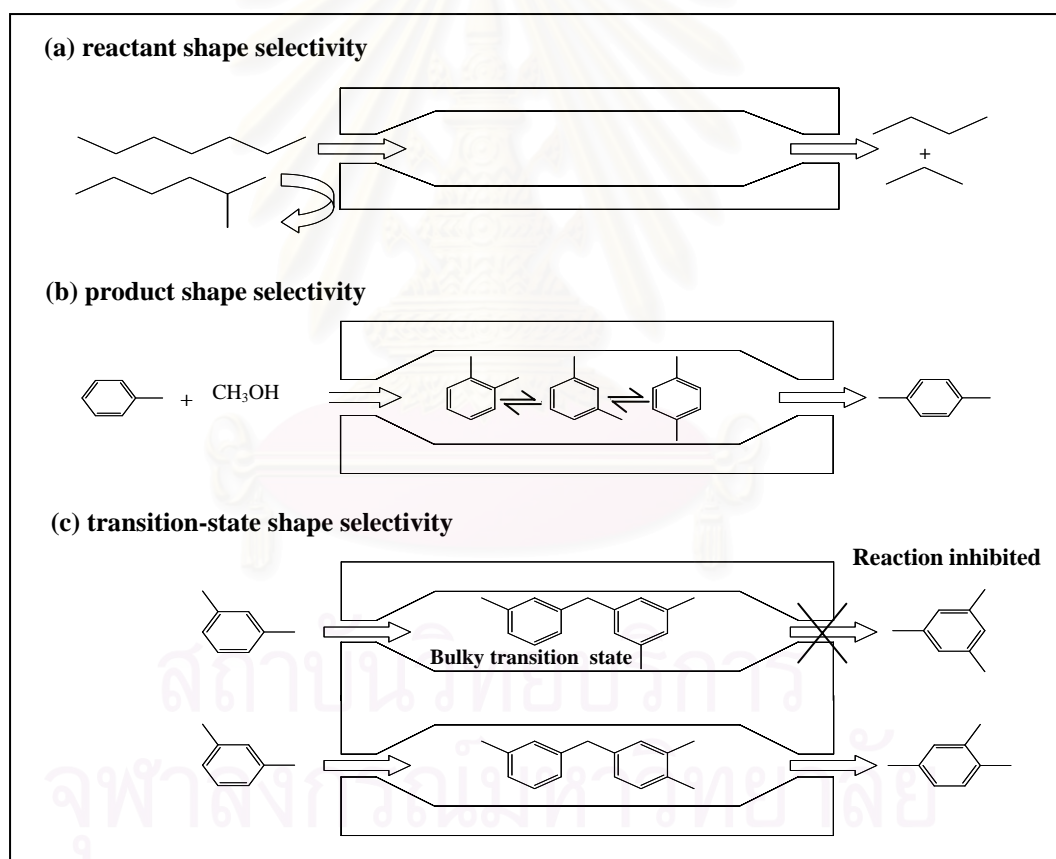
Figure 1.8 Three types of shape selectivity in zeolites: (a) reactant, (b) product, and (c) transition-state shape selectivity.[4]

1.4.3 Acid Sites of Zeolite ZSM-5

Classical Brønsted and Lewis acid models of acidity have been used for classifying the active sites on zeolites.[4] Brønsted acidity is proton-donor acidity, and occurs when protons play the role of charge-compensating cations to the framework anionic charge of zeolites. Proton-form zeolites are exceedingly important as industrial catalysts *e.g.*, for hydrocarbon conversion in the petroleum industry. The most active catalysts include relatively few H or Al sites per Si, typically the Si/Al ratio, *(x-y)/y*, is 10 or larger. Lewis acidity is electron acceptor acidity. An example is trigonally coordinated aluminium atom. In zeolite Brønsted acidity is generally believed to be weaker than Lewis acidity.[4,9]

To produce the zeolite acid catalyst, a first step is to remove large organic quaternary amine cations occluded during synthesis by combustion in air called calcination. The obtained material contains alkali cations (*e.g.* Na^+) and some protons as shown in Figure 1.9(a). Ammonium exchange of the alkali cations, followed by subsequent deammoniation *i.e.,* thermal treatment releasing ammonia gas and leaving proton, results in the structure shown in Equation 1.1 and Figure 1.9(b).

$$(NH_4)_y[(AlO_2)_y(SiO_2)_{x-y}] \rightarrow [(H\text{-}AlO_2)_y(SiO_2)_{x-y}] + yNH_3 \qquad (1.1)$$

Direct exchange with acid is also possible, but has to be done very carefully otherwise Al atoms will be extracted from the zeolite lattice.[4] Simultaneously, Brønsted acid sites are in equilibrium with Lewis acid if –OH groups are considered to bond totally to Si, leaving tricoordinated Al atoms (not shown in the Figure). Acid sites are transformed to Lewis acid sites by dehydration upon heating at high temperature, as shown in Figure 1.9(c). This process is reversible.
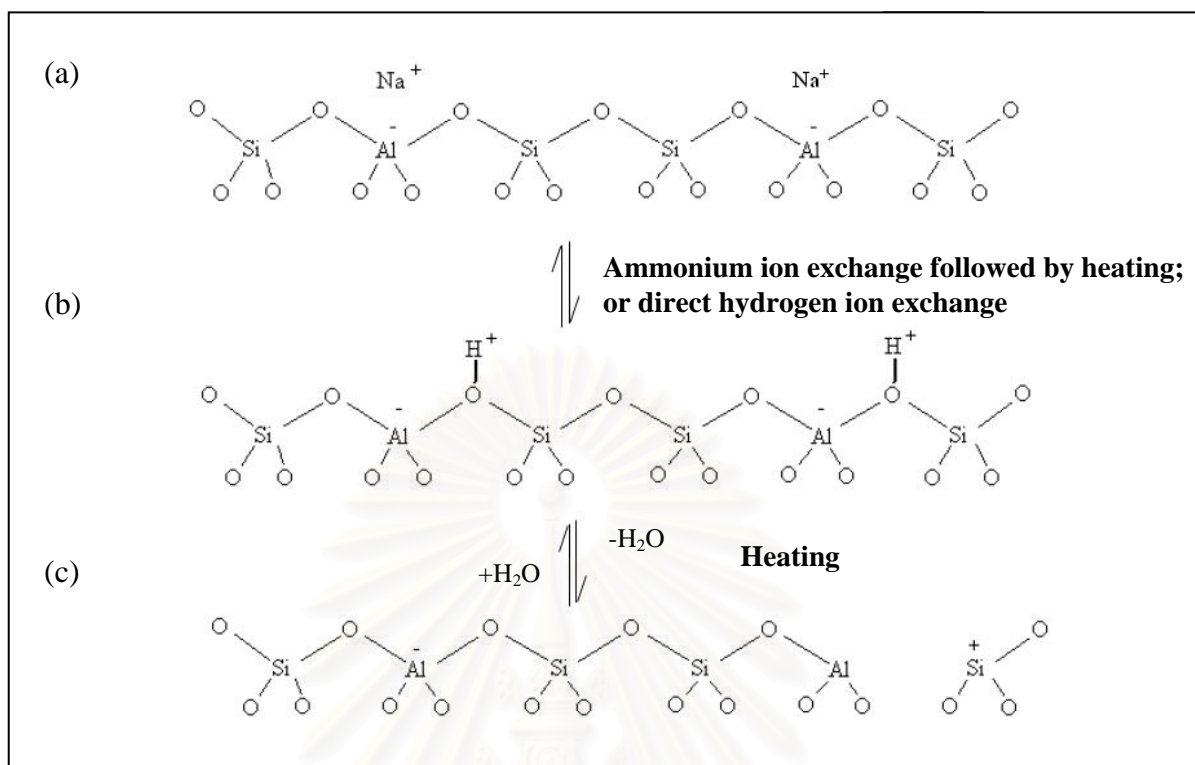
Figure 1.9 Acidities in zeolites. (a) calcined zeolite, (b) Brønsted-, and (c) Lewis acid.

1.4.4 Ion Exchange Properties of Zeolite ZSM-5

The cation exchange property of zeolite minerals was first observed more than 100 years ago. The cation exchange behavior of zeolites depends upon (1) the nature of the cation species, the cation size, and cation charge; (2) the temperature; (3) the concentration of the cation species in solution; (4) the anion species associated with the cation in solution; (5) the solvent; (6) the structural characteristic of the particular zeolite. Zeolite structures have unique features that lead to unusual types of cation selectivity and sieving.[4]

1.4.4.1 Basic Theory of Ion Exchange

Exchange between cation A^{Z_A}, initially in solution, and B^{Z_B}, initially in a zeolite, can be written as follows:

$$Z_B A^{Z_A} + Z_A \overline{B}^{Z_B} \quad \rightleftharpoons \quad Z_B \overline{A}^{Z_A} + Z_A B^{Z_B} \tag{1.2}$$
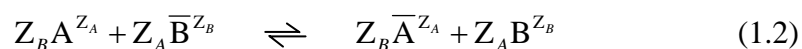
where $Z_{A,B}$ are the valencies of ions and the characters with a bar relate to a cation inside the zeolite crystal.[6]

1.5 Literature Review

1.5.1 Copper-Ion Exchanged ZSM-5

Iwamoto *et al.*[1,2] discovered the unique activity of copper-ion exchanged ZSM-5 (CuZSM-5) in nitrogen oxides (NO_x) direct decomposition to N_2 and O_2[1,2,13,14]. Trout *et al.*[3] reported that CuZSM-5 is the most active catalyst, many academics as well as industrial researchers have been engaged in the study of this catalyst from both environmental concerns and scientific interests.[1,2,3,15-20] Nitrogen oxides (NO_x) are unwanted byproducts from mobile and stationary sources of high-temperature combustion in the atmosphere. These are cause of acid rain and photochemical smog due to its detrimental impact on the environment.[21] Atmospheric emissions of nitrogen are predominantly in the form of gaseous compounds-oxidized nitrogen as nitric oxide (NO). Currently much of the NO emissions from combustion sources can be controlled by selective catalytic reduction (SCR)[23,24] as shown in Figure 1.10.
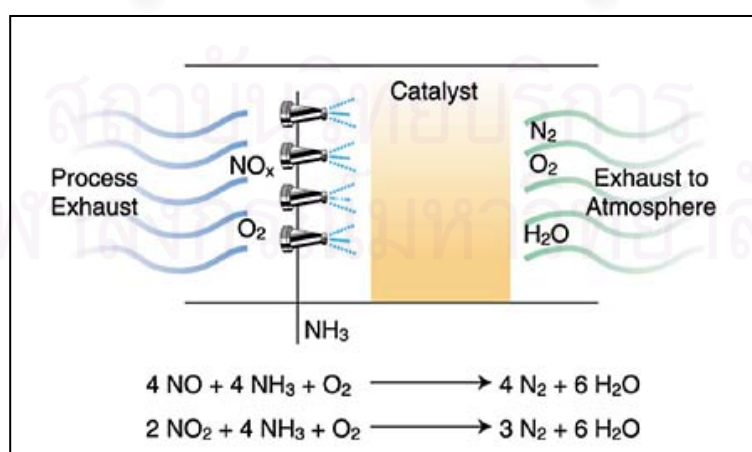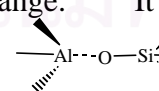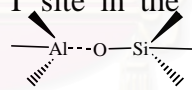
Figure 1.10 SCR process for remove nitrogen oxides (NO_x)[24]

In this process, NO is reduced in the presence of O_2 by NH_3 over titania-supported vanadia. While this technology is effective, the use of NH_3 as reductant is undesirable for number of reasons. First, large quantities of NH_3 must be stored either as liquid NH_3 or aqueous ammonia, raising the risk of release of a toxic compound. Second, the introduction of NH_3 to the SCR process must be carefully controlled to avoid NH_3 slippage into the effluent gases leaving the convertor. Third, the effluent NH_3 in the reactor can react with water and sulfur trioxide to produce ammonium sulfate with can deposit onto the surface of the heat exchanger thereby causing a reduction in heat transfer efficiency.[22] For all of these reasons, alternative for controlling NO emissions is using Copper ion exchange ZSM-5 catalyst. CuZSM-5 catalyst was obtained from a laboratory-synthesized sodium zeolite (NaZSM-5) by ionic exchange with a molar concentration ranging copper (II) acetate or copper (II) dichloride in aqueous solution that included pH and different Si/A1 ratio have been varied.[13,25,26] Other methods such as nitrogen adsorption, X-ray diffraction (XRD), scanning electron microscopy (SEM), energy-dispersive X-ray analysis (EDX), infrared spectroscopy (IR), thermal analysis (DTA-TG), temperature-programmed reduction (H_2-TPR), temperature-programmed desorption (TPD), and thermogravimetric measurements (TGA)[27] have provided indirect evidence concerning the oxidation state of copper (Cu) in CuZSM-5 zeolites.[25,26] Electron paramagnetic resonance (EPR) and X-ray absorption near-edge structure (XANES) investigations showed that all of the Cu in CuZSM-5 prepared by ion-exchange from aqueous solution is present as Cu^{2+}.[17,27] EPR spectroscopy has also been used to probe the structural environment of paramagnetic Cu^{2+} sites.[26] Particular interest has been focused on the Cu species oncoming in highly Cu- loaded ZSM-5, exhibiting the highest activity in NO decomposition. It has been assumed that the precursor of the active site is the $CuOH^+$ cation incorporated into the zeolite, which results in the copper overexchange.[26,29] It is believed that the Cu^{2+} cations are associated with isolated anionic $\;—Al\cdots O—Si—\;$ sites, and that the Cu^{2+} is present as $CuOH^+$. Infrared observations support this interpretation.[28] In rationalizing the redox chemistry of metal ions in zeolite cavities with widely spaced fixed negative charges, one should also keep in mind that Coulomb attraction between cations and the negative charges is favored by hydrolysis, *e.g.*

$$Cu^{2+} + H_2O \rightarrow Cu(OH)^+ + H^+ \tag{1.3}$$

as this process dissolves a (2+) charge into two (1+) charges which can each be positioned close to a negative charge of the zeolite matrix. The protons formed in reaction (Equation 1.2) can be detected by monitoring the IR band intensity of Si(OH)Al hydroxyl groups at 3610 cm^{-1}.[33] Protons also charge compensate these anionic sites[27] and the extent of Cu exchange is always less than the stoichiometric amount needed for a one-to-one correspondence between CuOH$^+$ species and anionic sites. Upon heating, as-exchanged CuZSM-5 undergoes autoreduction, a process in which a part of the Cu^{2+} is reduced to Cu$^+$ while, Larsen *et al.*[26] suggested formation of monovalent [CuO]$^+$ species obtained after dehydration of two CuOH$^+$ ions. In this paper easy reduction of the Cu ions adjacent to a single Al atom, leading Cu$^+$, is presented (see below).

$$[Cu^{II}OH]^+Z^- \rightleftharpoons Cu^IZ + \cdot OH$$

$$[Cu^{II}OH]^+Z^- + \cdot OH \rightleftharpoons [Cu^{II}O]^+Z^- + H_2O$$

$$\overline{2[Cu^{II}OH]^+Z^- \rightleftharpoons Cu^IZ + [Cu^{II}O]^+Z^- + H_2O} \tag{1.4}$$
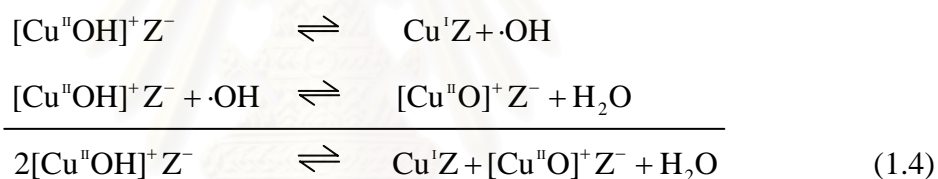
The symbol Z$^-$ represents an Al-substituted T site in the ZSM-5 zeolite, which is associated with a net negative charge, *i.e.*, $\overset{}{\underset{}{\text{Al}\cdots\text{O}\text{—Si}}}$. Isolated Cu^{2+} ions, oxocations such as [Cu-O-Cu]$^{2+}$, and CuO particles have been identified in CuZSM-5.[17,41] The oxocations [Cu-O-Cu]$^{2+}$ to get following reaction.[40]

$$Z^-CuOH^+Z^-CuOH^+ \rightarrow Z[Cu-O-Cu]^{2+}Z^- + H_2O \tag{1.5}$$
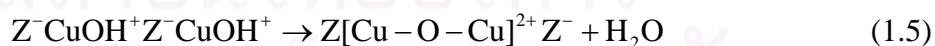
Lattice energy minimizations using interatomic potential functions early revealed that Cu$^+$ is coordinated to two oxygen atoms of the framework only, while Cu^{2+} has a coordination number of four or five.[42] The presence of Cu$^+$ cations in autoreduced CuZSM-5 has been observed directly by both XANES and fluorescence and indirectly by IR spectroscopy.[19, 29-31] The experimental results have suggested that the Cu$^+$ site is active for NO$_x$ decomposition in CuZSM-5.[32] The structure of the complex of NO$_2$

with a Cu^+ ion in the Zeolite is similar to the gas phase complex between NO_2 and naked Cu^+ ion, but the binding is much stronger.[3,43] A similar result has been obtained for the binding of NO.[39] The ability of the zeolite framework to 'activate' the Cu^+ ion for the binding of molecules seems to be the key for the catalytic activity. The extra binding results from partial $d^{10} \rightarrow d^9$ (sp) promotion which is facilitated by the strong electrostatic binding of the Cu^+ to the Zeolite framework.[39] For NO_x reduction over CuZSM-5, *in situ* XANES experiments show that the Cu^+ signal intensity correlates with the NO conversion[44] but which of the coexisting Cu species is reduced to Cu^+ is not clear.[33] Moreover, CuZSM-5 is studied by electron spin resonance (ESR) and electron spin echo modulation (ESEM) spectroscopies. It is found that in the hydrated zeolite the Cu^{2+} is octahedrally coordinated to six water molecules with the complex located at the intersection between two zeolitic channels.[35-39] We have begun a computational investigation of models $CuOH^+$ and Cu- complexes in water - ligand environments ($[Cu(H_2O)_n]$ n = 1-7) similar to what might be found in Cu-exchanged zeolites, with an initial emphasis on understanding the structure of $CuOH^+$ and Cu - water complexes in zeolite framework. However, the nature of the catalytically active site and the reaction mechanism were not understood in spite of active experimental research.

1.5.2 Structures and Stabilizations of Copper-Water Complexes

In part of structures and stabilizations of copper-water complexes, the copper-aqua complex has the 6-fold coordination with Jahn-Teller distorted octahedral (oct) structure. From accepted theory in the past, the most stable structure of copper-water complex is octahedral structure (oct)[73], yet in present this theory may not be correct because neutron diffraction experiment incorporating with the first principle Molecular Dynamics (MD) simulation suggested that the complex has 5-fold coordination with either square pyramid (spy) or trigonal bipyramid (tbp) structure.[74] While QM/MM MD simulation, on the other hand, confirmed the oct structure.[75] Therefore the structure of the complex should be reinvestigated. In this work, we performed calculations on possible structures of $[Cu(H_2O)_n]^{2+}$ for n=1-7 where their geometries were optimized and their energies were evaluated and compared. The

energies were calculated using quantum chemical calculations with various methods and basis sets.

1.6 The Objective of Study

1.6.1 Copper-Ion Exchanged ZSM-5

In this work, the suitable exchanged sites and the copper species in the cavity of ZSM-5 catalyst at high copper loading were studied. The natures of the active sites were determined by comparing configurations and exchanged energies of $CuOH^+$ in each exchanged site such as T6 T12, T8 T8, T7 T12 model 1 (M1T7 T18) and T7 T12 model 2 (M2T7 T12) for both one- and two- ion exchanged $CuOH^+$ in ZSM-5.

1.6.2 Structures and Stabilizations of Copper-Water Complexes

Find effect of stability and possible structures of $[Cu(H_2O)_n]^{2+}$ for n=1-7 by geometry optimized and compared their energies. The geometry optimization was performed at HF/6-31G(d,p) level. In addition, for each geometry single point energy calculations were carried out at MP2/6-31G(d,p) and B3LYP/6-31G(d,p). Moreover, for n=6 and 7, HF/6-31++G(d,p), HF/6-311G(d,p), and HF/6-311G(2df,p) were carried out for confirmed geometries of $[Cu(H_2O)_n]^{2+}$ complexes.

CHAPTER 2

THEORY

2.1 Background

A molecule may be considered as a set of positively charged nuclei surrounding by number of electrons. Roughly speaking, the Coulombic attraction between these two types of particle forms the basis for atoms and molecules.[45,46] The potential between two particles with charges q_i and q_j separated by a distance r_{ij} is given by

$$V_{ij} = V(r_{ij}) = \frac{q_i q_j}{r_{ij}}$$ (2.1)

Besides the interaction potential, an equation is also needed for describing the dynamics of the system, *i.e.* how the system evolves in time. In classical mechanic this is the Newton's second law

$$F = m\mathrm{a}$$
$$-\frac{dV}{dr} = m\frac{d^2r}{dt^2}$$ (2.2)

F is the force, **a** is the acceleration, r is the position vector and m the particle mass. Since electron is subatomic particles it cannot be described by classical mechanics. It displays both wave- and particle-like characteristics and can be described by wave function, Ψ.[45-47] The quantum mechanical equation corresponding to Newton's second law is the time dependent Shrödinger equation

$$\hat{H}\Psi = i\hbar\frac{\partial\Psi}{\partial t}$$ (2.3)

$\hat{H}$ is the Hamiltonian operator, $\hbar$ is Planks constant divided by 2π and i is the imaginary number. The simpler version of Equation 2.3 is the time-independent (or static) Schrödinger equation given by:

$$\hat{H}\Psi = E\Psi \tag{2.4}$$

For a general N particle system the Hamiltonian operator contains kinetic (T) and potential (V) operators for all particles.

$$\hat{H} = \text{T} + \text{V}$$

$$\text{T} = \sum_{i=1}^{N} \text{T}_i = -\sum_{i=1}^{N} \frac{\hbar^2}{2m_i}\nabla_i^2$$

$$\nabla_i^2 = \left(\frac{\partial^2}{\partial x_i^2} + \frac{\partial^2}{\partial y_i^2} + \frac{\partial^2}{\partial z_i^2} \right)$$

$$\text{V} = \sum_{i=1}^{N}\sum_{j \rangle 1} V_{ij} \tag{2.5}$$

The potential energy operator is the Coulomb potential (Equation 2.1). As nuclei are much heavier than electrons, their velocities are much smaller. The Schrödinger equation can therefore to a good approximation be separated into two parts, where one-part describes the electronic wave function for a fixed nuclear geometry, and another part describes the nuclear wave function. The energy from the electronic wave function plays the role of a potential energy. This separation is called *Born-Oppenheimer* approximation. The Born-Oppenheimer approximation is usually very good. For the hydrogen molecule the error is of the order of 10^{-4} a.u., and for systems with heavier nuclei, the approximation becomes better.[46]

Once the electronic Schrödinger equation has been solved for a large number of nuclear geometries (and possibly also for several electronic states) the *Potential Energy Surfaces* (PES) is known. This can then be used for solving the nuclear part of the Shrödinger equation. If there are N nuclei, there are $3N$ coordinates that define the geometry. Of these coordinates, three describe the overall translation of the molecule,

and three describe the overall rotation of the molecule with respect to three axes. For a linear molecule, only two coordinates are necessary for describing the rotation. This leaves 3N-6(5) coordinates to describe the internal movement of the nuclei, the vibrations, often chosen to be "vibration normal coordinates". It should be noted that nuclei are heavy enough for quantum effect to be almost negligible, they behave to a good approximation as classical particles.

The typical form of the Hamiltonian operator takes into account five contributions to the total energy of molecule; the kinetic energies of the electrons and nuclei, the attraction of the electrons to the nuclei, and the interelectronic and internuclear repulsions.[46] Casting the Hamiltonian into mathematical notation, we have

$$\hat{H} = -\sum_i \frac{\hbar^2}{2m_e}\nabla_i^2 - \sum_k \frac{\hbar^2}{2m_k}\nabla_k^2 - \sum_i\sum_k \frac{e^2 Z_k}{r_{ik}} + \sum_{i \langle j} \frac{e^2}{r_{ij}} + \sum_{k \langle l} \frac{e^2 Z_k Z_l}{r_{kl}}$$

$$= T_e + T_n + V_{ne} + V_{ee} + V_{nn} \tag{2.6}$$

where i and j run over electrons, k and l run over nuclei, m_e is the mass of the electron, m_k is the mass of nucleus k, e is the charge on the electron, Z is an atomic number, and r_{ab} is the distance between particles a and b.

Note that the Hamiltonian operator in (Equation 2.6) is composed of kinetic energy and potential energy where T_e denotes electronic kinetic, T_n denotes nuclear kinetic, V_{ne} denotes nuclear-electron attraction, V_{ee} denotes electron-electron repulsion and V_{nn} nuclear-nuclear repulsion.

Applying the Born- Oppenheimer approximation (Equation 2.6) is written as

$$\hat{H} = \hat{H}_{nu} + \hat{H}_{elec} \tag{2.7}$$

where $\hat{H}_{elec}$ is electronic Hamiltonian

$$\hat{H}_{elec} = -\sum_i \frac{\hbar^2}{2m_e}\nabla_i^2 - \sum_i\sum_k \frac{e^2 Z_k}{r_{ik}} + \sum_{i \langle j} \frac{e^2}{r_{ij}} \tag{2.8}$$

and $\hat{H}_{nu}$ is nuclear Hamiltonian. Thus,

$$
\begin{aligned}
\hat{H} &= -\sum_k \frac{\hbar^2}{2m_k}\nabla_k^2 + \left\langle -\sum_i \frac{\hbar^2}{2m_e}\nabla_i^2 - \sum_i\sum_k \frac{e^2 Z_k}{r_{ik}} + \sum_{i\langle j} \frac{e^2}{r_{ij}} \right\rangle + \sum_{k\langle l} \frac{e^2 Z_k Z_l}{r_{kl}} \\
&= -\sum_k \frac{\hbar^2}{2m_k}\nabla_k^2 + E_{\text{elec}}\left(\{r_k\}\right) + \sum_{k\langle l} \frac{e^2 Z_k Z_l}{r_{kl}} \\
&= -\sum_k \frac{\hbar^2}{2m_k}\nabla_k^2 + E_{\text{tot}}\left(\{r_k\}\right)
\end{aligned}
\tag{2.9}
$$

If the electronic Schrödinger equation $\left(H_{\text{ele}}\Psi_{\text{ele}} = \varepsilon\Psi\right)$ is solved, the nuclear Schrödinger equation can also be solved. However, even for the simplest molecular system the electronic Schrödinger equation can still not be solved exactly. Additional approximation is needed.

2.2 Spatial Orbitals and Spin Orbitals

We define an orbital as a wave function for a single particle, an electron. Because we are concerned with molecular electronic structure we will be using molecular orbitals for the wave functions of the electrons in a molecule. A spatial orbital $\psi_i(\mathbf{r})$, is a function of the position vector $\mathbf{r}$ and describes the spatial distribution of an electron such that $|\psi_i(\mathbf{r})|^2 d\mathbf{r}$ is the probability of finding the electron in the small volume element $d\mathbf{r}$ surrounding $\mathbf{r}$. Spatial molecular orbitals will usually be assumed to form an orthonormal set

$$
\int d\mathbf{r}\, \psi_i^*(\mathbf{r})\psi_j(\mathbf{r}) = \delta_{ij}
\tag{2.10}
$$

If the set of spatial orbitals $\{\psi_i\}$ were complete, then any arbitrary function $f(\mathbf{r})$ could be exactly expanded as

$$
f(\mathbf{r}) = \sum_{i=1}^{\infty} a_i\psi_i(\mathbf{r})
\tag{2.11}
$$

The wave function for an electron that describes both its spatial distribution and its spin is a spin orbital, $\chi(\mathrm{x})$, where x indicates both space and spin coordinates.[47]

$$\chi(\mathrm{x}) = \begin{cases} \psi(\mathrm{r})\alpha(\omega) \\ \text{or} \\ \psi(\mathrm{r})\beta(\omega) \end{cases} \tag{2.12}$$

2.3 The Hartree-Fock Approximation

The Hartree-Fock approximation constitutes the first step towards more accurate approximations.[47] The simplest antisymmetric wave function, which can be used to describe to ground state of an *N*-electron system, is a single Slater determinant,[51]

$$\Psi_0 = \left| \chi_1 \chi_2 \cdots \chi_N \right\rangle \tag{2.13}$$

where $\chi_i(\mathrm{r}_i, \omega_i)$ is the spin orbital which depends on spatial coordinate r and spin function ω. The variation principle states that the best wave function of this functional form (Equation 2.14) is the one which gives the lowest possible energy. The energy of this wave function, expressed in term of the set of spin orbitals $\{\chi_i | i = 1, 2, \ldots, N\}$, is given by (Equation 2.15),

$$E_0 = \left\langle \Psi_0 \left| \hat{H} \right| \Psi_0 \right\rangle \tag{2.14}$$

$$E_0 = \sum_i^N (i|h|i) + \frac{1}{2}\sum_i^N \sum_j^N (ii|jj) - (ij|ji) \tag{2.15}$$

For a closed-shell system, the wave function (Equation 2.13) contains $N/2$ spin orbitals with α spin function and $N/2$ spin orbitals with β spin fuction (Equation 2.15) can be written as

$$E_0 = 2\sum_{i}^{N/2}(i|h|i) + \sum_{ab}^{N/2}2(ii|jj) - (ij|ji) \qquad (2.16)$$

First, consider the one-electron terms

$$(i|h|i) = h_{ii} = \int dr\,\psi_i^*(\mathbf{r}_1)(-\frac{1}{2}\nabla_1^2 - \sum_{k=1}^{M}\frac{Z_k}{r_{1k}})\psi_i(\mathbf{r}_1) \qquad (2.17).$$

Thus h_{ii} is the average kinetic and nuclear attraction energy of an electron described by the wave function $\psi_i(\mathbf{r}_1)$. Next consider the two-electron integral

$$(ii|jj) = \int dr_1 dr_2 |\psi_i(\mathbf{r}_1)|^2 \frac{1}{r_{12}} |\psi_j(\mathbf{r}_2)|^2 \qquad (2.18)$$

which is the classical coulomb repulsion between the charge clouds $|\psi_i(\mathbf{r}_1)|^2$ and $|\psi_j(\mathbf{r}_2)|^2$. Thus, this integral is called a *coulomb* integral and is denoted by

$$J_{ij} = (ii|jj) = \langle ij|ij \rangle \qquad (2.19).$$

Finally, consider the two-electron integral

$$(ij|ji) = \int dr_1 dr_2 \psi_i^*(\mathbf{r}_1)\psi_j(\mathbf{r}_1)\frac{1}{r_{12}}\psi_j^*(\mathbf{r}_2)\psi_i(\mathbf{r}_2) \qquad (2.20).$$

This integral does not have classical interpretation. It is called an *exchange* integral and is denoted by

$$K_{ij} = (ij|ji) = \langle ij|ji \rangle \qquad (2.21)$$

Both exchange and coulomb integrals have positive values. Rewrite the Hartree-Fock energy of a closed-shell system in terms of coulomb and exchange integrals, we obtained

$$E_0 = 2\sum_a h_{ii} + \sum_{ij} 2J_{ij} - K_{ij} \qquad (2.22)$$

The variational flexibility in the wave function (Equation 2.13) is in the choice of spin orbitals. By minimizing E_0 with respect to the choice of spin orbitals, one can derive an equation, called the Hartree-Fock equation, which determines the optimal spin orbitals. The Hartree-Fock equation is an equation of the form

$$f(i)\chi(\mathrm{x}_i) = \varepsilon\chi(\mathrm{x}_i) \qquad (2.23)$$

where $f(i)$ is an effective one-electron operator, called the Fock operator. The Fock operator has the form

$$f(i) = -\frac{1}{2}\nabla_i^2 - \sum_{k=1}^{M}\frac{Z_k}{r_{ik}} + v^{\mathrm{HF}}(i) \qquad (2.24)$$

where $v^{\mathrm{HF}}(i)$ is the average potential experienced by the ith electron due to the presence of the other electrons. The essence of the Hartree-Fock approximation is to replace the complicated many electron problem by a one-electron problem in which electron-electron repulsion is treated in an average way. The procedure for solving the Hartree-Fock equation is called the self-consistent field (SCF) method.[47]

The basic idea of the SCF method is simple. By making an initial guess at the spin orbitals, one can calculate the average field (*i.e.*, v^{HF}) seen by each electron and then solve the eigenvalue equation (Equation 2.23) for a new set of spin orbitals. Using these new spin orbitals, one can obtain new fields and repeat the procedure until self-consistency is reached (*i.e.*, until the fields no longer change and the spin orbitals used to construct the Fock operator are the same as its eigenfunctions), as in Figure 2.1.
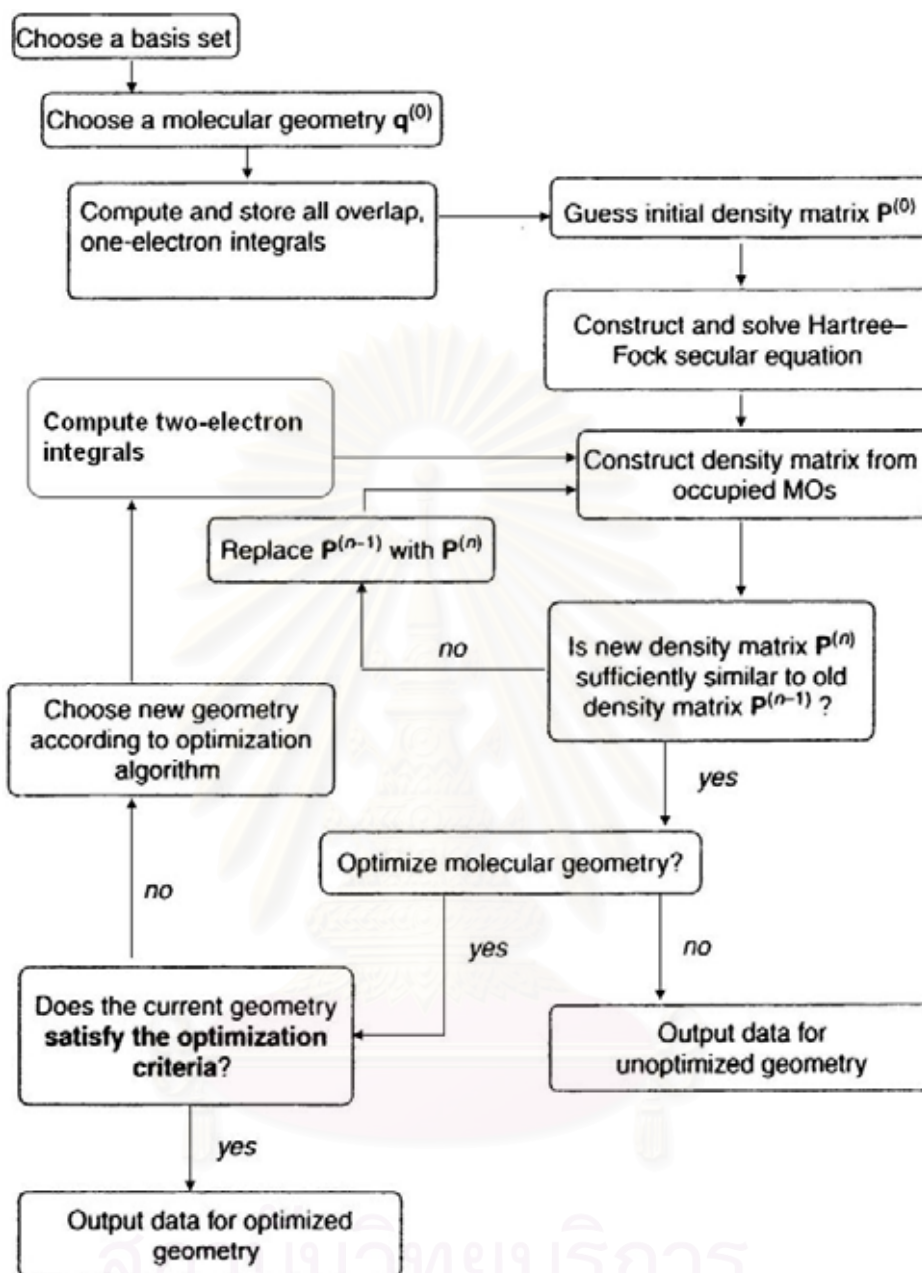
Figure 2.1 Flow chart of the HF SCF procedure. Note that data for an unoptimized geometry is referred to as deriving from a so-called 'single-point calculation'.[46]

The solution of the Hartree-Fock eigenvalue problem (Equation 2.23) yields a set $\{\chi_k\}$ of orthonormal Hartree-Fock spin orbitals with orbital energies $\{\varepsilon_k\}$. The N spin orbitals with the lowest energies are called the occupied or hole spin orbitals. The

Slater determinant formed from these orbitals is the Hartree-Fock ground state wave function and is the best variational approximation to the ground state of the system, of the single determinant form.

The Hartree-Fock equation can also be solved by introducing a finite set of spatial basis functions $\{\phi_\mu(r)|\mu=1,2,\ldots,K\}$. The spatial parts of the spin orbitals with the α and β spin function can then be expanded in terms of the known set of functions $\{\phi_\mu\}$ by using a basis set of K spatial functions $\{\phi_\mu\}$ leads to a set of $2K$ spin orbitals (K with α spin K and with β spin).

$$\psi_i = \sum_{i=1}^{2K} C_{\mu_i}\phi_\mu \tag{2.25}$$

2.3.1 The Restricted and Unrestricted Hartree-Fock Models

The Hartree-Fock solution is usually characterized by having doubly occupied spatial orbitals, *i.e.*, two spin orbitals χ_p and χ_q share the same spatial orbital $\psi_i(\text{r})$ connected with an α and a β spin function, respectively and have the same orbital energy. If we impose this double occupancy right from the start, we arrive at the *restricted* Hartree-Fock (RHF) approximation. Situations where the RHF picture is inadequate are provided by any system containing unpair electron or open shell. There are two possibilities for how one can treat such species within the Hartree-Fock approximation. Either we stay as closely as possible to the RHF picture and doubly occupy all spatial orbitals with pair electron and singly occupy all spatial orbital with unpair electron notion of doubly occupied spatial orbitals and allow each spin orbital to have its own spatial part. The former is the *restricted open shell* HF scheme (ROHF) while the latter is *unrestricted* Hartree-Fock variant (UHF). In UHF the α and β orbitals do not share the same effective potential but experience different potentials, $v^{\text{HF}}{}_\alpha$ and $v^{\text{HF}}{}_\beta$. As a consequence, the α- and β- orbitals differ in their spatial characteristics and have different orbital energies, as in Figure 2.3.
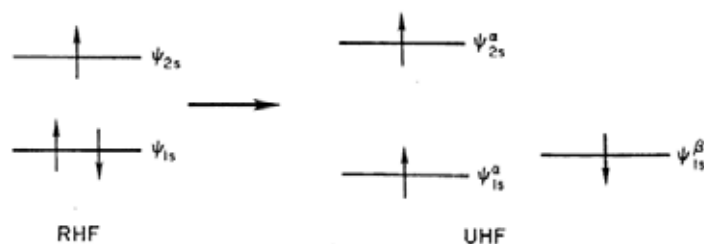
Figure 2.2 Relaxation of a restricted single determinant to an unrestricted single determinant.[47]

The UHF scheme affords equations that are much simpler than their ROHF counterparts. Particularly, the ROHF wave function is usually composed not of a single Slater determinant, but corresponds to a limited linear combination of a few determinants where the expansion coefficients are determined by the symmetry of the state. On the other hand, in the UHF scheme we are always dealing with single-determinants wave functions. However, the major disadvantage of the UHF technique is that unlike the true and also the ROHF wave function, a UHF slater determinant is no longer an eigenfunction of the total spin operator, $\hat{S}^2$. The more the $\left\langle \hat{S}^2 \right\rangle$, expectation value of $\hat{S}^2$ operator, deviates from the correct value -*i.e.*, $S(S+1)$ where S is the spin quantum number representing the total spin of the system- the more this unrestricted determinant is contaminated by functions corresponding to states of higher spin multiplicity and the less physically meaningful it obviously gets.

2.3.2 Electron Correlation

The difference between Hartree-Fock energy (E_0) and the exact ground state energy (E_{exact}) from the Born-Oppenheimer approximation and neglecting relativistic is following Löwdin[50], 1959, called the *correlation energy*

$$E_C^{HF} = E_{\text{exact}} - E_0 \tag{2.26}$$

E_C^{HF} is a negative quantity because E_0 and $E_{exact} < 0$ and $|E_{excat}| > |E_0|$. It is a measure for the error introduced through the HF scheme. Electron correlation is mainly caused by the instantaneous repulsion of the electrons, which is not covered by the effective HF potential. Pictorially speaking, the electron get often too close to each other in the Hartree-Fock scheme, because the electrostatic interaction is treated in only an average manner. As a consequence, the electron-electron repulsion term is too large resulting in E_0 being above E_{exact}. This part of the correlation energy is directly connected to the $1/r_{12}$ term controlling the electron-electron repulsion in the Hamitonian and is obviously the larger the smaller the distance r_{12} between electrons 1 and 2 is. It is usually called *dynamical* electron correlation because it is related to the actual movements of the individual electrons and is known to be a short range effect. The second main contribution to E_C^{HF} is the non-dynamical or static correlation. It is related to the fact that in certain circumstances the ground state Slater determinant is not a good approximation to the true ground state, because there are other Slater determinants with comparable energies. A typical example is provided by one of the famous laboratories of quantum chemistry, the H_2 molecule. The correlation error, which is almost exclusively due to dynamical correlation is small and amounts to only 0.04 E_h. However, as we stretch the bond the correlation gets larger and in the limit of very large distances converges to some 0.25 E_h as evident from Figure 2.3, which displays the computed (RHF and UHF) as well as the exact potential curves for the ground state of the hydrogen molecule.[49]

Obviously, this cannot be dynamical correlation because at $R_{H-H} \to \infty$ we have two independent hydrogen atoms with only one electron at each center and no electron-electron interaction whatsoever (because $1/R_{H-H} \to 0$).
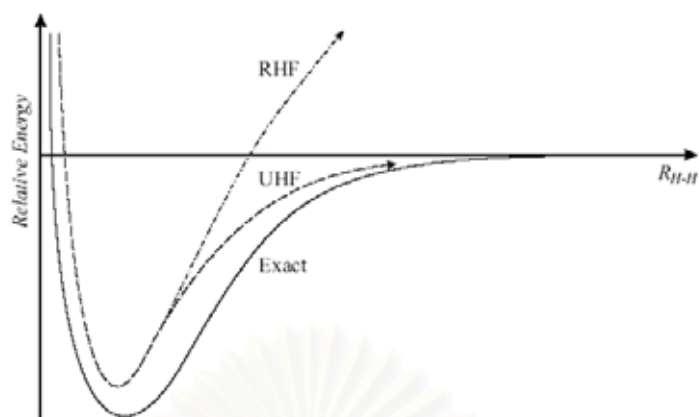
Figure 2.3 Potential curves for H_2.[49]

Unlike the dynamical correlation discussed before, these non-dynamical contributions are a long range effect and become the more important the more the bond is stretched (Cook and Karplus, 1987).[69] However, we also see from Figure 2.5 that using the unrestricted (UHF) scheme rather than RHF cures the problem. At a *H-H* distance of some 1.24Å an unrestricted solution lower than the RHF one appears and develops into a reasonable potential curve. However, resulting UHF wave function no longer resembles the H_2 singlet ground state. At large internuclear distances it actually converges to a physically unreasonable 1:1 mixture between a singlet ($S=0$, hence $S(S+1)=0$) and a triplet ($S=1$, hence $S(S+1)=2$) as indicate by the expectation value of the $\hat{S}^2$ operator, $\left\langle \hat{S}^2 \right\rangle = 1$. The correct energy emerges because the UHF wave function breaks the inversion symmetry inherent to a homonuclear diatomic such as H_2 and localizes one electron with spin down at one nucleus and the second one with opposite spin at the other nucleus.[47]

Finally, we want to point out that E_C^{HF} is not restricted to the direct contributions connected to the electron-electron interaction. As this quantity measures the difference between the expectation value of $\hat{H}$ with a Slater determinant $\left\langle \Psi | T + V_{ne} + V_{ee} | \Psi \right\rangle$ and the correct energy obtained from the true wave function Ψ_0, it should come as no surprise that there are also correlation contributions due to the kinetic energy or even the nuclear-electron term. If, for example, the average distance between the electrons

is too small at the Hartree-Fock level, this automatically will lead to a kinetic energy that is too large and nuclear-electron attraction which is too small (*i.e.*, too strong).

2.4 Density Functional Theory

Density functional theory (DFT) is an approach to the electronic structure of atoms and molecules which has enjoyed a dramatic surge of interest since the late 1980s and 1990s. In Hartree-Fock theory the many-electron wavefunction is expressed as a Slater determinant[51] which is constructed from a set of *N* single-electron wavefunction (*N* begin the number of electrons in the molecule). DFT also considers single-electron functions. However, whereas Hartree-Fock theory does indeed calculate the full *N*- electron wavefunction, density functional theory only attempts to calculate the total electronic energy and the overall electronic density distribution. The central idea underpinning DFT is that there is a relationship between the total electronic energy and the overall electronic density. This is not a particularly new idea; indeed an approximate model developed in the late 1920s (the Thomas-Fermi model)[52] contains some of the basic elements. However, the real break through came with a paper by Hohenberg and Kohn[55]in 1964, who showed that the ground-state energy and other properties of a system were uniquely defined by the electron density.[46,49,54]

2.4.1 Density Functions

For one-electron wave function, $\psi^2(\mathrm{r},\omega)d\tau d\omega$ give the chance of finding the electron in the spatial volume element $d\tau$ with spin coordinate between ω and $\omega + d\omega$.

For a many-electron system with wave function $\Psi(\mathrm{r}_1,\omega_1,\mathrm{r}_2,\omega_2,\ldots,\mathrm{r}_n\omega_n)$ then

$$\left|\Psi(\mathrm{r}_1,\omega_1,\mathrm{r}_2,\omega_2,\ldots,\mathrm{r}_n,\omega_n)\right|^2 d\tau_1 d\omega_1 d\tau_2 d\omega_2 \ldots d\tau_n d\omega_n \qquad (2.27)$$

gives the probability of finding simultaneously electron 1 in $d\tau_1 d\omega_1$, electron 2 in $d\tau_2 d\omega_2$,…, electron n in $d\tau_n d\omega_n$. The probability that electron 1 is in $d\tau_1 d\omega_1$ with other electrons anywhere is found by averaging over the remaining electrons.

$$\int(\cdots\int \left|\Psi(r_1,\omega_1,r_2,\omega_2,\ldots,r_n,\omega_n)\right|^2 d\tau_2 d\omega_2 \ldots d\tau_n d\omega_n) d\tau_1 d\omega_1 \qquad (2.28)$$

and, because electrons are indistinguishable, the probability must be the same for all electrons. We therefore define the *one-electron density function* as

$$\rho_1(r_1,\omega_1) = n(\int\cdots\int \left|\Psi(r_1,\omega_1,r_2,\omega_2,\ldots,r_n\omega_n)\right|^2 d\tau_2 d\omega_2 \cdots d\tau_n d\omega_n) \qquad (2.29)$$

The two-electron density function is

$$\rho_2(r_1,\omega_1,r_2,\omega_2) = n(n-1)(\int\cdots\int \left|\Psi(r_1,\omega_1,r_2,\omega_2,\ldots,r_n\omega_n)\right|^2 d\tau_3 d\omega_3 \cdots d\tau_n d\omega_n) \qquad (2.30)$$

which is related to the probability that any two electrons will be found simultaneously at point r_1,ω_1 and r_2,ω_2.

For every electron wave function that is an eigenfunction of the electron spin operator $\hat{S}^2$, the one-electron density function always comprises an α^2 spin part and a β^2 spin part, with no cross-term involving $\alpha\beta$.

$$\rho_1(r_1,\omega_2) = P^\alpha(r_1)\alpha^2(\omega_1) + P^\beta(r_1)\beta^2(\omega_1) \qquad (2.31)$$

The electron densities for α spin electrons and for β spin electrons are always equal in a singlet spin state, but in non-singlet spin states the densities may be different, giving a resultant spin density. If we evaluate the spin density function at the position of certain nuclei, it gives a value proportional to the isotropic hyperfine coupling constant that can be measured from electron spin resonance experiments.

2.4.2 The Hohenberg-Kohn Theorem

Hohenberg and Kohn's 1964 paper[55] was widely regarded by physicists, but its true importance in chemistry has only become apparent during the last decade or so. Density functional theory has become an increasingly important topic in chemistry. This culminated in the award of a half-part of the 1998 Chemistry Nobel Prize to Walter Kohn.[48]

Theorem 1

The electron density $\rho(\mathrm{r})$ determines the external potential. Suppose there are two external potentials $v_1(\mathrm{r})$ and $v_2(\mathrm{r})$ arising from the same electron density $\rho(\mathrm{r})$. There will be two Hamiltonians $\hat{H}_1$ and $\hat{H}_2$ with the same electron density with different wave functions Ψ_1 and Ψ_2. If E_1 and E_2 are the ground-state energies for $\hat{H}_1$ and $\hat{H}_2$ respectively, then

$$E_1 < \int \Psi_2^* \hat{H}_1 \Psi_2 d\tau \tag{2.32}$$

that can rearrange the right-hand side as follows:

$$\int \Psi_2^* \hat{H}_1 \Psi_2 d\tau = \int \Psi_2^* \hat{H}_2 \Psi_2 d\tau + \int \Psi_2^* (\hat{H}_1 - \hat{H}_2) \Psi_2 d\tau \tag{2.33}$$

which gives

$$E_1 < E_2 + \int \rho(\mathrm{r})[v_1(\mathrm{r}) - v_2(\mathrm{r})] d\tau \tag{2.34}$$

The above argument can be repeated with subscripts interchanged to give

$$E_2 < E_1 + \int \rho(\mathrm{r})[v_2(\mathrm{r}) - v_1(\mathrm{r})] d\tau \tag{2.35}$$

Addition of these two inequalities, (Equation 2.34 and 2.35), gives

$$E_1 + E_2 < E_2 + E_1 \qquad (2.36)$$

which is a contradiction.

Thus $v(\mathrm{r})$ is a unique function of the electron density; since $v(\mathrm{r})$ fixes the Hamiltonian we see that the full many-particle ground state is a unique functional of the electron density. Note that the theorem is restricted to electronic ground states. Therefore, the energy functional is given by

$$E(\rho(\mathrm{r})) = \int v(\mathrm{r})\rho(\mathrm{r})d\tau + F_{\mathrm{HK}}[\rho(\mathrm{r})]d\tau \qquad (2.37)$$
$$= V_{\mathrm{ne}}[\rho] + F_{\mathrm{HK}}[\rho]$$

where F_{HK} is Hohenberg-Kohn function.

Theorem 2

The second theorem proves by Hohenberg and Kohn in their 1964 contribution.[55] In plain words, this theorem states that $F_{\mathrm{HK}}[\rho(\mathrm{r})]$, the functional that delivers the ground state energy of the system, delivers the lowest energy if and only if the input density is the true ground state density, ρ. Thus,

$$E[\rho] < E[\tilde{\rho}] = T[\tilde{\rho}] + V[\tilde{\rho}] + U[\tilde{\rho}] \qquad (2.38)$$
$$= T[\tilde{\rho}] + V_{\mathrm{ne}}[\tilde{\rho}] + V_{\mathrm{ee}}[\tilde{\rho}]$$

$E(\tilde{\rho}(\mathrm{r}))$ assume its minimum value for the correct $\rho(\mathrm{r})$, if the admissible functions $\rho(\mathrm{r})$ satisfy the condition

$$\int \rho(\mathrm{r})d\tau = n \qquad (2.39)$$

where n is the number of electrons. Any approximate density $\tilde{\rho}(\mathrm{r})$, by theorem 1, determines the Hamiltonian and wave function $\tilde{\Psi}$. Using this wave function in the variational expression we obtain

$$E[\tilde{\rho}(\mathrm{r})] = \int \rho(\mathrm{r})\tilde{\rho}(\mathrm{r})d\tau + F_{\mathrm{HK}}[\tilde{\rho}] \qquad (2.40)$$
$$= \int \tilde{\Psi}^* \hat{H} \tilde{\Psi} d\tau \geq E[\rho(\mathrm{r})]$$

The main problem relating to practical applications of the Hohenberg and Kohn theorems are existence theorem and do not give us any clues as to calculation of the quantities involved.

2.4.3 The Kohn-Sham Equations

Kohn-Sham[53] provided a way to calculation (Equation 2.40). For non-interacting system,

$$E[\rho] = F_{HK}[\rho] + \int \rho(\mathrm{r})v(\mathrm{r})d\mathrm{r} \qquad (2.41)$$
$$= T_{\mathrm{S}}[\rho] + \int \rho(\mathrm{r})v(\mathrm{r})d\mathrm{r}$$

Applying non-interacting wave function $\psi_{\mathrm{S}} = \prod_{i=1}^{n} \phi_i$

$$T_{\mathrm{S}}[\rho] = \sum_i \left\langle \phi_i^{\mathrm{KS}} \left| -\frac{1}{2}\nabla_i^2 \right| \phi_i^{\mathrm{KS}} \right\rangle \qquad (2.42)$$

For interacting system,

$$E[\rho] = T_{\mathrm{S}}[\rho] + V_{\mathrm{ne}}[\rho] + J[\rho] + (T[\rho] + V_{\mathrm{ee}}[\rho] - T_{\mathrm{S}}[\rho] - J[\rho] \qquad (2.43)$$
$$= T_{\mathrm{S}}[\rho] + V_{\mathrm{ne}}[\rho] + J[\rho] + E_{\mathrm{XC}}[\rho]$$

$\left| \phi_i^{KS} \right\rangle$ is Kohn-Sham orbital which can be obtained from the Kohn-Sham equation.

$$ f^{KS}(i)\chi(\mathrm{x}_i) = \varepsilon\chi(\mathrm{x}_i) \tag{2.44} $$

which the one-electron Kohn and Sham operator f^{KS} defined as

$$ f^{KS} = -\frac{1}{2}\nabla^2 - \sum_{k=1}^{M}\frac{Z_k}{r_{ik}} + \int\frac{\rho(\mathrm{r}')}{\left|\mathrm{r}_i - \mathrm{r}'\right|}dr' + V_{XC} \tag{2.45} $$

$$ V_{XC} = \frac{\delta E_{XC}}{\delta\rho} $$

V_{XC} is a so-called functional derivative.

The Kohn-Sham equations look like standard HF equations, except that the exchange term is replaced with an exchange-correlation potential whose form is unknown. E_{XC}, to so-called exchange-correlation energy, contains not only the non-classical effects of self-interaction correction, exchange and correlation, which are contributions to the potential energy of the system, but also a portion belonging to the kinetic energy.[45,46,48,49]

2.4.4 The Local Density and Local Spin-Density Approximations

There is no systematic way in which the exchange correlation functional $V_{xc}[\rho]$ can be systematically improved. Starting from a model for which there is an exact solution, the uniform electron gas, E_{XC} can be written in the following form

$$ E_{XC}^{LDA}[\rho] = \int \rho(\mathrm{r})\varepsilon_{XC}(\rho(\mathrm{r}))d\mathrm{r} \tag{2.46} $$

Here, $\varepsilon_{XC}(\rho(\mathrm{r}))$ is the exchange-correlation energy per particle of a uniform electron gas of density $\rho(\mathrm{r})$. This energy per particle is weighted with the probability that there is in fact an electron at this position in space. Writing E_{XC} in this way defines

the *local density approximation*, LDA for short.[49] The quantity $\varepsilon_{XC}(\rho(\text{r}))$ can be further split into exchange and correlation contributions,

$$\varepsilon_{XC}(\rho(\text{r})) = \varepsilon_X(\rho(\text{r})) + \varepsilon_C(\rho(\text{r})) \tag{2.47}$$

The exchange part, ε_X, which represents the exchange energy of an electron in a uniform electron gas of a particular density is, apart from the pre-factor, equal to the form found by Slater in his approximation of the Hartree-Fock exchange and was originally derived by Bloch[56] and Dirac[57] in the late 1920's

$$\varepsilon_X = -\frac{3}{4}\sqrt[3]{\frac{3\rho(\text{r})}{\pi}} \tag{2.48}$$

On the basis of these results various authors have presented analytical expressions of ε_C based on sophisticated interpolation schemes. The most widely used representations of ε_C are the ones developed by Vosko, Wilk, and Nusair, 1980,[58] while the most recent and probably also most accurate one has been given by Perdew and Wang, 1992.[59] The common short hand notation for the former implementations of the correlation functional is VWN. Hence, instead of the abbreviation LDA, which defines the model of the local density approximation, one frequently finds the acronym SVWN to identify the particular functional. For open-shell situations with an unequal number of α and β electrons, functionals of the two spin densities consistently lead to more accurate results. But also for certain situations with an even number of electrons, such as the H_2 molecule at larger separation, the unrestricted functionals perform significantly better because they allow symmetry breaking. Up to this point the local density approximation was introduced as a functional depending solely on $\rho(\text{r})$. If we extend the LDA to the unrestricted case, we arrive at the *local spin-density approximation*, or LSDA. Formally, the two approximations differ only that instead of Equation 2.53 we now write

$$E_{XC}^{LSD}[\rho_\alpha, \rho_\beta] = \int \rho(r)\varepsilon_{XC}(\rho_\alpha(r)\rho_\beta(r))dr \qquad (2.49)$$

Just as for the simple, spin compensated situation where $\rho_\alpha(r) = \rho_\beta(r) = 1/2\rho(r)$, there are related expressions for the exchange and correlation energies per particle of the uniform electron gas characterized by $\rho_\alpha(r) \neq \rho_\beta(r)$ the so-called spin polarized case. The degree of spin polarization is often measured through the spin-polarization parameter

$$\xi = \frac{\rho_\alpha(r) - \rho_\beta(r)}{\rho(r)} \qquad (2.50)$$

ξ attains values from 0 (spin compensated) to 1 (fully spin polarized, *i. e.*, all electrons have only one kind of spin). In the following we do not differentiate between the local and the local spin-density approximation and use the abbreviation LDA for both, unless otherwise noted.

In general case of an open-shell atom or molecule. At a certain position r in this system we have the corresponding spin densities $\rho_\alpha(r)$ and $\rho_\beta(r)$. In the local spin-density approximation we now take these densities and insert them into (Equation 2.49) obtaining $E_{XC}(r)$. Thus, we associate with the densities $\rho_\alpha(r)$ and $\rho_\beta(r)$ the exchange and correlation energies and potentials that a homogeneous electron gas of equal, but constant density and the same spin polarization ξ would have. This is now repeated for each point in space and the individual contributions are integrated as schematically indicated in Figure 2.4. Obviously, this approximation hinges on the assumption that the exchange-correlation potentials depend only on the *local* values of $\rho_\alpha(r)$ and $\rho_\beta(r)$.
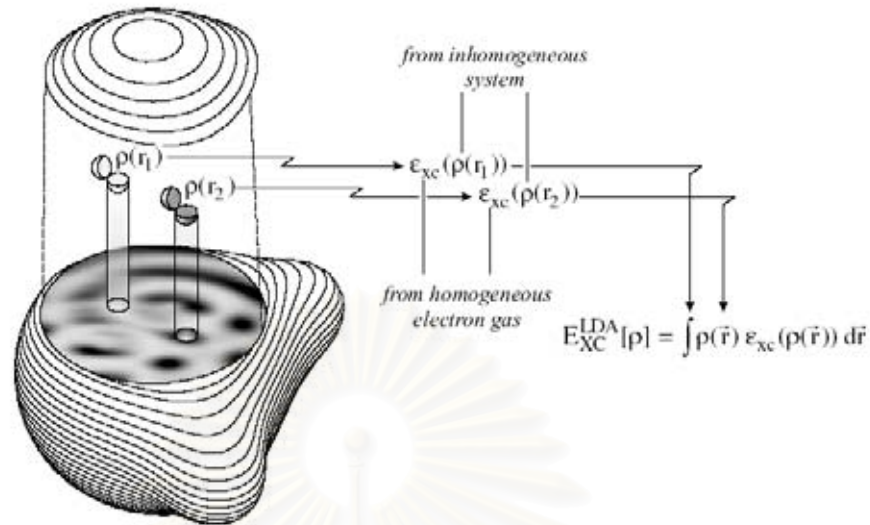
Figure 2.4 The local density approximation.[49]

2.4.5 The Generalized Gradient Approximation

The situation changed significantly in the early eighties when the first successful extensions to the purely local approximation were developed. The logical first step in that direction was the suggestion of using not only the information about the density $\rho(r)$ at a particular point r, but to supplement the density with information about the *gradient* of the charge density, $\nabla\rho(r)$ in order to account for the non-homogeneity of the true electron density. In other words, we interpret the local density approximation as the first term of a Taylor expansion of the uniform density and expect to obtain better approximations of the exchange-correlation functional by extending the series with the next lowest term. Thus we arrive at (with σ and σ' indicating α or β spin)

$$E_{XC}^{GEA}[\rho_\alpha, \rho_\beta] = \int \rho \varepsilon_{XC}(\rho_\alpha, \rho_\beta) d\mathbf{r} + \sum_{\sigma,\sigma'} \int C_{XC}^{\sigma,\sigma'}(\rho_\alpha, \rho_\beta) \frac{\nabla \rho_\sigma}{\rho_\sigma^{2/3}} \frac{\nabla \rho_{\sigma'}}{\rho_{\sigma'}^{2/3}} d\mathbf{r} + \dots \qquad (2.51)$$

This form of functional is termed the *gradient expansion approximation* (GEA) and it

can be shown that it applies to a model system where the density is not uniform but very slowly varying. Functionals include the gradients of the charge density and where the hole constraints have been restored in the above manner are collectively known as *generalized gradient approximations* (GGA).[49] These functionals are the workhorses of current density functional theory and can be generically written as

$$E_{XC}^{GGA}[\rho_\alpha, \rho_\beta] = \int f(\rho_\alpha, \rho_\beta, \nabla\rho_\alpha, \nabla\rho_\beta) d\mathbf{r} \qquad (2.52)$$

In practice, E_{XC}^{GGA} is usually split into its exchange and correlation contributions

$$E_{XC}^{GGA} = E_X^{GGA} + E_C^{GGA} \qquad (2.53)$$

and approximations for the two terms are sought individually. In fact, some of these functionals are not even based on any physical model. In other words, the actual form of E_X^{GGA} and E_C^{GGA} usually does not assist the understanding of the physics these functionals try to describe. This underlines the pragmatic character so typical for approximate density functional theory in general. We rewrite the exchange part of E_{XC}^{GGA} as

$$E_X^{GGA} = E_X^{LDA} - \sum_\sigma \int F(s_\sigma) \rho_\sigma^{4/3}(\mathbf{r}) d\mathbf{r} \qquad (2.54)$$

The argument of the function F is the *reduced density gradient* for spin σ

$$s_\sigma(\mathbf{r}) = \frac{|\nabla\rho_\sigma(\mathbf{r})|}{\rho_\sigma^{4/3}(\mathbf{r})} \qquad (2.55)$$

s_σ is to be understood as a local inhomogeneity parameter. It assumes large values not only for large gradients, but also in regions of small densities, such as the exponential tails far from the nuclei. Likewise, small values of s_σ occur for small gradients, typical

for bonding regions, but also for regions of large density. For example, the combination of large density gradients and large densities close to the nuclei typically leads to values of s_σ in this region which are in between the reduced density gradients in the bonding and tail regions, respectively. Of course, the homogeneous electron gas is characterized by $s_\sigma = 0$ everywhere. Finally, a word on why we divide by the 4/3 power of ρ and not just by ρ itself. This is needed to make s_σ a dimensionless quantity: the dimension of the density is the inverse dimension of volume and hence $[r]^{-3}$. Its gradient has therefore dimensions of $[r]^{-4}$. But this is just the same dimension that $\rho^{4/3}$ has, because of $([r]^{-3})^{4/3} = [r]^{-4}$ and we arrive at the desired dimensionless reduced gradient.

For the function F two main classes of realizations, the first one is based on a GGA exchange functional developed by Becke, 1988b.[60] As outlined above, this functional is abbreviated simply as B (sometimes one also finds B88)

$$F^B = \frac{\beta s_\sigma^2}{1 + 6\beta s_\sigma \sinh^{-1} s\sigma} \tag{2.56}$$

β is an empirical parameter that was determined to 0.0042 by a least-squares fit to the exactly known exchange energies of the rare gas atoms He through Rn. In addition to the sum rules, this functional was designed to recover the exchange energy density asymptotically far from a finite system.

The second class of GGA exchange functionals use for F a rational function of the reduced density gradient. Prominent representatives are the early functionals by Becke[61], 1986 (B86) and Perdew[62], 1986 (P), the functional by Lacks and Gordon, 1993 (LG) or the recent implementation of Perdew, Burke, and Ernzerhof, 1996 (PBE).[63] As an example, we explicitly write down F of Perdew's 1986 exchange functional, which, just as for the more recent PBE functional, is free of semiempirical parameters:

$$F^{P86} = \left(1 + 1.296\left(\frac{s_\sigma}{(24\pi^2)^{1/3}}\right)^2 + 14\left(\frac{s_\sigma}{(24\pi^2)^{1/3}}\right)^4 + 0.2\left(\frac{s_\sigma}{(24\pi^2)^{1/3}}\right)^6\right)^{1/15} \qquad (2.57)$$

Among the most widely used choices is the correlation counterpart of the 1986 Perdew exchange functional, usually termed P or P86. This functional employs an empirical parameter, which was fitted to the correlation energy of the neon atom. A few years later Perdew and Wang[62], 1991, refined their correlation functional, leading to the parameter free PW91. Another, nowadays even more popular correlation functional is due to Lee, Yang, and Parr[64], 1988 (LYP). Unlike all the other functionals mentioned so far, LYP is not based on the uniform electron gas but is derived from an expression for the correlation energy of the helium atom based on an accurate, correlated wave function presented in the context of wave function based theory by Colle and Salvetti, 1975.[65] The LYP functional contains one empirical parameter. It differs from the other GGA functionals in that it contains some local components.

In principle, each exchange functional could be combined with any of the correlation functionals, but only a few combinations are currently in use. The exchange part is almost exclusively chosen to be Becke's functional which is either combined with Perdew's 1986 correlation functional or the Lee, Yang, Parr usually abbreviated as BP86 and BLYP, respectively. Sometimes also the PW91 correlation functional is employed, corresponding to BPW91. To be fair, all these flavors of gradient-corrected KS-density functional theory deliver results of similar quality as demonstrated by several studies which assess the performance of these functional.

2.4.6 Hybrid Functionals

Hybrid exchange-correlation functions are now widely used. The straightforward and seemingly most appropriate strategy for arriving at a most accurate exchange-correlation energy seems to be to use the exact exchange energy and rely on approximate functionals only for the part missing in the HF picture, *i. e.*, the electron correlation,

$$E_{\text{XC}} = E_{\text{X}}^{\text{exact}} + E_{\text{C}}^{\text{KS}} \qquad (2.58)$$

In the adiabatic connection, the exchange-correlation potential energy is integrated over the λ-dependent, which is nothing else than the nonclassical contribution to the electron-electron interaction for different values of λ (note that E_{nu}^{λ} corresponds to the pure potential energy contributions, dependent on λ. Only the integration over λ introduces the kinetic energy part into E_{XC})

$$E_{\text{XC}} = \int_{0}^{1} E_{\text{nu}}^{\lambda} d\lambda \qquad (2.59)$$

Let us explore first the nature of the integrand E_{nu}^{λ} for the limiting cases. At λ = 0 we are dealing with an interaction free system, and the only component which is not included in the classical term is due to the antisymmetry of the fermion wave function. On the other hand, for λ = 1, the non-classical contributions are those of the fully interacting system, containing exchange as well as electron correlation parts. This interacting exchange-correlation energy is not known, but can be approximated – more or less satisfactorily – by any E_{XC} functional. The simplest approximation to solve Equation 2.60 is to assume that E_{nu}^{λ} is a linear function in λ. This leads to

$$E_{\text{XC}}^{\text{HH}} = \frac{1}{2} E_{\text{XC}}^{\lambda=0} + \frac{1}{2} E_{\text{XC}}^{\lambda=1} \qquad (2.60)$$

and corresponds to the situation shown schematically in Figure 2.5a. Using the LDA exchange- correlation functional for $E_{\text{XC}}^{\lambda=1}$, Equation 2.60 represents the so-called *half-and half* (HH) combination of 'exact' exchange and density functional exchange-correlation as introduced by Becke, 1993a.
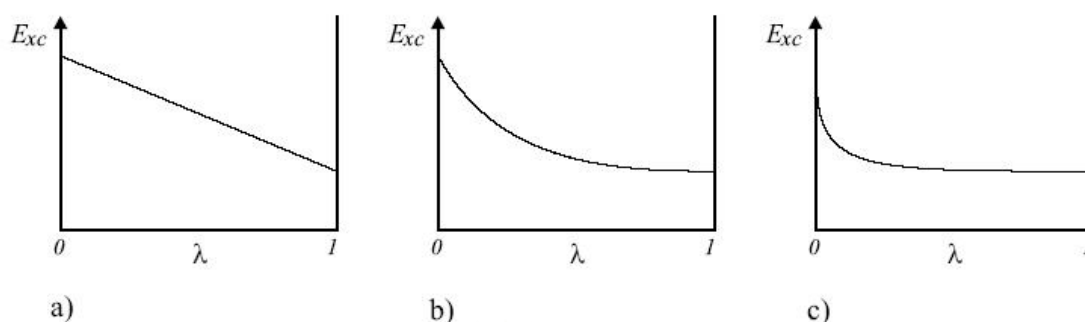
Figure 2.5 λ-dependence of E_{XC}.[49]

Hence, the amount of exact exchange was reduced relative to the earlier half-and-half scheme, indicative of a large slope of $E_{XC}^{\lambda=0}$, see Figure 2.5b. Of course one should keep in mind that the parameters a, b, and c were fitted to exactly these data and it is a priori completely unclear whether a similarly good performance can also be expected in general. Functionals of this sort, where a certain amount of exact exchange is incorporated are frequently called DFT/HF *hybrid* functionals, because they represent a hybrid between pure density functionals for exchange and exact Hartree-Fock exchange. They are also sometimes referred to as ACM functionals, where the acronym stands for *adiabatic connection method.*

Currently, the most popular hybrid functional is known as B3LYP and was suggested by Stephens *et al.*[66], 1994. The B3LYP exchange-correlation energy expression is

$$E_{XC}^{B3LYP} = (1-a)E_X^{LSD} + aE_{XC}^{\lambda=0} + bE_X^{B88} + cE_C^{LYP} + (1-c)E_C^{LSDA} \tag{2.61}$$

In particular the B3LYP functional is the most popular and most widely used functional. This amazing success was fueled by the surprisingly good performance B3LYP and related functionals demonstrated in many chemical applications, including such difficult areas as open-shell transition-metal chemistry

2.5 Basis Set

A basis set is a set of functions used to describe the shape of the orbitals in an atom. Molecular orbitals and all wave functions are created by taking linear combinations of basis functions and angular functions.[49] The basis functions should have large amplitude in regions of space where the electron probability density is also large, and small amplitudes where the probability density is small. There are two guidelines for choosing the basis functions. One is that they should have a behavior which agrees with the physics of the problem; this ensures that convergence as more basis functions are added is reasonably rapid. The second guideline is practical: the chosen functions should make it easy to calculate all the required integrals.

The orbitals χ_i which are expressed through the $\{\eta_\mu\}$ are used to construct the approximate wave function. It has long been recognized that very large basis sets are needed if high quality wave functions that take also into account electron correlation are the target. In particular, basis functions with complex nodal structures (polarization functions) are necessary and in highly correlated calculations the basis set requirements soon lead to computationally very demanding procedures. On the other hand, in the Kohn-Sham scheme the orbitals play an indirect role and are introduced only as a tool to construct the charge density according to

$$\rho(\mathbf{r}) = \sum_i^N |\varphi_i(\mathbf{r})|^2 \qquad (2.62)$$

One should therefore expect that the basis set requirements in Kohn-Sham calculations are less severe than in wave function based ones. In conventional wave function based approaches, such as the Hartree-Fock or configuration-interaction schemes, the set $\{\eta_\mu\}$ is almost universally chosen to consist of so-called cartesian *Gaussian-type-orbitals*, GTO of the general form

$$\eta^{\text{GTO}} = N x^l y^m z^n \exp\left[-\alpha \mathbf{r}^2\right] \qquad (2.63)$$

N is a normalization factor which ensures that $\langle \eta_\mu | \eta_\mu \rangle = 1$ (but note that the η_μ are not orthogonal, *i.e.*, $\langle \eta_\mu | \eta_\nu \rangle \neq 0$ for $\mu \neq \nu$). α represents the orbital exponent which determines how compact (large α) or diffuse (small α) the resulting function is. $L = l + m + n$ is used to classify the GTO as s-functions ($L = 0$), p-functions ($L = 1$), d-function ($L = 2$), etc. Note, however that for $L > 1$ the number of cartesian GTO functions exceeds the number of $(2l + 1)$ physical functions of angular momentum l. For example, among the six cartesian functions with $L = 2$, one is spherically symmetric and is therefore not a d-type but an s-type functions. Similarly the ten cartesian $L = 3$ functions include an unwanted set of three p-type functions.

The preference for GTO basis functions in HF and related methods is motivated by the computational advantages these functions offer, because very efficient algorithms exist for analytically calculating the huge number of four-center-two-electron integrals occurring in the Coulomb and HF- exchange terms. On the other hand, from a physical point of view, *Slater-type-orbitals* (STO) seem to be the natural choice for basis functions.[47,49] They are simple exponentials that mimic the exact eiganfunctions of the hydrogen atom. Unlike the GTO functions, Slater-type-orbitals exhibit the correct cusp behavior at $r \to 0$ with a discontinuous derivative (while a GTO has a slope of zero at $r \to 0$) and the desired exponential decay in the tail regions as $r \to \infty$ (GTO fall off rapidly). A typical STO is expressed as

$$\eta^{STO} = N r^{n-1} \exp[-\zeta r] Y_{lm}(\Theta, \phi) \tag{2.64}$$

Here, n corresponds to the principal quantum number, the orbital exponent is termed ζ and Y_{lm} are the usual spherical harmonics that describe the angular part of the function. In fact as a rule of thumb one usually needs about three times as many GTO than STO functions to achieve a certain accuracy. Unfortunately, many-center integrals are notoriously difficult to compute with STO basis sets so we employ contracted GTO basis sets, in which several primitive Gaussian Functions (typically between three and six linear combination to give one *contracted Gaussian function* (CGF)

$$\eta_{\tau}^{\text{CGF}} = \sum_{a}^{A} d_{a\tau} \eta_{a}^{\text{GTO}} \qquad (2.65)$$

The original motivation for contracting was that the contraction coefficients $d_{s\tau}$ can be chosen in a way that the CGF resembles as much as possible a single STO function.

We should also mention that basis sets which do not actually comply with the LCAO scheme are employed under certain circumstances in density functional calculations, *i.e.*, *plane waves*. These are the solutions of the Schrödinger equation of a free particle and are simple exponential functions of the general form

$$\eta^{\text{PW}} = \exp[i k \mathbf{r}] \qquad (2.66)$$

where the vector k is related to the momentum p of the wave through $p = \hbar k$. Plane waves are not centered at the nuclei but extend throughout the complete space. They enjoy great popularity in solid state physics for which they are particularly adapted because they implicitly involve the concept of periodic boundary conditions. Unfortunately, the number of plane waves needed to arrive at an acceptable accuracy is usually daunting at best and for this and other reasons applications employing plane wave basis sets are very rare in molecular quantum chemistry.

Irrespective of whether we use Gaussian functions, Slater type exponentials of numerical sets, certain categories of functions that can help to characterize the quality of a basis set have become customary in quantum chemistry. The simplest and least accurate expansion of the molecular orbitals utilizes only one basis function (or one contracted function in the case of CGF sets) for each atomic orbital up to and including the valence orbitals. These basis set are for obvious reasons called *minimal sets*. A typical representative is the STO-3G basis set. For carbon, this basis set consists of five functions, one each describing the 1s and 2s atomic orbitals and three functions for the 2p shell (p_x, p_y, and p_z). One should expect no more than only qualitative results from minimal sets and nowadays they are hardly used anymore. The next level of sophistication is the *double-zeta* basis sets. Here, the set of functions is doubled, *i.e.*,

there are two functions for each orbital (the generic name 'double-zeta' for such basis set still points to the beginnings of computational quantum chemistry, when STO functions were in use, where the orbital exponent is called Zeta(ζ). If we take into account that it is in the valence space where change in the electronic wave function occur during chemical processes, we can limit the double set of functions to the valence orbitals, while the chemically mostly inert core electrons are still treated in a minimum set. This defines the *split-valence* type sets. Typical examples are the 3-21G or 6-31G Gaussian basis set developed by Pople and coworkers.[67] In most applications, such basis sets are augmented by *polarization functions*, *i.e.*, functions of higher angular momentum than those occupied in the atom, *e.g.*, p-functions for hydrogen or d-functions for the first row elements. Polarization functions have by definition more angular nodal planes than the occupied atomic orbitals and thus ensure that the orbitals can distort from their original atomic symmetry and better adapt to the molecular environment. Polarized double-zeta or split valence basis set are the mainstay of routine quantum chemical applications since usually they offer a balanced compromise between accuracy and efficiency. In terms of CGF type basis sets, typical examples are the standard 6-31G(d,p) sets of Hehre, Ditchfield, and Pople[68], 1972, and Hariharan and Pople, 1973, or the more recent SVP (split-valence polarization) sets of Schäfer, Horn, and Ahlrichs, 1992. Equivalents consisting of two STO functions per atomic orbital or two numerical functions are of comparable importance in their respective domains. In the latter case the doubing of the numerical functions can be achieved, for example, by adding numerically generated atomic orbitals from calculations only doubly or even higher positively charged ions.

It is obvious how these schemes can be extended by increasing the number of functions in the various categories. This results in triplet- or quadruple-zeta basis sets which are augmented by several sets of polarization functions including functions of even higher angular momentum.

The exponents and contraction coefficient of most Gaussian basis sets have been optimized within the Hartree-Fock or correlated wave function based schemes. In the beginning it was not at all clear whether one could in fact use basis sets that were optimized for representing molecular orbitals in a HF or configuration interaction context to construct the density, as in the Kohn-Sham scheme. However, it fortunately

turned out that the results are fairly insensitive with respect to the way the exponents and contraction coefficients have been determined, in particular for the calculation of properties such as energies or equilibrium geometries. Hence, in general it is probably not necessary to use basis sets explicitly optimized for a density functional approach, even though there are a number of special cases where this statement is an oversimplification. Nevertheless, most modern applications of Kohn-Sham density functional theory using Gaussian functions simply employ one of the many standard basis sets, irrespective of their origin in wave function based approaches. In most contemporary program packages the popular sets are provided in an internal basis set library. Should the desired set not be included in that internal library of the program chosen, it can usually be conveniently downloaded even in the appropriate input format from the web-site http://www.emsl.pnl.gov:2080/forms/basisform.html (Feller, Schuchardt, and Jones, 1998).[49]

CHAPTER 3

DETAILS OF THE CALCULATIONS

3.1 Preparation of Structures of ZSM-5

Starting geometries of ZSM-5 (MFI) have been taken from Molecular Dynamics (MD) simulations of the MFI type structure when 2 Si atoms were replaced by 2 Al atoms (Si/Al ratio=47). Acidic protons associated to the substitution were also added to balance excess charges. The MFI structure was taken for library and Al substitutions were carried out using Crystal Builder program, in Cerius2 package.[70] Table 3.1 shows all possible di-substituted MFI. There are totally 23 possible of such substitutions[9] which create ZSM-5 with Si/Al of 47. The location of such substitutions in ZSM-5 is illustrated in Figure 3.1.

Table 3.1 Investigated all Al substitution sites of 23 Al configurations[7,9] as shown in Figure 3.1.

Al Substitution sites			
1) T11 T11	7) T3 T3	13) T3 T9	19) T2 T5
2) T8 T8	8) T7 T9	14) T6 T12	20) T4 T10
3) T6 T6	9) T7 T9	15) T4 T4	21) T4 T4
4) T5 T5	10) T7 T12	16) T9 T10	22) T9 T12
5) T1 T1	11) T7 T12	17) T7 T12	23) T5 T12
6) T2 T2	12) T1 T7	18) T1 T6	
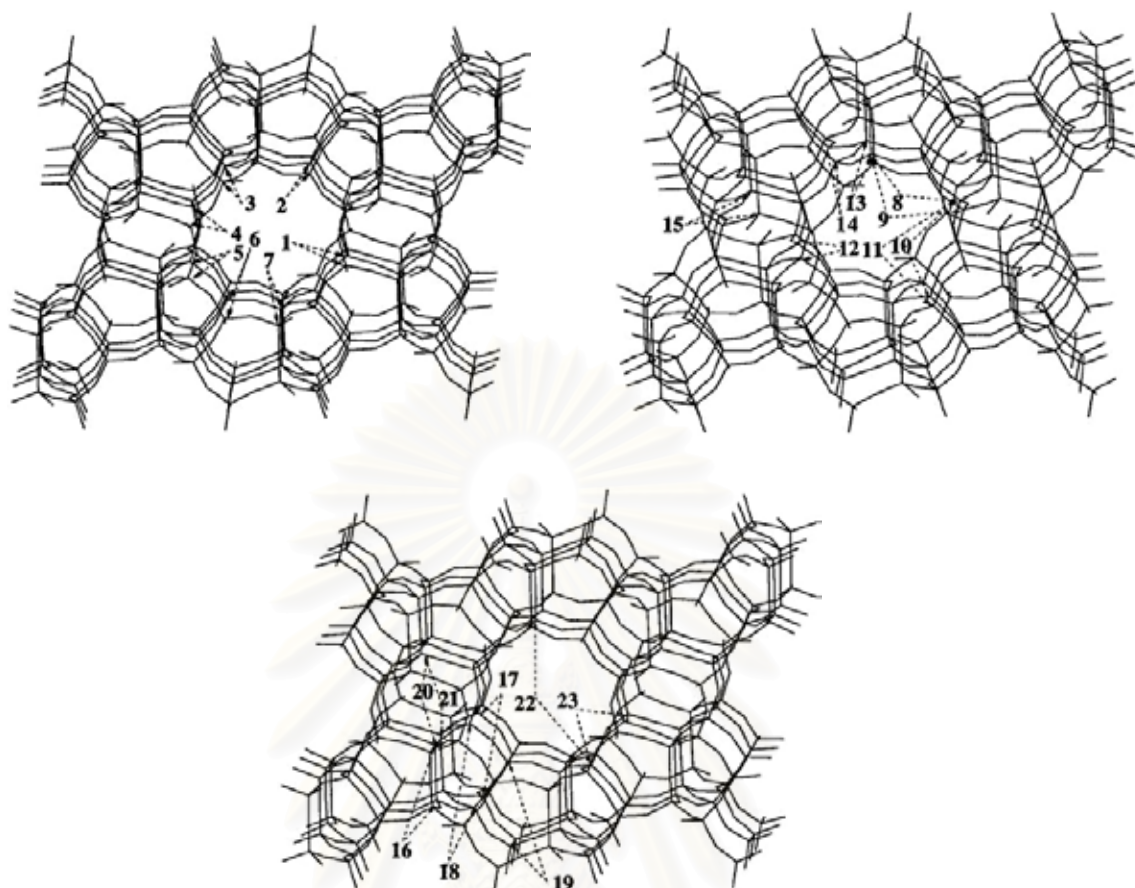
Figure 3.1 Al substitution sites of 23 Al configurations.[9]

However, only 4 Al substitution sites or "exchanged sites" were studied, *i.e.* T6 T12, T8 T8, T7 T12 model 1 (M1T7 T12) and T7 T12 model 2 (M2T7 T12). These 4 sites were selected because they represent exchanged sites in the cavity of the straight channel. Particularly, the site T12 is at the intersection between straight and sinusoidal channels. Illustrations of these exchanged sites were given in Figure 3.2. The MD simulations were carried out using CVFF force field with NVT ensemble setting temperature at 300 K. The simulation runtime is set to 2000 ps or until equilibrium was reached where time step of 0.1 fs was applied. The MD simulations were not done in this work but taken from study by Mr. Ukrid Poompub.[72]
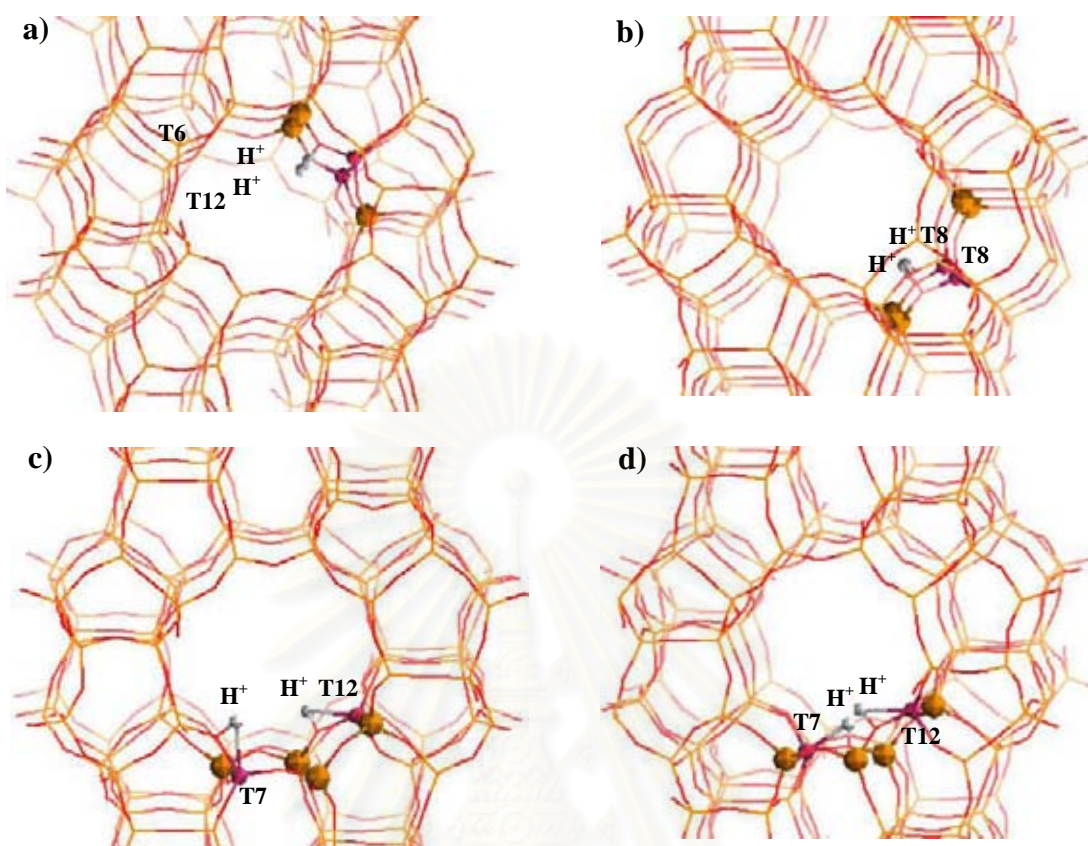
Figure 3.2 Exchanged sites at a) T6 T12, b) T8 T8, c) M1T7 T12, and d) M2T7 T12
used in this study.

3.2 Preparation of Cluster Models of CuZSM-5

The geometries of ZSM-5 zeolite with different Al substitutions from MD
simulations were used to prepare cluster models of ZSM-5. Five- or six-T ring
representing the exchanged sites was chosen as the cluster model. The edge of cluster
(Si-O bond) was then saturated with H atoms. The position of H^+, O-H bond lengths,
and T-O-H bond angles were optimized using B3LYP/6-31G(d,p) while other
geometrical parameters were frozen. All O-H bond lengths and $\angle$T-O-H bond angles
were set as one parameter for bond length and another one parameter for bond angle.
Geometry optimizations were performed using the Gaussian98 program.[71] Schematic
representations of cluster models are shown in Figure 3.3.
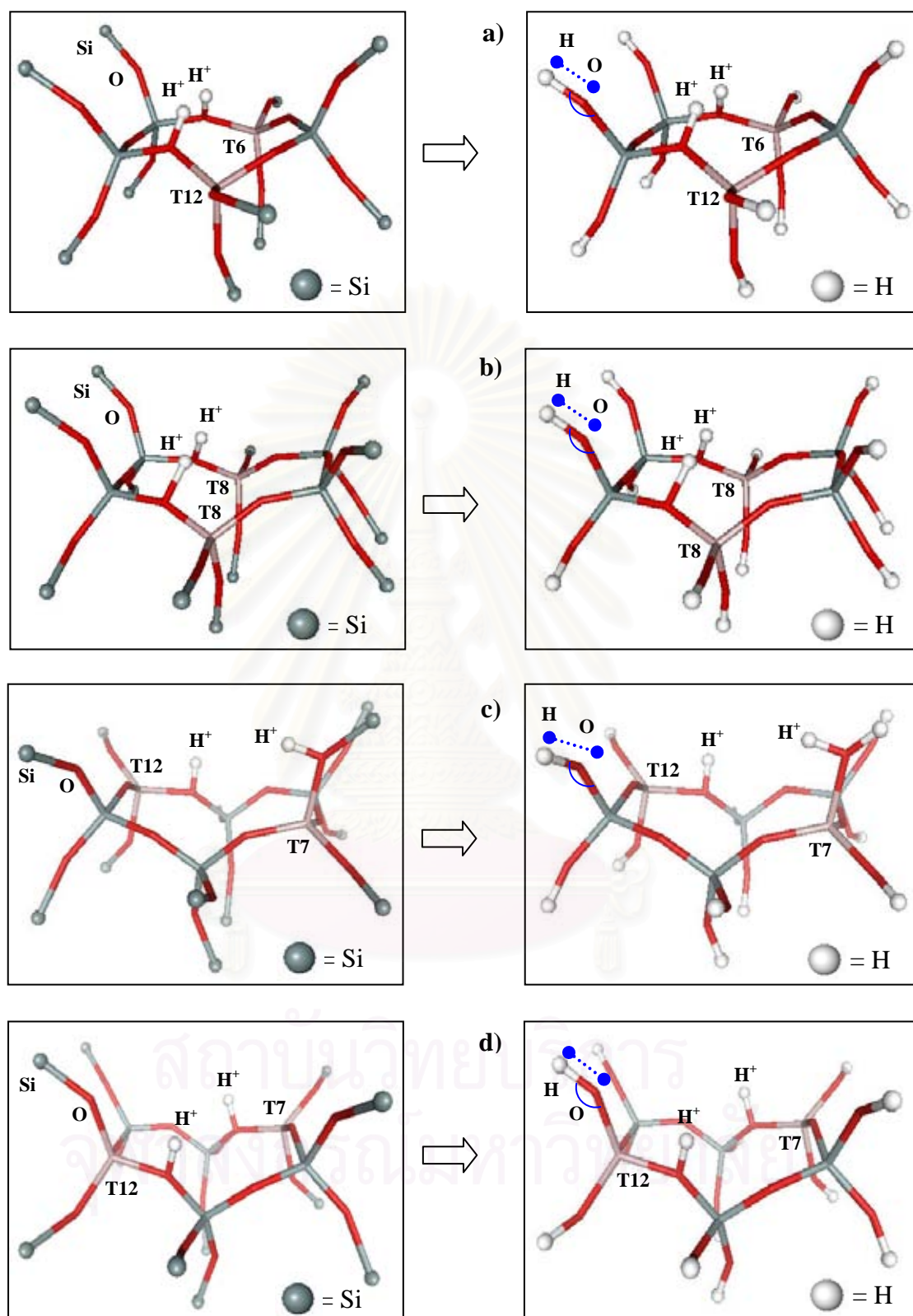
Figure 3.3 Cluster models cut from ZSM-5 structure after saturated with H at the edge
(Si-O) of a) T6 T12, b) T8 T8, c) M1T7 T12, and d) M2T7 T12.

After obtained optimized geometries for each ZSM-5 cluster model, structures of CuZSM-5 were prepared. Cluster models of CuZSM-5 are classified into two groups, one- and two-ion exchanged CuZSM-5. $CuOH^+$ was added to the model replacing H^+ in ZSM-5 cluster models. Positions of H^+ and $CuOH^+$ as well as geometries of $CuOH^+$ were optimized using B3LYP/6-31G(d,p) (while ZSM-5's framework was fixed). Schematic representations for all one- and two-ion exchanged CuZSM-5 being studied are shown in Figure 3.4.
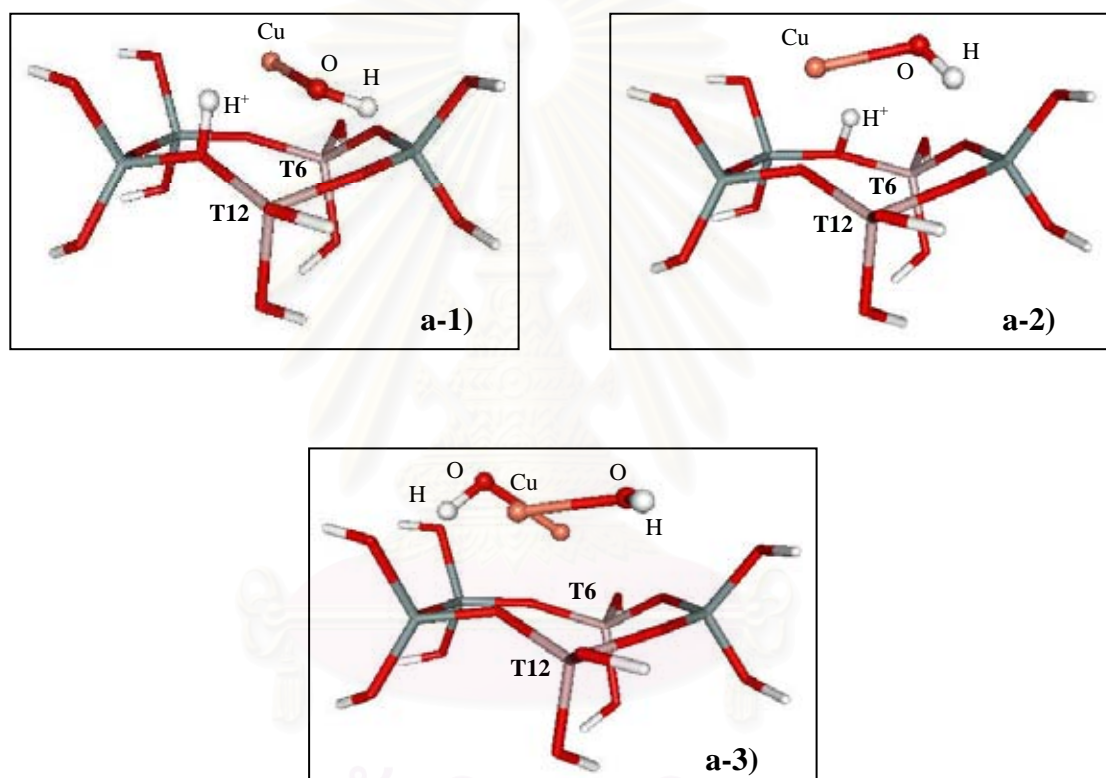
Figure 3.4 Cluster models of single- and double-proton exchanged CuZSM-5 at T6 T12 a-1) $T6CuOH^+$ $T12H^+$, a-2) $T6H^+$ $T12CuOH^+$, and a-3) $T6CuOH^+$ $T12CuOH^+$, at T8 T8 b-1) $T8CuOH^+$ $T8H^+$, b-2) $T8H^+$ $T8CuOH^+$, and b-3) $T8CuOH^+$ $T8CuOH^+$, at M1T7 T12 c-1) $M1T7CuOH^+$ $T12H^+$, c-2) $M1T7H^+$ $T12CuOH^+$, and c-3) $M1T7CuOH^+$ $T12CuOH^+$, and at M2T7 T12 d-1) $M2T7CuOH^+$ $T12H^+$, d-2) $M2T7H^+$ $T12CuOH^+$, and d-3) $M2T7CuOH^+$ $T12CuOH^+$, respectively.
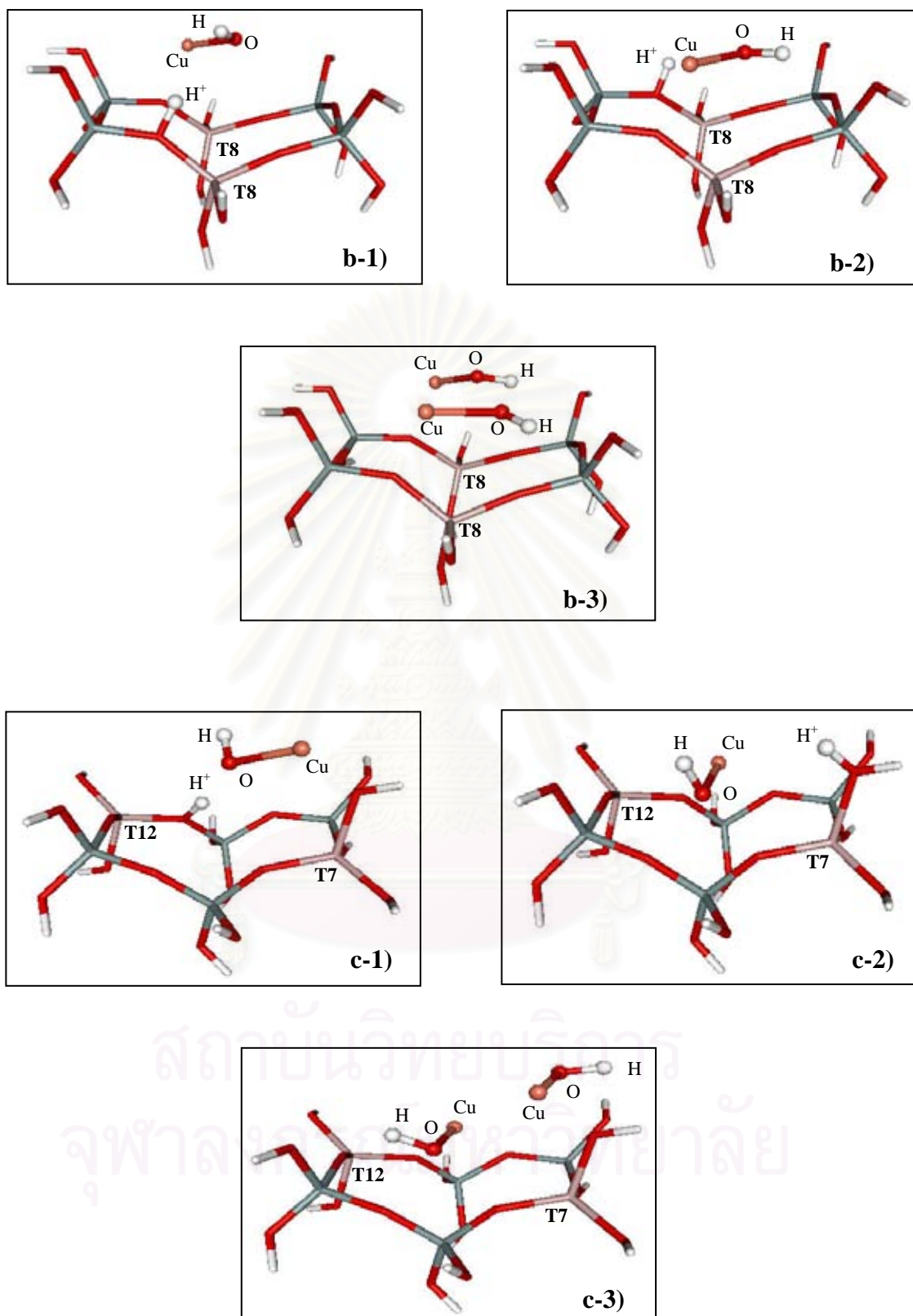
Figure 3.4 (continued).
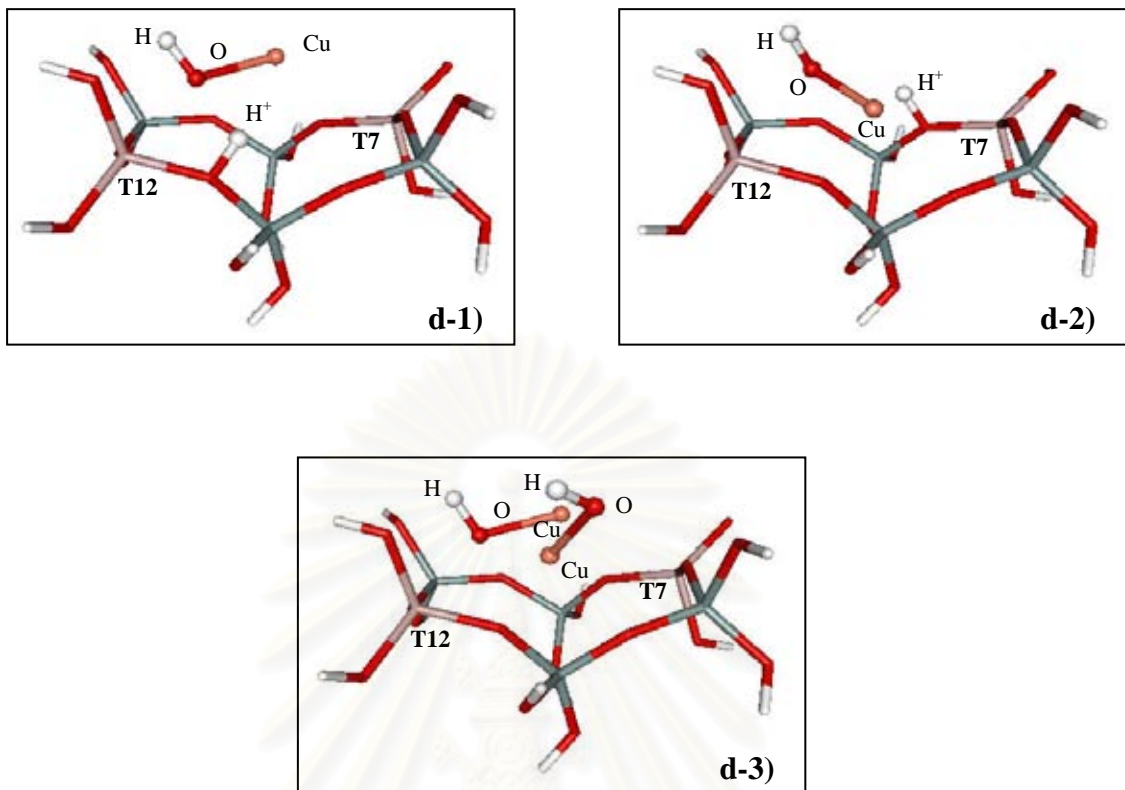
Figure 3.4 (continued).

3.3 Exchanged Energies

After optimized structures of CuZSM-5 were obtained, exchanged energies, E_{exc}, at various exchanged sites were computed using following equation.

$$ZH_2 + nCuOH^+ \rightarrow Z(CuOH)_n H_{2-n} + nH^+$$

$$E_{exc} = E(Z(CuOH)_n H_{2-n}) - E(ZH_2) - nE(CuOH^+) \tag{3.1}$$

where ZH_2 and $Z(CuOH)_n H_{2-n})$ denote HZSM-5 and CuZSM-5, respectively.

3.4 Structures and Stabilizations of Copper-Water Complexes.

Possible structures of $[Cu(H_2O)_n]^{2+}$ for n=1-7 as given in Table 3.2 were optimized and their energies were evaluated and compared. The energies were calculated using quantum chemical calculations with various methods and basis sets.

The geometry optimizations were performed at HF/6-31G(d,p) level. Then, for each geometry single point energy calculation was carried out at MP2/6-31G(d,p) and B3LYP/6-31G(d,p). In addition, for n=6 and 7, HF/6-31++G(d,p), HF/6-311G(d,p), and HF/6-311G(2df,p) calculations were performed. Then, copper-water complex stabilization energies (CSE) were computed using

$$CSE = E([Cu(H_2O)_n]^{2+}) - E(Cu^{2+}) - nE(H_2O) \qquad (3.2)$$

Table 3.2 The possible geometries of $[Cu(H_2O)_n]^{2+}$ for n=1-7.

n	No. of possible geometries investigated	Structure
1	1	linear
2	1	linear
3	1	trigonal
4	2	square planar (spl), tetrahedral (td)
5	3	square pyramidal (spy), trigonal bipyramidal (tbp), td+H_2O
6	2	Octahedral (oct), tbp+H_2O
7	2	oct+H_2O, tbp+2H_2O

CHAPTER 4

RESULTS AND DISCUSSIONS

4.1 Optimized Geometries of HZSM-5

Partial optimizations for cluster models T6 T12, T8 T8, M1T7 T12, and, M2T7 T12 yielded O-H bond length of 0.96 Å and ∠T-O-H bond angle between 115.0°-119.0°. More details of the calculations at different exchanged sites were described in sections 4.1.1-4.1.4.

4.1.1 Optimized Geometries of T6 T12 Exchanged Sites

Figure 4.1 displays optimized geometry of HZSM-5 cluster model at T6 T12 site and Table 4.1 lists geometrical parameters for the skeleton for T6 T12 ZSM-5 (ZSM-5 with Al substitutions at T6 T12 sites) which were fixed throughout geometry optimization.
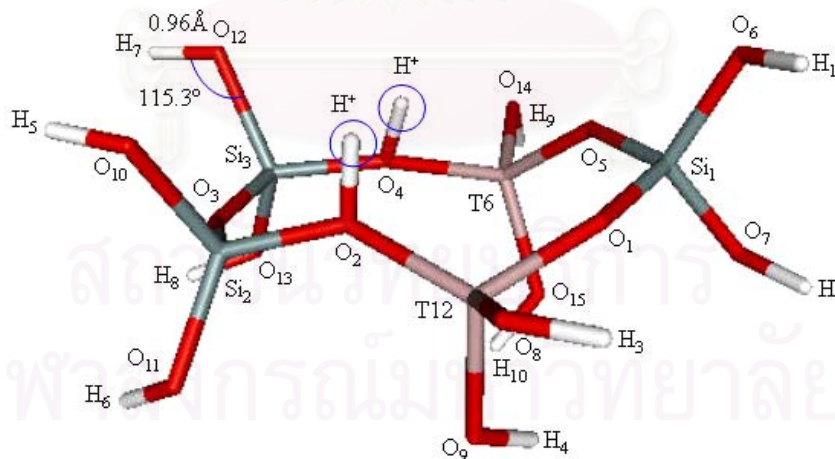
Figure 4.1 Cluster model for T6 T12 substitution of HZSM-5.

Al-O bond lengths at both exchanged sites (Al_{T6}-O and Al_{T12}-O) are between 1.70-1.80 Å, 0.16-0.26 Å longer than bond lengths of Si-O which are between 1.54-1.80 Å. Bond lengths of Si_2-O_{10} and Si_3-O_{12} are longer than others Si-O bond lengths. This is owing to the difference in size between Al and Si.

Table 4.1 Geometrical T6 T12 substitutions obtained from MD simulations.

T6 T12 adsorb sites	Structural parameters (Å)
Si1 – O1	1.59
Si1 - O5	1.62
Si1 - O6	1.60
Si1 - O7	1.60
Al_{T12} - O1	1.70
Al_{T12} - O2	1.74
Al_{T12} - O8	1.75
Al_{T12} - O9	1.78
Si2 - O2	1.54
Si2 - O3	1.61
Si2 - O10	1.73
Si2 - O11	1.62
Si3 - O3	1.58
Si3 - O4	1.57
Si3 - O12	1.80
Si3 - O13	1.64
Al_{T6} - O4	1.74
Al_{T6} - O5	1.74
Al_{T6} - O14	1.79
Al_{T6} - O15	1.80

Table 4.2 shows optimized parameters for terminal Si-O-H and position of H^+. From Table 4.2, the terminal Si-O-H has bond lengths of 0.96 Å, and bond angles of 115.3º. The H^+-O distances are 0.99 Å thus, H^+ binds very tightly with O.

Table 4.2 Terminal Si-O-H and H^+ associated geometrical parameters obtained at B3LYP/6-31G(d,p).

$T6H^+$ $T12H^+$ model	Structural parameters
O – H	0.96 Å
∠T- O - H	115.3º
H^+-O4	0.99 Å
H^+-O2	0.99 Å

4.1.2 Optimized Geometries of T8 T8 Exchanged Sites

Figure 4.2 displays optimized geometry of HZSM-5 cluster model at T8 T8 site and Table 4.3 lists geometry parameters for the skeleton for T8 T8 ZSM-5 which were fixed throughout geometry optimizations.
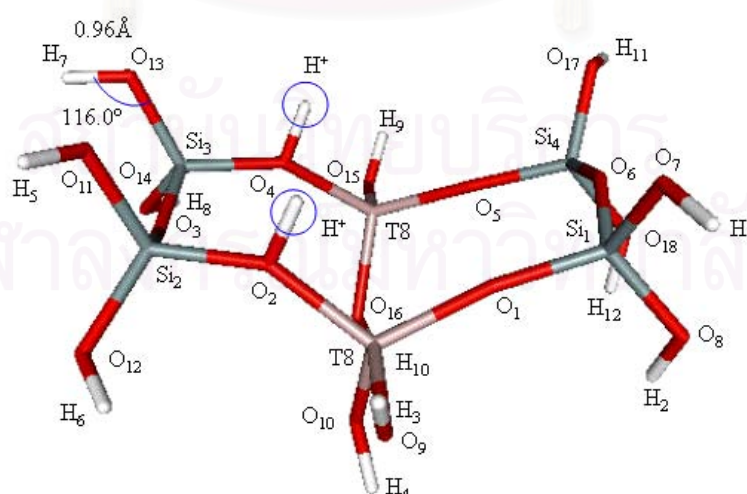
Figure 4.2 Cluster model for T8 T8 substitution of HZSM-5.

In Table 4.3, Al-O bond lengths at both exchanged sites (Al_{T8out}-O and Al_{T8in}-O) are between 1.75-1.82 Å, 0.15-0.22 Å longer than bond lengths of Si-O which are between 1.60-1.67 Å. Similar behavior to that of T6 T12 site was observed.

Table 4.3 Geometrical parameters for T8 T8 substitutions obtained from MD simulations.

T8 T8 adsorb sites	Structural parameters (Å)
Si1 - O1	1.64
Si1 - O6	1.60
Si1 - O7	1.67
Si1 - O8	1.65
Al_{T8out} - O1	1.82
Al_{T8out} - O2	1.79
Al_{T8out} - O9	1.75
Al_{T8out} - O10	1.76
Si2 - O2	1.66
Si2 - O3	1.63
Si2 - O11	1.66
Si2 - O12	1.66
Si3 - O3	1.61
Si3 - O4	1.64
Si3 - O13	1.64
Si3 - O14	1.61
Al_{T8in} - O4	1.82
Al_{T8in} - O5	1.77
Al_{T8in} - O15	1.76
Al_{T8in} - O16	1.79
Si4 - O5	1.65
Si4 - O6	1.65
Si4 - O17	1.65
Si4 - O18	1.66

Table 4.4 shows optimized parameters for terminal Si-O-H and position of H$^+$. From Table 4.4, the terminal Si-O-H has bond lengths of 0.96 Å and bond angles of 116.0º. The H$^+$-O distances are 0.98 Å. These parameters are similar to those of T6 T12 model.

Table 4.4 Terminal Si-O-H and H$^+$ associated optimized parameters obtained at
B3LYP/6-31G(d,p).

T8$_{in}$H$^+$ T8$_{out}$H$^+$ model	Structural parameters
O – H	0.96 Å
∠T- O - H	116.0º
H$^+$-O4	0.98 Å
H$^+$-O2	0.98 Å

4.1.3 Optimized Geometries of M1T7 T12 Exchanged Sites

Figure 4.3 displays optimized geometry of HZSM-5 cluster model at T7 T12 site model1 (M1T7 T12).

Figure 4.3 Cluster model for M1T7 T12 substitution of HZSM-5.

Table 4.5 lists geometry parameters for the skeleton of M1T7 T12 ZSM-5 which were fixed throughout geometry optimizations. In Table 4.5, bond lengths of both exchanged sites (Al_{T7}-O and Al_{T12}-O) are between 1.72-1.83 Å, 0.2-0.31 Å longer than bond lengths of Si-O which are between 1.56-1.67 Å. Similar behavior to T6 T12 site was observed.

Table 4.5 Geometrical parameters for M1T7 T12 substitutions obtained from MD
simulations.

M1T7 T12 adsorb sites	Structural parameters (Å)
Si1 - O1	1.59
Si1 - O6	1.60
Si1 - O7	1.66
Si1 - O8	1.62
Al_{T7} - O2	1.77
Al_{T7} - O8	1.72
Al_{T7} - O9	1.82
Al_{T7} - O10	1.79
Si2 - O2	1.59
Si2 - O3	1.56
Si2 - O11	1.58
Si2 - O12	1.60
Si3 - O3	1.57
Si3 - O4	1.68
Si3 - O13	1.58
Si3 - O14	1.66
Al_{T12} - O4	1.72
Al_{T12} - O5	1.78
Al_{T12} - O15	1.83
Al_{T12} - O16	1.72
Si4 - O5	1.61
Si4 - O6	1.67
Si4 - O17	1.59
Si4 - O18	1.65

Table 4.6 shows optimized parameters for terminal Si-O-H and position of H$^+$. From Table 4.6, the terminal Si-O-H has bond lengths of 0.96 Å and bond angles of 118.5°. The H$^+$-O4 and H$^+$-O2 distances are 0.97 Å and 0.98 Å respectively. These parameters are similar to those of T6 T12 model.

Table 4.6 Terminal Si-O-H and H$^+$ associated optimized parameters obtained at B3LYP/6-31G(d,p).

M1T7H$^+$ T12$^+$ model	Structural parameters
O – H	0.96 Å
∠T- O - H	118.5°
H$^+$-O9	0.97 Å
H$^+$-O5	0.98 Å

4.1.4 Optimized Geometries of M2T7 T12 Exchanged Sites
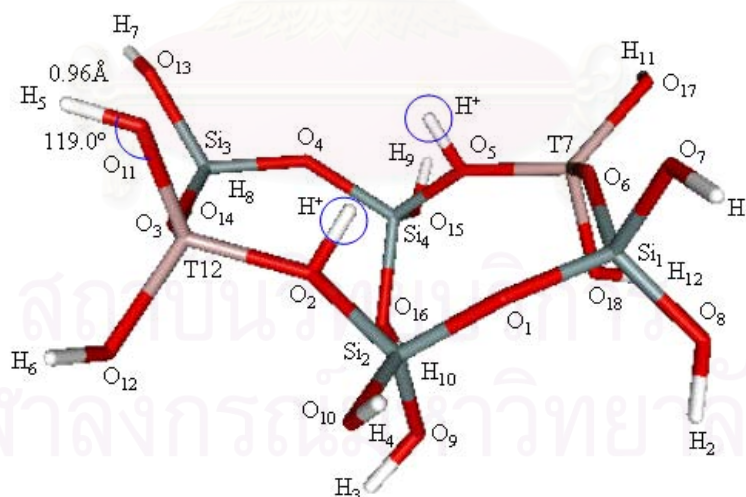
Figure 4.4 Cluster model for M2T7 T12 substitution of HZSM-5.
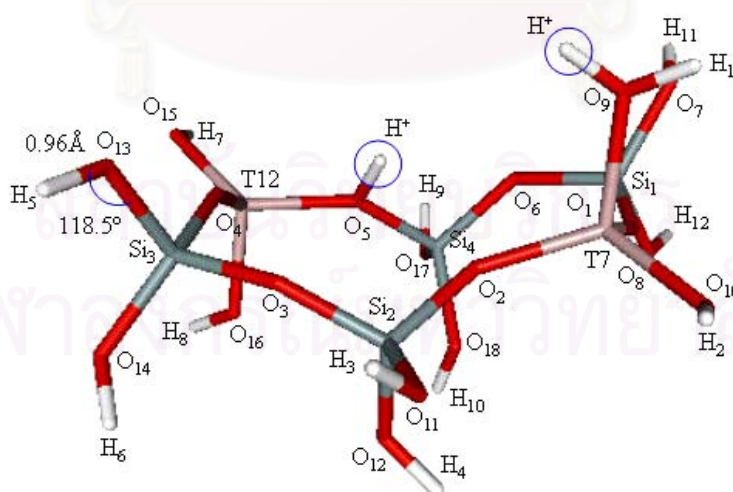
Table 4.7 lists geometry parameters for the skeleton of M1T7 T12 ZSM-5 which were fixed throughout geometry optimizations. The data also shows that, bond lengths of both exchanged sites (Al_{T7}-O and Al_{T12}-O) are between 1.72-1.88 Å, 0.18-0.34 Å longer than bond lengths of Si-O which are between 1.54-1.71 Å. Similar behavior to T6 T12 site was observed.

Table 4.7 Geometrical parameters for M2T7 T12 substitutions obtained from MD simulations.

M2T7 T12 adsorb sites	Structural parameters (Å)
Si1 - O1	1.58
Si1 - O6	1.59
Si1 - O7	1.64
Si1 - O8	1.63
Si2 - O1	1.56
Si2 - O7	1.57
Si2 - O10	1.54
Si2 - O12	1.63
Al_{T12} - O2	1.75
Al_{T12} - O3	1.75
Al_{T12} - O11	1.72
Al_{T12} - O12	1.79
Si3 - O13	1.66
Si3 - O14	1.62
Si3 - O3	1.63
Si3 - O4	1.58
Si4 - O4	1.68
Si4 - O5	1.59
Si4 - O15	1.55
Si4 - O16	1.71
Al_{T7} - O5	1.73
Al_{T7} - O6	1.80
Al_{T7} - O17	1.88
Al_{T7}- O18	1.72

Table 4.8 shows optimized parameters for terminal Si-O-H and position of H^+. From Table 4.8, the terminal Si-O-H has bond lengths of 0.96 Å and bond angles of 119.0º. The H^+-O4 and H^+-O2 distances are 0.98 Å and 0.99 Å respectively. These parameters are similar to those of T6 T12 model.

Table 4.8 Terminal Si-O-H and H^+ associated optimized parameters obtained at B3LYP/6-31G(d,p).

$M2T7H^+$ $T12H^+$ model	Structural parameters
O – H	0.96 Å
∠T- O - H	119.0º
H^+- O2	0.98 Å
H^+- O5	0.99 Å

4.2 Optimized Geometries of One- Ion Exchanged CuZSM-5

4.2.1 T6 T12 Exchanged Sites

4.2.1.1 $T6H^+$ $T12CuOH^+$ Model

The $CuOH^+$ was placed in the position of H^+ at T12 site at the start of the geometry optimization. After optimization was completed, we found that the OH^- group is protonated by the available H^+ at T6 and dissociated from $CuOH^+$. This leaves only bare Cu^{2+} and H_2O in the cluster as seen from Figure 4.5. This maneuver is established to reduce repulsion between 2 charges species, $CuOH^+$ and H^+.
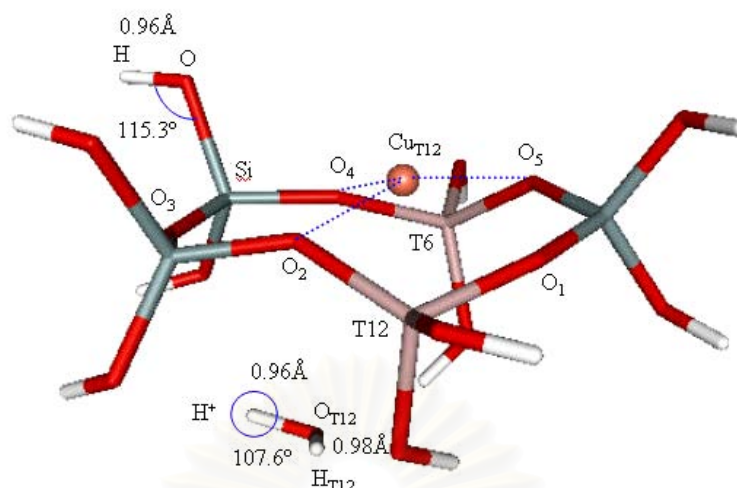
Figure 4.5 Optimized cluster model for $T6H^+$ $T12CuOH^+$ CuZSM-5.

Table 4.9 displays optimized parameters for $CuOH^+$ and H^+ in $T6H^+$ $T12CuOH^+$. The closest Cu-O(Z) distances are 1.96 Å (with O_2), 1.99 Å (with O_4) and 2.13 Å (at O_5) where the O(Z) represents oxygen atom in ZSM-5 skeleton. Thus Cu^{2+} forms tri-coordination with zeolites.

Table 4.9 Optimized structural parameters for $CuOH^+$ and H^+ of $T6H^+$ $T12CuOH^+$ model.

$T6H^+$ $T12CuOH^+$ model	Structural parameters
Cu_{T12}-O_{T12}	3.91 Å
O_{T12}-H_{T12}	0.98 Å
∠Cu_{T12}-O_{T12}-H_{T12}	72.0 °
∠H_{T12}-O_{T12}-H^+	107.6°
∠Cu_{T12}-O_{T12}-H^+	98.1°
Cu_{T12}-O1	2.30 Å
Cu_{T12}-O2	1.96 Å
Cu_{T12}-O4	1.99 Å
Cu_{T12}-O5	2.13 Å

4.2.1.2 T6CuOH$^+$ T12H$^+$ Model

After the optimization was completed, we found that H$^+$ at T12 is bound to O of CuOH$^+$ to form [CuOH$_2$]$^{2+}$ as seen in Figure 4.6. This is probably to reduce repulsion between 2 charged species.

Figure 4.6 Optimized cluster model for T6CuOH$^+$ T12H$^+$ CuZSM-5.

Table 4.10 displays optimized parameters for CuOH$^+$ and H$^+$ in T6CuOH$^+$ T12H$^+$. From Cu-O(Z) distances, there are 2 Cu-O with distances around 2 Å. Thus, for this site the coordination of Cu^{2+} is 2.

Table 4.10 Optimized structural parameters for $CuOH^+$ and H^+ of $T6CuOH^+$ $T12H^+$ model.

$T6CuOH^+$ $T12H^+$ model	Structural parameters
Cu_{T6}-O_{T6}	1.97 Å
O_{T6}-H_{T6}	0.98 Å
$\angle Cu_{T6}$-O_{T6}-H_{T6}	112.7º
$\angle Cu_{T6}$-O_{T6}-H^+	115.0º
H_{T6}-$O6$	2.18 Å
H^+-O_{T6}	0.97 Å
$\angle H_{T6}$-$O6$-H^+	107.9º
Cu_{T6}-$O1$	2.57 Å
Cu_{T6}-$O2$	2.05 Å
Cu_{T6}-$O4$	1.97 Å
Cu_{T6}-$O5$	2.27 Å

4.2.2 T8 T8 Exchanged Sites

4.2.2.1 $T8inH^+$ $T8outCuOH^+$ Model

After the optimization was completed, we found that H^+ at $T8_{in}$ is bound to O of $CuOH^+$ to form $[CuOH_2]^{2+}$ as seen in Figure 4.7. This is probably to reduce repulsion between 2 charged species.
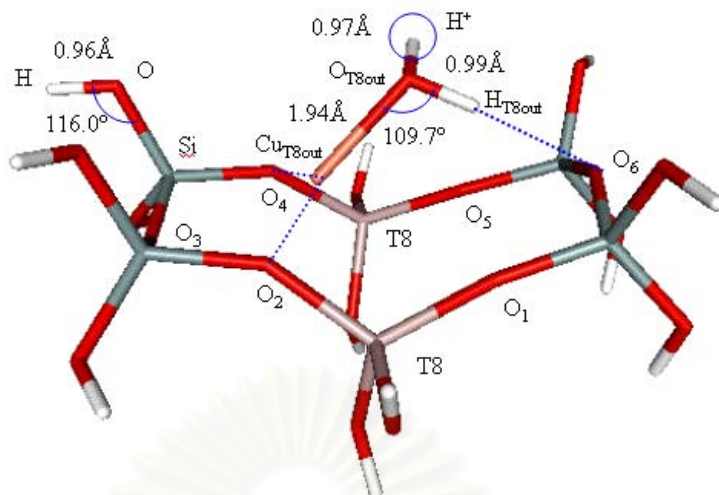
Figure 4.7 Optimized cluster model for T8inH$^+$ T8outCuOH$^+$ CuZSM-5.

Table 4.11 displays optimized parameters for CuOH$^+$ and H$^+$ in T8inH$^+$ T8outCuOH$^+$. From Cu-O(Z) distances, there are 2 Cu-O with distances around 2 Å. Thus, in this site the coordination of Cu^{2+} is 2.

Table 4.11 Optimized structural parameters for CuOH$^+$ and H$^+$ of T8inH$^+$ T8outCuOH$^+$ model.

T8inH$^+$ T8outCuOH$^+$ model	Structural parameters
Cu$_{T8out}$-O$_{T8out}$	1.94 Å
O$_{T8out}$-H$_{T8out}$	0.99 Å
∠Cu$_{T8out}$-O$_{T8out}$-H$_{T8out}$	109.7°
∠Cu$_{T8out}$-O$_{T8out}$-H$^+$	115.9°
∠H$_{T8out}$-O$_{T8out}$-H$^+$	104.6°
H$^+$-O$_{T8out}$	0.97 Å
H$_{T8out}$-O6	2.10 Å
Cu$_{T8out}$-O2	2.01 Å
Cu$_{T8out}$-O3	2.65 Å
Cu$_{T8out}$-O4	2.05 Å

4.2.2.2 T8inCuOH$^+$ T8outH$^+$ Model

After the optimization was completed, we found that H$^+$ at T8$_{out}$ is bound to O of CuOH$^+$ to form [CuOH$_2$]$^{2+}$ is seen in Figure 4.8. This is probably to reduce repulsion between 2 charged species.
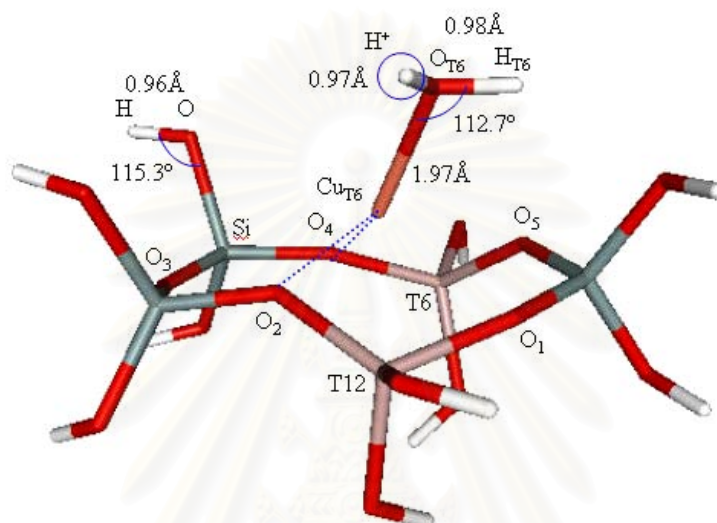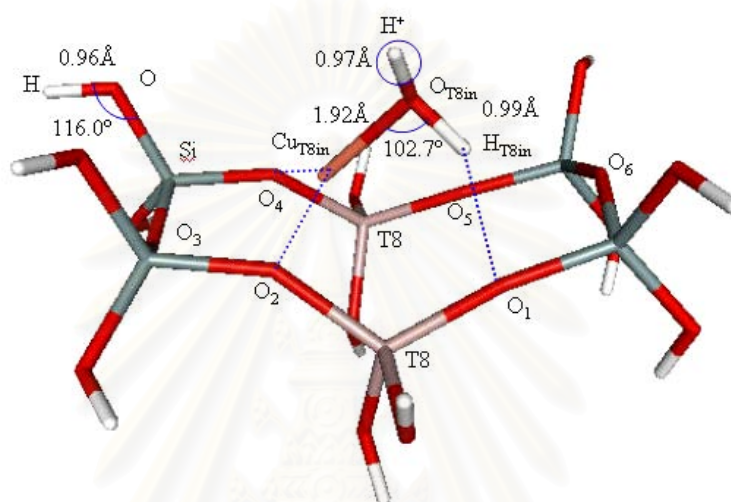

Figure 4.8 Optimized cluster model for T8inCuOH$^+$ T8outH$^+$ CuZSM-5.

Table 4.12 displays optimized parameters for CuOH$^+$ and H$^+$ in T8inCuOH$^+$ T8outH$^+$. From Cu-O(Z) distances, there are 2 Cu-O with distances around 2 Å. Thus, in this site the coordination of Cu^{2+} is 2.

Table 4.12 Optimized structural parameters for CuOH$^+$ and H$^+$ of T8inCuOH$^+$ T8outH$^+$ model.

T8inCuOH$^+$ T8outH$^+$ model	Structural parameters
Cu$_{T8in}$-O$_{T8in}$	1.92Å
O$_{T8in}$-H$_{T8in}$	0.99 Å
∠Cu$_{T8in}$-O$_{T8in}$-H$_{T8in}$	102.7º
H$^+$-O$_{T8in}$	0.97 Å
∠Cu$_{T8in}$-O$_{T8in}$-H$^+$	125.3º
∠H$_{T8in}$-O$_{T8in}$-H$^+$	108.6º
H$_{T8in}$-O1	1.88 Å
Cu$_{T8in}$-O2	2.14 Å
Cu$_{T8in}$-O3	2.71 Å
Cu$_{T8in}$-O4	1.97 Å

4.2.3 M1T7 T12 Exchanged Sites

4.2.3.1 M1T7H$^+$ T12CuOH$^+$ Model

Interestingly for M1T7H$^+$ T12CuOH$^+$, H$^+$ at T7 does not bind on CuOH$^+$ like in other cases as seen from Figures 4.6-4.8. The H$^+$ does also not attach on O$_1$ which is on zeolite's skeleton but on O$_9$.
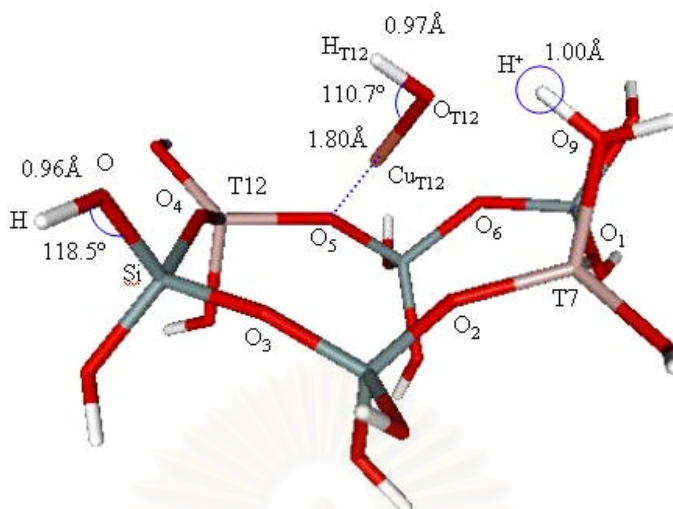
Figure 4.9 Optimized cluster model for M1T7H$^+$ T12CuOH$^+$ CuZSM-5.

Table 4.13 display optimized parameters for CuOH$^+$ and H$^+$ in M1T7H$^+$ T12CuOH$^+$. From Cu-O(Z) distances, there are 1 Cu-O with distances around 2 Å. Thus, in this site the coordination of Cu^{2+} is 1.

Table 4.13 Optimized structural parameters for CuOH$^+$ and H$^+$ of M1T7H$^+$ T12CuOH$^+$ model.

M1T7H$^+$ T12CuOH$^+$ model	Structural parameters
Cu$_{T12}$ - O$_{T12}$	1.80Å
O$_{T12}$-H$_{T12}$	0.97 Å
∠Cu$_{T12}$ -O$_{T12}$-H$_{T12}$	110.7°
H$^+$-O$_{T12}$	1.61 Å
H$^+$-O9	1.00 Å
Cu$_{T12}$ - O2	2.85 Å
Cu$_{T12}$ - O4	2.76 Å
Cu$_{T12}$ - O5	1.89 Å
Cu$_{T12}$ - O6	2.61 Å

4.2.3.2 M1T7CuOH$^+$ T12H$^+$ Model

        Like M1T7CuOH$^+$ T12H$^+$, H$^+$ does not bind to CuOH$^+$ as seen in Figure 4.9.
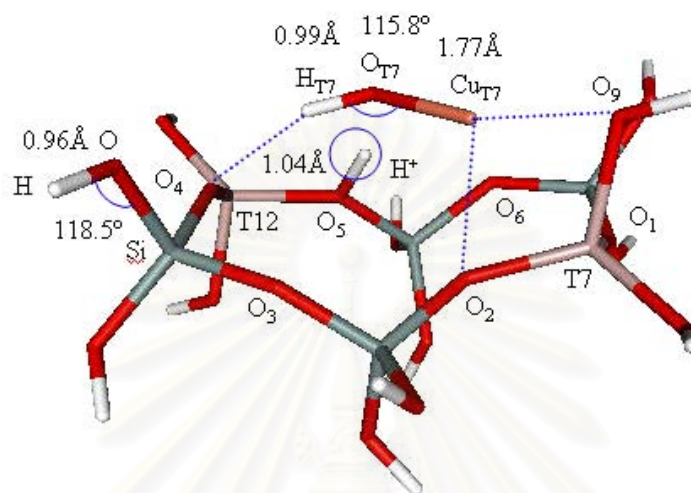
Figure 4.10 Optimized cluster model for M1T7CuOH$^+$ T12H$^+$ CuZSM-5.

        Table 4.14 display optimized parameters for CuOH$^+$ and H$^+$ in M1T7CuOH$^+$ T12H$^+$. From Cu-O(Z) distances, there are 2 Cu-O with distances around 2 Å. Thus, in this site the coordination of Cu^{2+} is 2. We also found H$_{T7}$ - O4 of 1.79 Å which is the region of H-bond. Thus other than coordinates with Cu^{2+} for this system there is also coordination between H of CuOH$^+$ and O in ZSM-5.

Table 4.14 Optimized structural parameters for $CuOH^+$ and H^+ of $M1T7CuOH^+$ $T12H^+$ model.

$M1T7CuOH^+$ $T12 H^+$ model	Structural parameters
Cu_{T7} - O_{T7}	1.77 Å
O_{T7} - H_{T7}	0.99 Å
$\angle Cu_{T7}$ - O_{T7}-H_{T7}	115.80º
H^+-O_{T7}	1.61 Å
H^+-O5	1.04 Å
H_{T7} - O4	1.79 Å
Cu_{T7} - O2	2.15 Å
Cu_{T7} - O9	1.97 Å

4.2.4 M2T7 T12 Exchanged Sites

4.2.4.1 $M2T7H^+$ $T12CuOH^+$ Model

After the optimization was completed, we found that H^+ at T7 is binds to O of $CuOH^+$ to form $[CuOH_2]^{2+}$ as seen in Figure 4.11. This is probably to reduce repulsion between 2 charged species.

Figure 4.11 Optimized cluster model for M2T7H$^+$ T12CuOH$^+$ CuZSM-5.

Table 4.15 displays optimized parameters for CuOH$^+$ and H$^+$ in M2T7H$^+$ T12CuOH$^+$. From Cu-O(Z) distances, there are 2 Cu-O with distances around 2 Å. Thus, in this site the coordination of Cu^{2+} is 2. We also found H$_{T12}$-O6 of 1.74 Å which is the region of H-bond. Thus other than coordinate with Cu^{2+} for this system there is also coordination between H of CuOH$^+$ and O in ZSM-5.

Table 4.15 Optimized structural parameters for CuOH$^+$ and H$^+$ of M2T7H$^+$ T12CuOH$^+$ model.

M2T7H$^+$ T12CuOH$^+$ model	Structural parameters
Cu$_{T12}$-O$_{T12}$	1.93 Å
O$_{T12}$-H$_{T12}$	1.00 Å
∠Cu$_{T12}$-O$_{T12}$-H$_{T12}$	107.9°
∠H$_{T12}$-O$_{T12}$-H$^+$	113.5°
H$_{T12}$-O6	1.74 Å
Cu$_{T12}$-O6	2.95 Å
Cu$_{T12}$-O4	2.57 Å
Cu$_{T12}$-O5	2.12 Å
Cu$_{T12}$-O2	1.95 Å

4.2.4.2 M2T7CuOH$^+$ T12H$^+$ Model

        After the optimization was completed, we found that H$^+$ at T12 binds to O of CuOH$^+$ to form [CuOH$_2$]$^{2+}$ as seen in Figure 4.12. This is probably to reduce repulsion between 2 charged species.
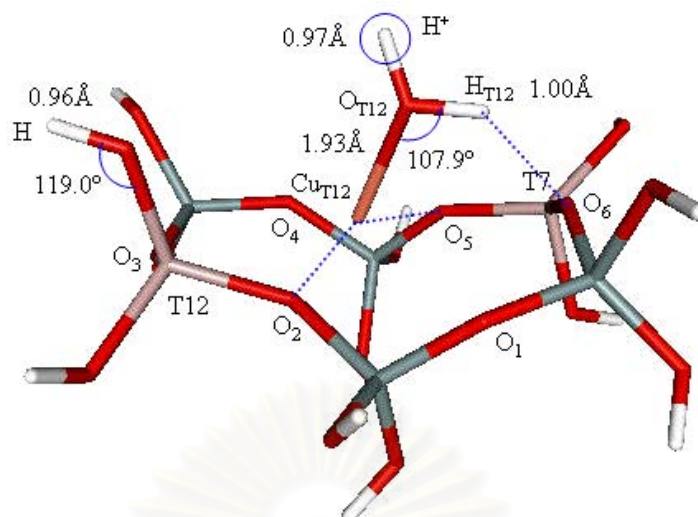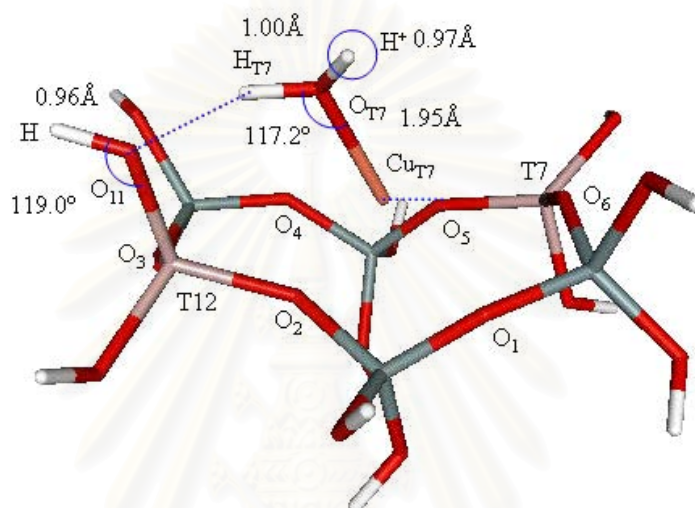

Figure 4.12 Optimized cluster model for M2T7CuOH$^+$ T12H$^+$ CuZSM-5.

        Table 4.16 displays optimized parameters for CuOH$^+$ and H$^+$ in M2T7CuOH$^+$ T12H$^+$. From Cu-O(Z) distances, there are 2 Cu-O with distances around 2 Å. Thus, in this site the coordination of Cu^{2+} is 2.

Table 4.16 Optimized structural parameters for $CuOH^+$ and H^+ of $M2T7CuOH^+$ $T12H^+$ model.

$M2T7CuOH^+$ $T12H^+$ model	Structural parameters
$Cu_{T7}-O_{T7}$	1.95 Å
$O_{T7}-H_{T7}$	1.00 Å
$\angle Cu_{T7}-O_{T7}-H_{T7}$	117.2º
$O_{T7}-H^+$	0.97 Å
$H_{T7}-O11$	1.76 Å
$\angle Cu_{T7}-O_{T7}-H^+$	119.0º
$\angle H_{T7}-O_{T7}-H^+$	107.0º
$Cu_{T7}-O1$	2.96 Å
$Cu_{T7}-O2$	2.12 Å
$Cu_{T7}-O4$	2.92 Å
$Cu_{T7}-O5$	2.12 Å

4.3 Optimized Geometries of Two- Ion Exchanged CuZSM-5

4.3.1 T6 T12 Exchanged Sites

From the calculations, we found that both $CuOH^+$ like to exchange as $CuOH^+$. No protonation at O position of $CuOH^+$ as seen on Figure 4.13.
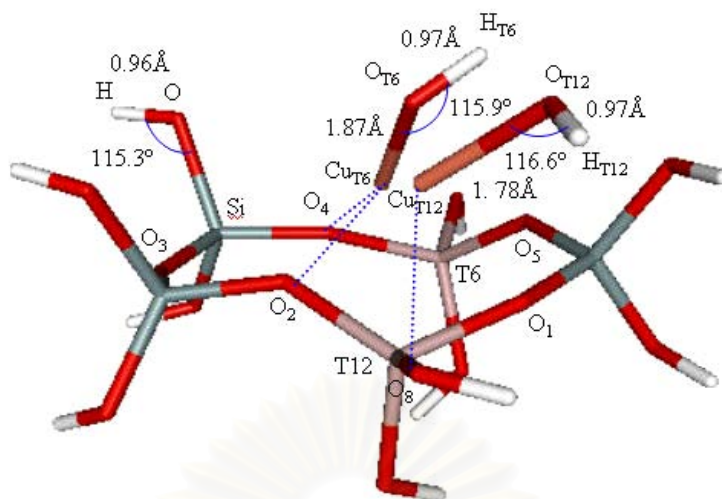
Figure 4.13 Optimized structure of two- ion exchanged CuZSM-5 at T6 T12 site.

From Table 4.17, the shortest Cu-O distance is 2.02 Å (Cu_{T6} –O4). We also found Cu_{T12} attached to O_{T6} (2.00 Å). Thus, some kind of dimer is formed. Longer Cu-O distance was found as compared to one- ion exchanged $CuOH^+$. The $CuOH^+$ does not as tightly bind to zeolites as one- ion exchanged one.

Table 4.17 Structural parameters of $T6CuOH^+$ $T12CuOH^+$ model.

$T6CuOH^+$ $T12CuOH^+$ model	Structural parameters
$Cu_{T6}-O_{T6}$	1.87 Å
$O_{T6}-H_{T6}$	0.97 Å
$\angle Cu_{T6}-O_{T6}-H_{T6}$	115.9º
$Cu_{T12}-O_{T12}$	1.78 Å
$O_{T12}-H_{T12}$	0.97 Å
$\angle Cu_{T12}-O_{T12}-H_{T12}$	116.6º
$\angle Cu_{T12}-O_{T6}-H_{T6}$	106.9º
$Cu_{T12}-O_{T6}$	2.00 Å
$Cu_{T6}-O1$	2.65 Å
$Cu_{T6}-O2$	2.14 Å
$Cu_{T6}-O4$	2.02 Å
$Cu_{T6}-O5$	2.30 Å
$Cu_{T12}-O1$	2.66 Å
$Cu_{T12}-O2$	2.81 Å
$Cu_{T12}-O8$	2.10 Å

4.3.2 T8 T8 Exchanged Sites

From calculations, we found that both $CuOH^+$ like to form into Cu(II)-O-Cu(II) where both Cu(II) share O_{T8in}. Moreover, H of $CuOH^+_{T8in}$ form bond with framework oxygen (see Figure 4.14).
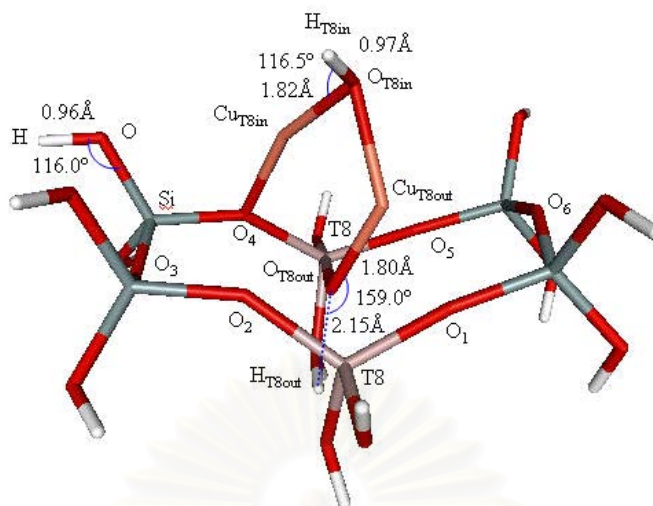
Figure 4.14 Optimized structure of two- ion exchanged CuZSM-5 at T8 T8 site.

Table 4.18 shows optimized parameters for two- ion exchanged CuOH$^+$ in T8 T8 site. The shortest Cu-O distance is 1.87 Å for Cu$_{T8in}$-O4. The 2nd shortest is 2.01 Å for Cu$_{T8out}$-O1. It seems that CuOH$^+$ binds tightly with zeolite.

Table 4.18 Structural parameters of $T8_{in}CuOH^+$ $T8_{out}CuOH^+$ model.

T8inCuOH$^+$ T8outCuOH$^+$ model	Structural parameters
$Cu_{T8in}-O_{T8in}$	1.82 Å
$O_{T8in}-H_{T8in}$	0.97 Å
$\angle Cu_{T8in}-O_{T8in}-H_{T8in}$	116.5º
$Cu_{T8out}-O_{T8out}$	1.80 Å
$O_{T8out}-H_{T8out}$	2.15 Å
$\angle Cu_{T8out}-O_{T8out}-H_{T8out}$	159.0º
$Cu_{T8in}-Cu_{T8out}$	2.24 Å
$Cu_{T8out}- O_{T8in}$	1.94 Å
$\angle Cu_{T8out}-O_{T8in}-H_{T8in}$	117.5º
$\angle Cu_{T8in}-O_{T8in}-Cu_{T8out}$	72.9º
$H_{T8out}-O10$	2.11 Å
$H_{T8out}-O16$	1.00 Å
$Cu_{T8in}-O4$	1.87 Å
$Cu_{T8out}-O1$	2.01 Å
$Cu_{T8out}-O2$	2.76 Å
$Cu_{T8out}-O5$	2.57 Å
$Cu_{T8out}-O6$	2.59 Å

4.3.3 M1T7 T12 Exchanged Sites

From calculations, we found that both CuOH$^+$ like to form bridging di copper compound where 2 O of CuOH$^+$ act as bridging atom. For this dimer, not only 2 Cu atoms but also 2 H atoms are coordinated with zeolite framework as seen in Figure 4.15.

Figure 4.15 Optimized structure of two- ion exchanged CuZSM-5 at M1T7 T12 sites.

From Table 4.19 where structural parameters for two- ion exchanged $CuOH^+$ in M1T7 T12 were listed, the shortest Cu-O distances are 1.88 Å and 1.97 Å for Cu_{T7} - O9 and Cu_{T12} - O5 respectively. The H_{T7}-O4 and H_{T12}-O7 are also 1.75 Å and 1.99 Å respectively. These bond distances are in the rangs of H-bond.

Table 4.19 Structural parameters of M1T7CuOH$^+$ T12CuOH$^+$ model.

M1T7CuOH$^+$ T12CuOH$^+$ model	Structural parameters
Cu$_{T7}$ - O$_{T7}$	1.85 Å
O$_{T7}$ - H$_{T7}$	1.00 Å
∠Cu$_{T7}$ - O$_{T7}$-H$_{T7}$	127.6º
Cu$_{T12}$- O$_{T12}$	1.91 Å
O$_{T12}$ - H$_{T12}$	0.98 Å
∠Cu$_{T12}$- O$_{T12}$-H$_{T12}$	119.0º
Cu$_{T7}$ - O$_{T12}$	1.91 Å
Cu$_{T7}$- Cu$_{T12}$	2.52 Å
Cu$_{T12}$- O$_{T7}$	1.89 Å
H$_{T7}$ - O4	1.75 Å
H$_{T12}$ - O7	1.99 Å
Cu$_{T7}$ - O2	2.75 Å
Cu$_{T7}$ - O9	1.88 Å
Cu$_{T12}$ - O5	1.97 Å
Cu$_{T12}$ - O6	2.13 Å

4.3.4 M2T7 T12 Exchanged Sites

Form calculations, we found that both CuOH$^+$ like to exchange as CuOH$^+$. However, Cu$_{T12}$ can coordinate with O$_{T7}$ like in the case of exchange at T6 T12 site.
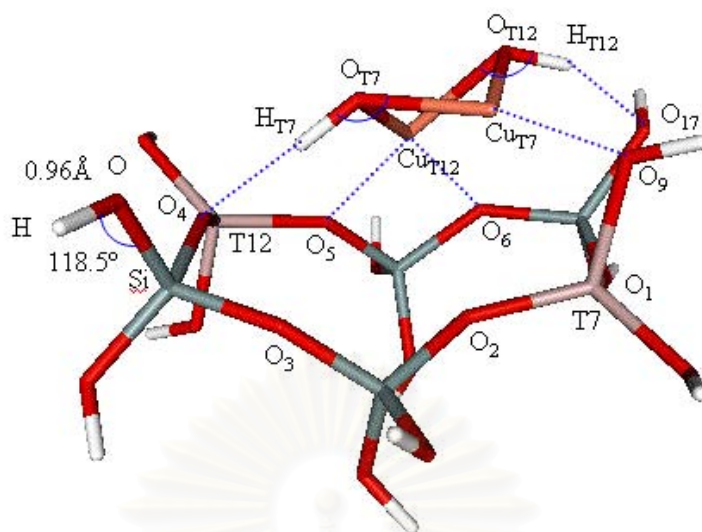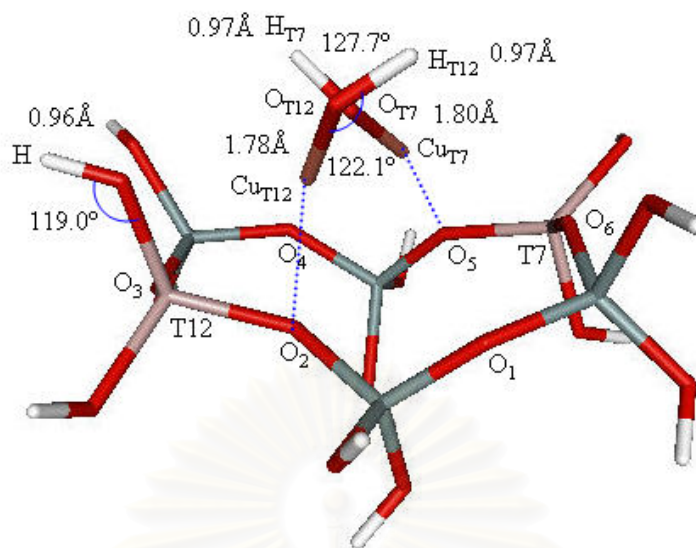
Figure 4.16 Optimized structure of two- ion exchanged CuZSM-5 at M2T7 T12 sites.

Table 4.20 shows structural parameters for two- ion exchanged $CuOH^+$ in M2T7 T12. The shortest Cu-O distances are 1.84 Å and 2.09 Å for Cu_{T7}-O5 and Cu_{T12}-O2 respectively. Each Cu has the coordination of 1 to the framework.

Table 4.20 Structural parameters of M2T7CuOH$^+$ T12CuOH$^+$ model.

M2T7CuOH$^+$ T12CuOH$^+$ model	Structural parameters
Cu$_{T7}$-O$_{T7}$	1.80 Å
O$_{T7}$-H$_{T7}$	0.97 Å
∠Cu$_{T7}$-O$_{T7}$-H$_{T7}$	127.7°
Cu$_{T12}$-O$_{T12}$	1.78 Å
O$_{T12}$-H$_{T12}$	0.97 Å
∠Cu$_{T12}$-O$_{T12}$-H$_{T12}$	122.1°
Cu$_{T7}$-Cu$_{T12}$	2.94 Å
Cu$_{T12}$-O$_{T7}$	1.49 Å
∠Cu$_{T12}$-O$_{T7}$-H$_{T7}$	93.4°
Cu$_{T7}$-O4	2.78 Å
Cu$_{T7}$-O5	1.84 Å
Cu$_{T7}$-O6	2.74 Å
Cu$_{T12}$-O1	2.98 Å
Cu$_{T12}$-O2	2.09 Å

4.4 Exchange of CuOH$^+$ to ZSM-5

Exchanged energies of one- and two- ion exchanged CuOH$^+$ at different exchanged sites were shown in Table 4.21. Exchanged energies are ranging between -32.47 and 75.61 kcal/mol. For one- and two- ion exchanged CuZSM-5, T6 T12 exchanged sites (T6H$^+$ T12CuOH$^+$ and T6CuOH$^+$ T12H$^+$) appears to possess best exchanged energies, -14.11 and -32.47 kcal/mol, respectively. While M1T7 T12 exchanged sites (M1T7H$^+$ T12CuOH$^+$ and M1T7CuOH$^+$ T12H$^+$) possess the highest exchanged energies, 22.06 and 33.49 kcal/mol respectively. For M2T7 T12 and T8 T8 exchanged sites, small positive and negative exchanged energies were observed, between -5.36-3.47 kcal/mol, where M2T7 T12 (M2T7CuOH$^+$ T12H$^+$) having lower exchanged energies. For two- ion exchanged CuZSM-5, very high positive exchanged energies were observed, 12.61-75.61

kcal/mol. From exchanged energies calculations in Table 4.21, it can be concluded that two- ion exchanged of $CuOH^+$ in CuZSM-5 is not preferable to one- ion exchanged and the most preferred exchanged site is T6 T12. M2T7 T12 and T8 T8 exchanged site are also possible but with quite smaller populations.

Table 4.21 Exchanged Energies of CuZSM-5 for each model.

Models		**Exchanged Energies (E_{ads}) kcal/mol**
T6 T12	$T6H^+ T12CuOH^+$	-14.11
	$T6CuOH^+ T12H^+$	-32.47
	$T6CuOH^+ T12CuOH^+$	12.61
T8 T8	$T8_{in}H^+ T8_{out}CuOH^+$	-0.11
	$T8_{in}CuOH^+ T8_{out}H^+$	3.47
	$T8_{in}CuOH^+ T8_{out}CuOH^+$	48.28
M1T7 T12	$M1T7H^+ T12CuOH^+$	22.06
	$M1T7CuOH^+ T12H^+$	33.49
	$M1T7CuOH^+ T12CuOH^+$	32.76
M2T7 T12	$M2T7H^+ T12CuOH^+$	-2.25
	$M2T7CuOH^+ T12H^+$	-5.36
	$M2T7CuOH^+ T12CuOH^+$	75.61

The exchange of Cu species in T6 T12, the most preferred site, is not in $[CuOH]^+$ but rather $[CuOH_2]^{2+}$. The protonation of $CuOH^+$ reduces charge on both H^+ and $CuOH^+$ which in turns reduces repulsion and stabilizes the exchanged complex. Therefore, Cu species is likely being exchanged as $[CuOH_2]^{2+}$. Similar trends were also found in M2T7 T12 and T8 T8 sites but not in M1T7 T12 site. Owing to repulsion between positive charges, two- ion exchanged CuZSM-5 is unfeasible. However, this repulsion could be reduced in the present of water in ZSM-5 cavities, the possibility of existence of water has not been considered in this work.

4.5 Structures and Stabilizations of Copper-Water Complexes

The geometries of possible $[Cu(H_2O)_n]^{2+}$ for n=1-7 structures were obtained at HF/6-31G(d,p). Energies of all calculated species were more accurately determined at B3LYP/6-31G(d,p) and MP2/6-31G(d,p). The optimized structures of all calculations are presented in Figure 4.17, in which bond lengths and bond angles of $[Cu(H_2O)_n]^{2+}$ for n=1-7 were demonstrated. We found that bond lengths of Cu-O are ranging from 1.90-2.24Å.

a) *n*=1 linear
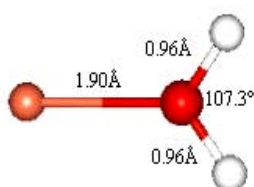
b) *n*=2 linear
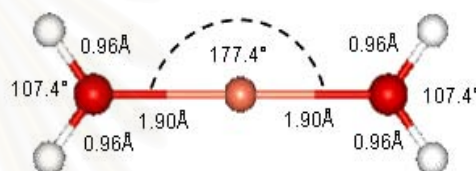
c) *n*=3 trigonal
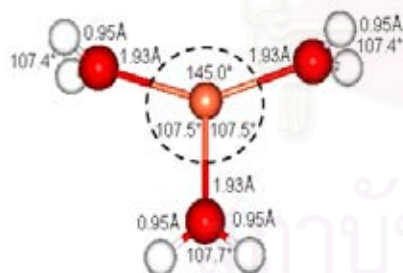
d) *n*=4 square planar (spl)
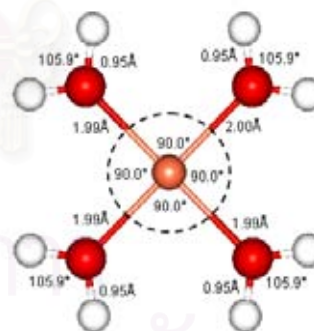
Figure 4.17 Show the optimized structures of $[Cu(H_2O)_n]^{2+}$ for n=1-7 a) $[Cu(H_2O)]^{2+}$, b) $[Cu(H_2O)_2]^{2+}$, c) $[Cu(H_2O)_3]^{2+}$, d) $[Cu(H_2O)_4]^{2+}$ (**spl**), e) $[Cu(H_2O)_4]^{2+}$ (**td**), f) $[Cu(H_2O)_5]^{2+}$ (**spy**), g) $[Cu(H_2O)_5]^{2+}$ (**td+H₂O**), h) $[Cu(H_2O)_5]^{2+}$ (**tbp**), i) $[Cu(H_2O)_6]^{2+}$ (**tbp+H₂O**), j) $[Cu(H_2O)_6]^{2+}$ (**oct**), k) $[Cu(H_2O)_7]^{2+}$ (**tbp+2H₂O**), l) $[Cu(H_2O)_7]^{2+}$ (**oct+H₂O**).

e) *n*=4 tetrahedral (td)
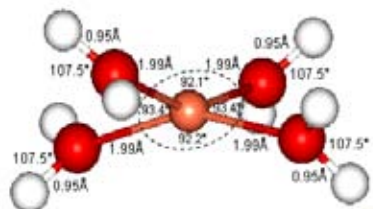
f) *n*=5 square pyramidal (spy)
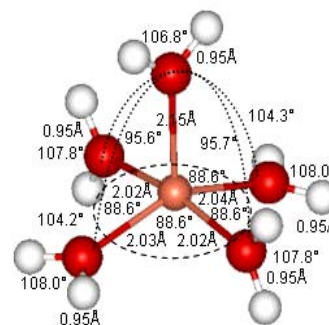
g) *n*=5 tetrahedral + H₂O (td+ H₂O)
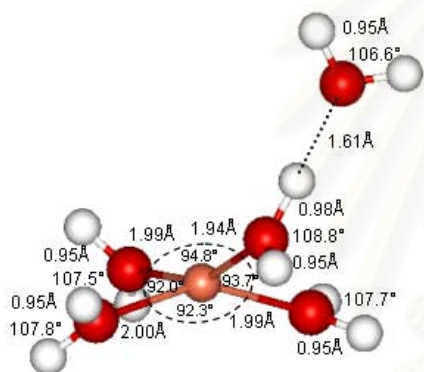
h) *n*=5 trigonal bipyramidal (tbp)
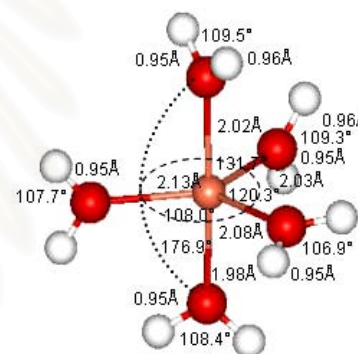
i) *n*=6 trigonal bipyramidal + H₂O (tbp+ H₂O)
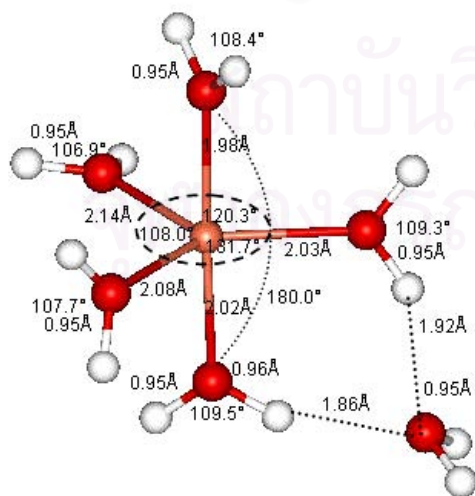
j) *n*=6 octahedral (oct)
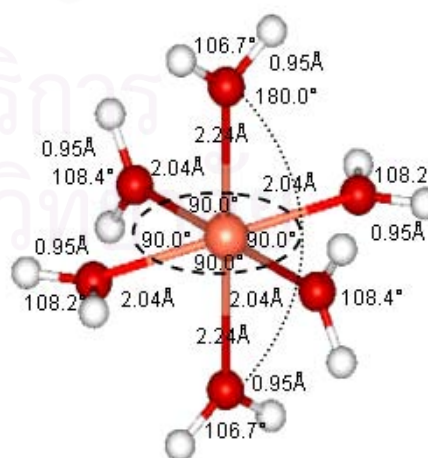
Figure 4.17 (continued).

k) *n*=7 trigonal bipyramidal + 2H$_2$O
   (tbp+ 2H$_2$O)

l) *n*=7 octahedral + H$_2$O (oct+ H$_2$O)
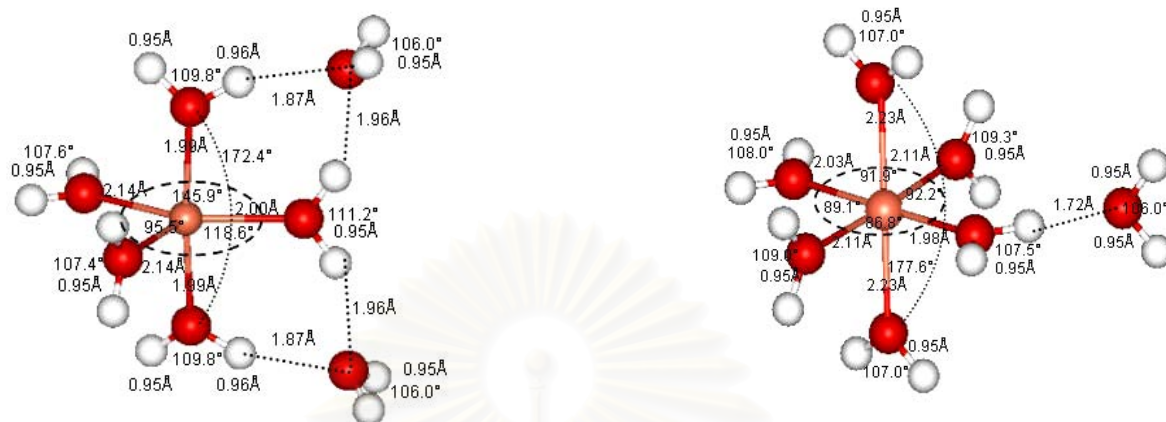
Figure 4.17 (continued).

For *n*=1-3, there are only sole geometry for each complex. For *n*=4-7, there are more than one possible geometries. These possible geometries were compared as given in Tables 4.22-4.26 for *n*=4, 5, 6, 7 respectively.

Table 4.22 Relative Energies (ΔE) in kcal/mol of $[Cu(H_2O)_n]^{2+}$ *n*=4.

Species	Relative Energies (ΔE) kcal/mol		
	HF/6-31G(d,p)	MP2/6-31G(d,p)	B3LYP/6-31G(d,p)
$[Cu(H_2O)_4]^{2+}$ spl	5.96	6.55	7.62
$[Cu(H_2O)_4]^{2+}$ td	0.00	0.00	0.00

Table 4.23 Relative Energies (ΔE) in kcal/mol of $[Cu(H_2O)_n]^{2+}$ n=5.

Species	Relative energies (ΔE) kcal/mol		
	HF/6-31G(d,p)	MP2/6-31G(d,p)	B3LYP/6-31G(d,p)
$[Cu(H_2O)_5]^{2+}$ td+ H_2O	9.09	7.64	3.63
$[Cu(H_2O)_5]^{2+}$ tbp	3.05	2.51	1.95
$[Cu(H_2O)_5]^{2+}$ spy	0.00	0.00	0.00

Table 4.24 Relative Energies (ΔE) in kcal/mol of $[Cu(H_2O)_n]^{2+}$ n=6.

Species	Relative energies (ΔE) kcal/mol					
	Basis set 6-31G(d,p)			HF method		
	MP2	B3LYP	HF	6-31++G(d,p)	6-311G(d,p)	6-311G(2df,p)
$[Cu(H_2O)_6]^{2+}$ oct	4.11	11.81	1.49	-0.58	-3.74	-3.24
$[Cu(H_2O)_6]^{2+}$ tbp+H_2O	0.00	0.00	0.00	0.00	0.00	0.00

Table 4.25 Relative Energies (ΔE) in kcal/mol of $[Cu(H_2O)_n]^{2+}$ n=7.

Species	Relative energies (ΔE) kcal/mol					
	Basis set 6-31G(d,p)			HF method		
	MP2	B3LYP	HF	6-31++G(d,p)	6-311G(d,p)	6-311G(2df,p)
$[Cu(H_2O)_7]^{2+}$ oct+H_2O	8.88	13.43	5.46	3.35	0.83	1.06
$[Cu(H_2O)_7]^{2+}$ tbp+2H_2O	0.00	0.00	0.00	0.00	0.00	0.00

For $n=4$, tetrahedral (td) structure is the most stable and 6.54 kcal/mol (MP2/6-31G(d,p)) below the square planar (spl) one. For $n=5$, all basis sets and methods give the square pyramidal (spy) structure as the most stable and gives trigonal bipyramidal (tbp) structure more stable than tetrahedral+ H_2O (td+ H_2O) structure. For $n=6$, at 6-31G(d,p) it appears that the oct is less stable than tbp+H_2O for all methods while when increasing size of basis set the oct then becomes more stable. Similar trend is also observed for $n=7$. However, the tbp form remains more stable. Table 4.26 listed CSE of the most stable $[Cu(H_2O)_n]^{2+}$ for $n=1-7$.

Table 4.26 Complex Stabilization Energies (CSE) kcal/mol of $[Cu(H_2O)_n]^{2+}$ for $n=1-7$ only the most stable.

Species	Complex Stabilization Energies (CSE) kcal/mol		
	HF/6-31G(d,p)	MP2/6-31G(d,p)	B3LYP/6-31G(d,p)
$[Cu(H_2O)]^{2+}$	-92.55	-101.65	-119.73
$[Cu(H_2O)_2]^{2+}$	-174.87	-192.54	-210.01
$[Cu(H_2O)_3]^{2+}$	-244.56	-267.85	-291.74
$[Cu(H_2O)_4]^{2+}$ td	-292.21	-320.49	-344.24
$[Cu(H_2O)_5]^{2+}$ spy	-327.28	-358.05	-379.37
$[Cu(H_2O)_6]^{2+}$ tbp+H_2O	-354.74	-389.99	-415.83
$[Cu(H_2O)_7]^{2+}$ tbp+$2H_2O$	-380.30	-419.64	-443.45

We found that the stability of the complex increases when more waters are included. However, for $n=6$ and $n=7$ only 5-fold and 6-fold coordination complexes were found. The 5-fold consists of spy and tbp structures and the 6-fold consists of distorted oct structure. For $n=6$, at 6-31G(d,p) basis all methods predicted tbp as the most stable whereas HF/6-31++G(d,p), HF/6-311G(d,p), and HF/6-311G(2df,p) suggested oct as the lowest. For $n=7$ all methods and basis sets agree that tbp is the most stable (tbp-like structure with 5 waters within 2.14Å and 2 waters within 3.89Å is the most stable form) but the energy difference is reduced when larger basis were employed. Thus, oct and tbp structures should co-exist in solution where tbp is more abundant.

CHAPTER 5

CONCLUSION

5.1 Exchange of One- and Two- Proton Exchanged CuOH$^+$ in ZSM-5

Partial optimizations of all HZSM-5 cluster models by using B3LYP/6-31G(d,p) gave O-H bond length of 0.96Å, $\angle$T-O-H bond angle between 115.0°-119°. In part of partial optimization CuZSM-5, all cases of one- and two-ion exchanged CuOH$^+$ gave Cu-O(Z) distances (Cu to framework oxygen distance) between 1.84-2.15 Å. The most preferred exchanged sites for both one- and two-ion exchanged CuOH$^+$ in the cavity of ZSM-5 with Si/Al of 47 is T6 T12, with exchanged energies of -32.03 and +12.54 kcal/mol respectively. Interestingly,exchanged copper species is not in the form of [CuOH]$^+$ but rather as [CuOH$_2$]$^{2+}$. Thus, Cu species is likely being exchanged as [CuOH$_2$]$^{2+}$. All two-ion exchanged CuZSM-5 have positive adsorption energies. It is, thus, unlikely to find two- proton exchanged [CuOH]$^+$.

5.2 Structures and Stabilizations of Copper-Water Complexes

The stability of [Cu(H$_2$O)$_n$]$^{2+}$ n=1-7 complex increases as n increase. For n=6, at 6-31G(d,p) basis set tpb-like structure is the most stable. However, when the site of basis set increased, the oct-like structure becomes more stable. Thus, while basis set effect favor oct-like structure, tbp-like structure more stabilized at higher level of accuracy. Another observation is as more waters are added tbp-like structure becomes more stable. For n=7, tbp-like structure with 5 waters within 2.14 Å and 2 waters within 3.89 Å is the most stable form. While the oct-like structure with 7th water at 4.14 Å is 1.06 kcal/mol higher in energy (HF/6-311G(2df,p)) and is Jahn-Teller distorted (axial=2.03-2.11 Å, equatorial=2.23 Å). Therefore [Cu(H$_2$O)$_n$]$^{2+}$ should have 5 fold coordination with tbp-like structure. But this structure could co-exist with 6 fold coordination oct-like structure since the energy difference is not very large.

SUGGESTION FOR FUTURE WORK

Exchange of other Cu species such as $[Cu(H_2O)_n]^{2+}$ and $[Cu\text{-}O\text{-}Cu]^{2+}$ could be explored. Roles of water in ion-exchange process can be further investigated. Both studies could use the knowledge from this thesis as a starter.

REFERENCES

1. Iwamoto, M.; Yokoo, S.; Sakai, K.; Kagawa, S. "Catalytic Decomposition of Nitric Oxide over Copper (II) –Exchanged Y-Type Zeolites", *J. Chem. Soc., Faraday Trans. l*, **1981**, *77*, 1629-1638.

2. Iwamoto, M.; Furukawa, H.; Mine, Y.; Uemura, F.; Mikuriya, S.; Kagawa, S. "Copper (II) Ion-Exchanged ZSM-5 Zeolite as Highly Active Catalysts for Direct and Continuous Decomposition of Nitrogen Monoxide", *J. Chem. Soc., Chem. Commun.*, **1986**, 1272-1273.

3. Trout, B. L.; Chakraborty, A. K.; Bell, A. T. "Analysis of the Thermochemistry of NO_x Decomposition over CuZSM-5 Based on Quantum Chemical and Statistical Mechanical Calculations", *J. Phys. Chem.,* **1996**, *100*, 17582-17592.

4. Szostak, R. Molecular Sieves: Principles of Synthesis and Identification. New York: Van Nostrand Reinhold, **1989**.

5. Breck, D. W. Zeolite Molecular Sieves: Structure, Chemistry, and Use. Florida: Robert E. Krieger Publishing Company, **1973**.

6. Dyer, A. An Introduction to Zeolite Molecular Sieves. New York: John Wiley & Sons, **1988**.

7. Argauer, R. J.; Landolt, G. R. "Crystalline Zeolite ZSM-5 and Method of Preparing the Same", *United States Patent*, **1972**, *3*, 702-886.

8. Meimer, W. M.; Olson, D. H. Atlas of Structure Type. London: Butterworth-Heinemann, **1992**.

9. Schreiner, P. R. Zeolites: Applications of Computational Methods" in Encyclopedia of Computational Chemistry. Wiley: Chichester Schleyer, P. v. R., **1998**.

10. Olson, D. H.; Kokotailo, G. T.; Lawton, S. L.; Meier, W. M. "Crystal Structure and Structure-Related Properties of ZSM-5", *J. Phys. Chem.*, **1981**, *85*, 2238-2243.

11. Sayle, D. C.; Catlow, C. R. A.; Gale, J. D.; Perrin, M. A.; Nortier, P. "Computer Modeling of the Active-Site Configurations within the NO Decomposition Catalyst Cu-ZSM-5", *J. Phys. Chem. A*, **1997,** *101,* 3331-3337.

12. Teraishi, K.; Ishida, M.; Irisawa, J.; Kume, M.; Takahashi, Y.; Nakano, T.; Nakamura, H.; Miyamoto, A. "Active Site Structure of Cu/ZSM-5: Computational Study", *J. Phys. Chem. B,* **1997,** *101,* 8079-8085.

13. Dĕdeček, J.; Wichterlova, B. "Siting and Redox Behavior of Cu Ions in CuH-ZSM-5 Zeolites. Cu^+ Photoluminescence Study", *J. Phys. Chem.,* **1994**, *98,* 5721-5727.

14. Lamberti, C.; Bordiga, S.; Salvalaggio, M.; Spoto, G.; Zecchina, A.; Geobaldo, F.; Vlaic, G.; Bellatreccia, M. "XAFS, IR, and UV-Vis Study of the CuI Environment in CuI-ZSM-5", *J. Phys. Chem. B,* **1997**, *101*, 344-360.

15. Iwamoto, M.; Furukawa, H.; Kagawa, S. In New Developments in Zeolite Science and Technology. Amsterdam: Elsevier**, 1986**.

16. Iwamoto, M.; Hamada, H. "Removal of Nitrogen Monoxide from Exhaust Gases through Novel Catalytic Processes", *Catal. Today,* **1991**, *10*, 57-71.

17. Iwamoto, M.; Yahiro, H.; Tanada, K.; Mozino, Y.; Mine, Y.; Kagawa, S. "Removal of Nitrogen Monoxide through a Novel Catalytic Process. 1. Decomposition on Excessively Copper Ion Exchanged ZSM-5 Zeolites", *J. Phys. Chem.*, **1991**, *95*, 3727-3730.

18. Moden, B.; Costa, P. D.; Lee, D. K.; Iglesia, E. "Transient Studies of Oxygen Removal Pathways and Catalytic Redox Cycles during NO Decomposition on Cu-ZSM-5", J. *Phys. Chem. B,* **2002***, 106*, 9633-9641.

19. Iwamoto, M.; Yahiro, H.; Mizuno, N.; Zhang, W.; Mine, Y.; Furukawa, H.; Kagawa, S. "Removal of Nitrogen Monoxide through a Novel Catalyst Process. 2. Infrared Study on Surface Reaction of Nitrogen Monoxide Adsorbed on Copper Ion-Exchanged ZSM-5 Zeolltes", *J. Phys. Chem.*, **1992**, *96*, 9360-9366.

20. Zhang, Y.; Flytzani, -S. M. In Environmental Catalysis. Washington: ACS Symposium Series 552, American Chemical Society, **1994**.

21. Adtke, F.; Koeppel, R. A.; Baiker, A. "Formation of Hydrogen Cyanide over Cu/ZSM-5 Catalyst Used for the Removal of Nitrogen Oxides from Exhausts of Lean-Bum Engines", *Environ. Sci. Tech.*, **1995**, *29*, 2703-2705.

22. Bell, A. T. "Experimetal and Theoretical Studies of NO Decomposition and Reduction over Metal-Exchanged ZSM-5", *Catal. Today,* **1997**, *38*, 151-156.

23. Shelef, M. "Selective Catalytic Reduction of NOx with N-Free Reductants", *Chem. Rev.,* **1995**, *95*, 209-225.

24. Ceramic Industry. Available from: http://www.ceramicindustry.com/.../ 0, 2710, 71657, 00.html[**2004**, Aug 31]

25. Quincoces, C. E.; Kikot, A.; Basaldella, E. I.; González, M. G. "Effect of Hydrothermal Treatment on Cu-ZSM-5 Catalyst in the Selective Reduction of NO", *Ind. Eng. Chem. Res.,* **1999**, *38,* 4236-4240.

26. Larsen, S. C.; Aylor, A.; Bell, A. T.; Reimer, J. A. "Electron Paramagnetic Resonance Studies of Copper Ion-Exchanged ZSM-5", *J. Phys. Chem.,* **1994**, *98,* 11533-11540.

27. Li, Y.; Hall, W. K. "Catalytic Decomposition of Nitric Oxide over Cu-Zeolites", *J. Catal.,* **1991,** *129,* 202-215.

28. Valyon, J.; Hall, W. K. "On the Preparation and Properties of CuZSM-5 Catalysts for Nitric Oxide Decomposition" *Catal. Lett.* **1993**, *19*, 109-119.

29. Valyon, J.; Hall, W. K. "Studies of the Surface Species Formed from Nitric Oxide on Copper Zeolites", *J. Phys. Chem.*, **1993**, *97*, 1204-1212.

30. Valyon, J.; Hall, W. K. "Effects of Reduction and Reoxidation on the Infrared Spectra from Cu-Y and Cu-ZSM-5 Zeolites", *J. Phys. Chem.*, **1993**, *97*, 7054-7060.

31. Spoto, G.; Zecchina, A.; Bordiga, S.; Ricchiardi, G.; Martra, G. "Cu(I)-ZSM-5 Zeolites Prepared by Reaction of H-ZSM-5 with Gaseous CuCl: Spectroscopic Characterization and Reactivity towards Carbon Monoxide and Nitric Oxide", *Appl. Catal. B: Environ.*, **1994**, *3*, 151-172.

32. Lei, G. D.; Adelman, B. J.; Sarkany, J.; Sachtler W. M. H. "Identification of Copper (II) and Copper (I) and Their Interconversion in Cu/ZSM-5 De-NOx Catalysts", *Appl. Catal. B,* **1995**, *5*, 245-256.

33. Beutel, T.; Sarkany, J.; Lei, G. -D.; Yan, J. T.; Sachtler, M. H. "Redox Chemistry of Cu/ZSM-5", *J. Phys. Chem.*, **1996**, *100*, 845-851.

34. Liu, D.-J.; Robota, H. "In Situ Characterization of Cu-ZSM-5 by X-ray Absorption Spectroscopy: XANES Study of the Copper Oxidation State during Selective Catalytic Reduction of Nitric Oxide by Hydrocarbons", *Appl. Catal. B,* **1994**, *4*, 155-165.

35. Schneider, W. F.; Hass, K. C. "Cluster Models of Cu Binding and CO and NO Adsorption in Cu-Exchanged Zeolites", *J. Phys. Chem.,* **1996,** *100,* 6032-6046.

36. Ramprasad, R.; Schneider, W. F.; Hass, K. C.; Adams, J. B. "Theoretical Study of CO and NO Vibrational Frequencies in Cu-Water Clusters and Implications for Cu-Exchanged Zeolites", *J. Phys. Chem. B*, **1997,** *101,* 1940-1949.

37. Rice, M. J.; Chakraborty, A. K.; Bell, A. T. "A Density Functional Theory Study of the Interactions of H_2O with H-ZSM-5, Cu-ZSM-5, and Co-ZSM-5", *J. Phys. Chem. A,* **1998**, *102*, 7498-7504.

38. Trout, B. L.; Chakraborty, A. K.; Bell, A. T. "Local Spin Density Functional Theory Study of Copper Ion-Exchanged ZSM-5", *J. Phys. Chem.,* **1996**, *100,* 4173-4179.

39. Yokomichi, Y.; Yamabe, T.; Ohtsuka, H.; Kakumoto, T. "Theoretical Study of NO Decomposition on Cu-ZSM-5 Catalyst Models Using the Density Functional Method", *J. Phys. Chem.,* **1996**, *100*, 14424-14429.

40. Rice, M. J.; Chakraborty, A. K.; Bell, A. T. "Theoretical Studies of the Coordination and Stability of Divalent Cations in ZSM-5", *J. Phys. Chem. B,* **2000**, *104,* 9987-9992.

41. Grünert, W.; Hayes, N. W.; Joyner, R. W.; Shpiro, E. S.; Siddiqui, M. R. H.; Baeva, G. N. "Structure, Chemistry, and Activity of Cu-ZSM-5 Catalysts for the

Selective Reduction of NO, in the Presence of Oxygen", *J. Phys. Chem.,* **1994**, *98*, 10832-10846.

42. Sayle, D. C.; Perrin, M. A.; Nortier, P.; Catlow, C. R. A. "Simulation Study of Copper (I) and Copper (II) Species in ZSM-5 Zeolite", *J. Chem. Soc., Chem. Commun.,* **1995***, 945-947.

43. Rodriguez, -S. L.; Sierka, M.; Branchadell, V.; Sodupe, M.; Sauer, J. "Coordination of Cu^+ Ions to Zeolite Frameworks Strongly Enhances Their Ability to Bind NO2. An ab Initio Density Functional Study", *J. Am. Chem. Soc.,* **1998**, *120,* 1545-1551.

44. Anderson, M. W.; Kevan, L. "Study of Cu*+-Doped Zeolite NaH-ZSM-5 by Electron Spin Resonance and Electron Spin Echo Modutation Spectroscopies", *J. Phys. Chem.,* **1987**, *91,* 4174-4179.

45. Levine, I. N. Quantum Chemistry 5th Edition. New Jersey: Prentice-Hall, Inc., **2000**.

46. Cramer, C. J. Essentials of Computational Chemistry Theories and Models. New York: John Wiley & Sons, **2002**.

47. Szabo, A.; Ostlund, N. S. Modern Quantum Chemistry: Introduction to Advanced Electronic Structure Theory. New York: MacMillan Publishing Co., **1989**.

48. Hinchiffe, A. Modelling Molecular Structures. New York: John Wiley & Sons, **2000**.

49. Koch, W.; Holthausen, M. C. A Chemist's Guide to Density Functional Theory: Second Edition. New York: Wiley-VCH Verlag GmbH, **2001**.

50. Löwdin, P.-O. "Correlation Problem in Many-Electron Quantum Mechanics", *Adv. Chem. Phys.*, **1959**, *2*, 207-322.

51. Slater, J. C. "A Simplification of the Hartree-Fock Method", *Phys. Rev.*, **1951,** *81*, 385-390.

52. Thomas, L. H. "The Calculation of Atomic Fields", *Proc. Camb. Phil. Soc.*, **1927**, *23*, 542-548.

53. Kohn, W.; Sham, L. J. "Self Consistent Equations Including Exchange and Correlation Effects", *Phys. Rev.*, **1965**, *140,* A1133-A1138.

54. Kohn, W.; Becke, A. D.; Parr, R. G. "Density Functional Theory of Electronic Structure", *J. Phys. Chem.*, **1996**, *100*, 12974-12980.

55. Hohenberg, P.; Kohn, W. "Inhomogeneous Electron Gas", *Phys. Rev.*, **1964**, *136*, B864-B871.

56. Bloch, F. "The Electron Theory of Ferromagnetism and Electrical Conductivity", *Z. Physik*, **1929,** *57*, 545-555.

57. Dirac, P. A. M. "Note on Exchange Phenomena in the Thomas Atom", *Proc. Camb. Phil. Soc.*, **1930**, *26,* 376-385.

58. Vosko, S. J.; Wilk, L.; Nusair, M. "Accurate Spin-Dependent Electron Liquid Correlation Energies for Local Spin Density Calculations: A Critical Analysis", *Can. J. Phys.*, **1980**, *58*, 1200-1211.

59. Perdew, J. P.; Wang, Y. "Accurate and Simple Analytic Representation of the Electron Gas Correlation Energy", *Phys. Rev. B.*, **1992**, *45*, 13244-13249.

60. Becke, A. D. "A Multicenter Numerical Integration Scheme for Polyatomic Molecules", *J. Chem. Phys.*, **1988**, *88*, 2547-2553.

61. Becke, A. D. "Density Functional Calculations of Molecular Bond Energies", *J. Chem. Phys.*, **1986**, *84*, 4524-4529.

62. Perdew, J. P.; Wang, Y. "Accurate and Simple Density Functional for the Electronic Exchange Energy: Generalized Gradient Approximation", *Phys. Rev. B*, **1986**, *33*, 8800-8802.

63. Perdew, J. P.; Burke, K.; Ernzerhof, M. "Generalized Gradient Approximation Made Simple", *Phys. Rev. Lett.*, **1996,** *77,* 3865-3868.

64. Lee, C.; Yang, W.; Parr, R. G. "Development of the Colle-Salvetti Correlation-Energy Formula into a Functional of the Electron Density", *Phys. Rev. B*, **1988**, *37*, 785-789.

65. Colle, R.; Salvetti, O. "Approximate Calculation of the Correlation Energy for the Closed Shells", *Theor. Chim. Acta*, **1975**, *37*, 329-334.

66. Stephens, P. J.; Devlin, J. F.; Chabalowski, C. F.; Frisch, M. J. "Ab Initio Calculations of Vibrational Absorption and Circular Dichroism Spectra Using SCF, MP2,

and Density Functional Theory Force Fields", *J. Phys. Chem.*, **1994**, *98*, 11623-11627.

67. Pople, J. A.; Gill, P. M. W.; Handy, N. C. "Spin-Unrestricted Character of Kohn-Sham Orbitals for Open-Shell Systems", *Int. J. Quant. Chem.*, **1995**, *56*, 303-327.

68. Hehre, W. J.; Ditchfield, R.; Pople, J. A. "Self-Consistent Molecular Orbital Methods. XII. Further Extensions of Gaussian-Type Basis Sets for Use in Molecular Orbital Studies of Organic Molecules", *J. Chem. Phys.*, **1972**, *56*, 2257-2261.

69. Cook, M.; Karplus, M., "Electron Correlation and Density-Functional Methods", *J. Phys. Chem.*, **1987**, *91*, 31-37.

70. DMol Insight II release 96.0, User Guide. San Diego: Molecular Simulations, **1996**.

71. Frisch, M. J.; Trucks, G. W.; H. B. Schlegel, G. E. S.; Robb, M. A.; Cheeseman, J. R.; Zakrzewski, V. G.; Montgomery, J. A.; Stratmann, R. E.; Burant, J. C.; Dapprich, S.; Millam, J. M.; Daniels, A. D.; Kudin, K. N.; Strain, M. C.; Farkas, O.; Tomasi, J.; Barone, V.; Cossi, M.; Cammi, R.; Mennucci, B.; Pomelli, C.; Adamo, C.; Clifford, S.; Ochterski, J.; Petersson, G. A.; Ayala, P. Y.; Cui, Q.; Morokuma, K.; Malick, D. K.; Rabuck, A. D.; Raghavachari, K.; Foresman, J. B.; Cioslowski, J.; Ortiz, J. V.; Stefanov, B. B.; Liu, G.; Liashenko, A.; Piskorz, P.; Komaromi, I.; Gomperts, R.; Martin, R. L.; Fox, D. J.; Keith, T.; Al-Laham, M. A.; Peng, C. Y.; Nanayakkara, A.; Gonzalez, C.; Challacombe, M.; Gill, P. M. W.; Johnson, B. G.; Chen, W.; Wong, M. W.; Andres, J. L.; Head-Gordon, M.; Replogle, E. S.; Pople, J. A. Gaussian 98 (ReVision A.7) (Theory and Calculation). Pittsburgh: PA, **1998**.

72. Poompub, U. Structures and Acidities of H-ZSM-5 with Si/Al Ratio of 47 and 95. Master's Thesis, Petrochemistry and Polymer Science, Faculty of Science, Graduate School, Chulalongkorn University, Thailand, **2004**.

73. Cotton, F. A.; Wilkinson, G. Advanced Inorganic Chemistry, 4th edition. New York: Wiley-Interscience, **1980**.

74. Pasquarello, A.; Petri, I.; Salmon, P. S.; Parisel,O.; Car, R.; Toth, E.; Powell, D. H.; Fischer, H. E.; Helm, L.; Merbach, A. E. "First Solvation Shell of the Cu (II) Aqua Ion: Evidence for Fivefold Coordination", *Science*, **2001,** *291*, 856-859.

75. Schwenk, C. T.; Rode, B. M. "Extended ab initioquantum mechanical/molecular mechanical molecular dynamics simulations of hydrated Cu^{2+}", *J. Chem. Phys.*, **2003***, 119*, 9523-9531.

76. Akesson, R.; Pettersson, L. G. M.; Sandstrom, M.; Wahlgren, U. "Theoretical Calculations of the Jahn-Teller Effect in the Hexahydrated Copper (II), Chromium (II), and Manganese (III) Ions, $[Cu(H_2O)_6]^{2+}$, $[Cr(H_2O)_6]^{2+}$, and $[Mn(H_2O)_6]^{3+}$, and Comparisons wfth the Hexahydrated Copper (I), Chromium (III), and Manganese (II) Clusters", *J. Phys. Chem.,* **1992,** *96*, 150-156.

77. Korshin, G. V.; Frenkel, A. I.; Stern, E. A. "EXAFS Study of the Inner Shell Structure in Copper (II) Complexes with Humic Substances", *Environ. Sci. Technol.*, **1998**, *32*, 2699-2705.

VITAE

NAME: Kanjarat Sukrat

DATE AND PLACE OF BIRTH: 6 November 1978 in Samutsakorn, Thailand

ELEMENTARY SCHOOL:

1985-1991 Somreudee School, Samutsakorn

SECONDARY SCHOOL:

1991-1997 Sirinthorn Rachawitayalai School, Nakornpatom

UNIVERSITY EDUCATION:

1997-2001 B. Sc. in Chemistry, Department of Chemistry, Faculty of Science,
Chulalongkorn University, Bangkok

2001-2004 M. Sc. in Physical Chemistry, Department of Chemistry, Faculty of Science,
Chulalongkorn University, Bangkok